

600839  
600838  
600837

204-P-3-50  
OFFICE OF NAVAL RESEARCH  
CONTRACT Nonr-1866(24)

NR - 384 - 903

TECHNICAL MEMORANDUM  
No. 57

THRESHOLDS OF ACOUSTIC CAVITATION

BY

James E. Barger

APRIL 1964

DDC  
REPRODUCED  
JUN 3 1964

NSIA

ACOUSTICS RESEARCH LABORATORY  
DIVISION OF ENGINEERING AND APPLIED PHYSICS  
HARVARD UNIVERSITY - CAMBRIDGE, MASSACHUSETTS

## **DISCLAIMER NOTICE**

**THIS DOCUMENT IS BEST QUALITY  
PRACTICABLE. THE COPY FURNISHED  
TO DTIC CONTAINED A SIGNIFICANT  
NUMBER OF PAGES WHICH DO NOT  
REPRODUCE LEGIBLY.**

Office of Naval Research

Contract Nonr-1866(24)

Technical Memorandum No. 57

## THRESHOLDS OF ACOUSTIC CAVITATION IN WATER

by

James E. Barger

May 1964

### Abstract

Cavitation thresholds in water have been measured as a function of frequency, dissolved gas, ambient pressure, and suspended particle size. The apparatus used comprises a two-liter volume of water enclosed by a spherical glass shell driven at its radially symmetric resonance frequencies by eight multiresonant piezoelectric transducers. Large acoustic pressures can be produced, ranging from 10 bars at 27 kc/s to 200 bars at 1.16 Mc/s. The threshold data can be divided into three regions. In region A, defined by  $f < 200$  kc/s, acoustic pressure,  $P_a < 3$  bars, and air saturation pressure  $P_s > 600$  mm Hg, small air bubbles grow by rectified diffusion and stabilize at the pressure nodes. In region B, defined by  $f < 200$  kc/s,  $P_a > 3$  bars, and  $P_s < 500$  mm Hg, transient cavities are formed that can be detected visually and aurally. In region C,  $f > 200$  kc/s,  $P_a > 3$  bars, for any value of  $P_s$ , transient cavities are formed, but their presence can be detected only acoustically. Experiments on cavitation at pressures larger than the threshold indicate that only a finite number of cavitation events can be produced in a given sample of water when it is isolated from contamination by airborne motes. In this way water can be "strengthened" by a factor of at least 8 by repeated cavitation.

Acoustics Research Laboratory

Division of Engineering and Applied Physics

Harvard University, Cambridge, Massachusetts

## TABLE OF CONTENTS

	Page
ABSTRACT	i
TABLE OF CONTENTS	iii
LIST OF FIGURES	vi
LIST OF TABLES	vii
Chapter	
I      INTRODUCTION	1
The Interest in Cavitation	1
The Concept of Acoustic Cavitation	6
The Strength of a Nucleus	10
Nucleation Theories	18
Theories Which Do Not Consider Nuclei	26
Experimental Cavitation Thresholds	29
Statement of the Problem	36
II     EXPERIMENTAL APPARATUS	40
The Resonator	44
The Transducers	46
Performance of the Resonator	52
The Power Amplifier	56
Pressure Probes	59
Automatic Frequency Control System	60

The Probe Amplifier	70
Cavitation Detection Circuit	71
Water Control Apparatus	74
III EXPERIMENTAL PROCEDURE AND OBSERVATIONS	76
Threshold Measurements	77
Measurements Above Threshold	89
IV EXPERIMENTAL RESULTS	97
Cavitation Thresholds	97
Cavitation Threshold as a Function of Ambient Pressure	101
Number of Cavitation Events Produced as a Function of Acoustic Pressure	102
Statistical Distribution of the Time Between Cavitation Events	106
The Effect of a Paraffin Screen on the Cavitation Rate	108
V DISCUSSION OF THE RESULTS	110
The Threshold for the Formation of Gas Bubbles (Region A)	111
Motion of Small Gas Bubbles in a Radial Sound Field	115
The Formation of Transient Cavities at Low Frequencies (Region B)	123
Translational Motions of Transient Cavities	130
Cavitation Thresholds at High Frequencies (Region C)	135
The Cavitation Nucleus	137
Recommendations for Future Study	143
ACKNOWLEDGMENTS	149

Appendix A	RESONATOR MODAL FREQUENCIES AND DRIVING SENSITIVITIES	151
Appendix B	MULTIRESONANT TRANSDUCER CALCULATIONS	157
Appendix C	PROBE-HYDROPHONE RECEIVING-SENSITIVITY CALCULATIONS	163
LIST OF REFERENCES		170

## LIST OF FIGURES

Number	Followi ng Page
1. Experimental cavitation thresholds	30
2. Cavitation thresholds (from Galloway, Reference 28)	36
3. Photograph of the experimental apparatus	44
4. Photograph of the spherical resonator and driver transducers	44
5. Schematic diagram of the experimental apparatus	44
6. Power amplifier chassis	58
7. Low- and high-voltage power supplies	58
8. Construction of the pressure probes	60
9. Probe calibration apparatus	62
10. Automatic frequency control chassis	70
11. Probe amplifier	70
12. Photographs of transient cavities	88
13. Cavitation threshold for water (equilibrium air saturation pressure: 10 mm Hg)	98
14. Cavitation threshold for water (equilibrium air saturation pressure: 100 mm Hg)	98
15. Cavitation threshold for water (equilibrium air saturation pressure: 250 mm Hg)	98
16. Cavitation threshold for water (equilibrium air saturation pressure: 700 mm Hg)	98
17. Cavitation threshold for water (equilibrium air saturation pressure: 760 mm Hg)	98
18. Cavitation threshold as a function of ambient pressure	102
19. Pressure distributions of cavitation events in water	102

V

	Following Page	Page
20. Number of cavitation events/cm <sup>3</sup> as a function of the maximum foreign particle size	106	
21. Distribution of intervals between events	106	
22. Time history of cavitation events showing effect of paraffin screen	108	
23. Geometry of an interface in a crack		139
24. Receiving sensitivity of solid core hydrophones of PZT-5		166

## LIST OF TABLES

I The experimental apparatus used by Esche	30
II Resonator performance characteristics	53
III Experimental cavitation thresholds for water	98
IV Total number of cavitation events produced in two liters of water by an acoustic pressure of 38 bars	105

## Chapter I

### INTRODUCTION

#### The Interest in Cavitation

Cavitation is a rather general term applied to the formation of ruptures or bubbles within a liquid that is being subjected to a sufficiently low pressure. A more concrete definition of the term will be given in the following section. The negative pressure necessary for cavitation may be applied steadily, as a result of fluid flow, or acoustically. The eruptive boiling of a superheated liquid and the effervescence of liquids supersaturated with dissolved gases can be considered to be related to the phenomenon of cavitation.

The word cavitation itself was introduced in 1895 by Robert Froude to describe the cavities observed to form in the water near the surfaces of ship propellers.<sup>1</sup> The first theoretical treatment of the problem was undertaken by Rayleigh,<sup>2</sup> who studied the collapse of a vapor-filled cavity under steady external pressure. He concluded that cavities which form on the low-pressure side of a propeller collapse with such violence that the resulting pressure shock created in the water erodes the surface of the propeller. Later, high performance hydrodynamic machinery was observed to suffer damage due to cavitation activity.

---

1. Sir John Thornycroft and Sidney W. Barnaby, "Torpedo Boat Destroyers," Proc. Inst. Civil Engrs. 122, 51 (1895).
2. Lord Rayleigh, "On Pressure Developed in a Liquid During the Collapse of a Spherical Cavity," Phil. Mag. 34, 94 (1917).

Acoustic cavitation at the face of sonar transducers has been observed to limit the acoustic power a given transducer can radiate into the water. This power limitation and the damage suffered by the transducers motivated a great deal of the research in acoustic cavitation. Recently, however, cavitation in liquids has been used to perform a wide range of industrial and experimental tasks. The trend toward the beneficial use of acoustic cavitation has generated interest in the acquisition of more complete knowledge of the phenomenon.

The ultrasonic cleaner has recently found wide industrial acceptance, although, aside from the fact that cavitation is necessary for the cleaning process to take place, little is known of the mechanism by which the action occurs. Knowledge of the dependence of the threshold for cavitation on acoustic and geometric parameters is necessary for the efficient design of these devices.

Cavitation has been shown to be an effective means for promoting dispersion and emulsification of solids and liquids in liquids. Olaf<sup>3</sup> has conducted experiments in which jeweler's rouge was dispersed in water; and oil, grease, and wax were dispersed in trichlorethylene. The dispersion of metal particles removed from a surface by cavitation was also accomplished. Bisa, Dirnagl, and Esche<sup>4</sup> have dispersed small water droplets in air with an intense sound field in the water below the air-water interface. It was reported that the diameters of the water drops

---

3. J. Olaf, "Oberflachenreinigung mit Ultraschall," *Acustica* 7, 253 (1957).

4. K. Bisa, K. Dirnagl, and R. Esche, *Siemens-Zeitschrift* 28, 341 (1954).

were about equal to the wavelength of surface waves at the exciting frequency.

Nyborg, Gould, Jackson, and Adams<sup>5</sup> have reported on the effect of cavitation on chemical reactions. They have shown that the rate of several chemical reactions can be increased even in "weak cavitation." In this type of cavitation small bubbles were observed to form in the region of the transducer. The authors attributed the increased rates of reaction to the intense rates of shear in the neighborhood of the oscillating bubbles. In addition to the acceleration of chemical reactions, cavitation can be used to promote chemical reactions which would not otherwise occur.

Several experimenters have shown that the molecular structure of matter can be altered by cavitation. In studies on peroxide formation in water, it has been established<sup>6</sup> that the reaction is due partly to water molecules that have been broken up:  $H_2O \rightarrow H^+ + OH^-$ ;  $OH^- + OH^- \rightarrow H_2O_2$ . When dissolved oxygen takes part in the chemical action, del Duca, Yeager, Davies, and Hovorka<sup>7</sup> have shown by isotope techniques that the two atoms from one oxygen molecule are incorporated into one peroxide molecule.

---

5. W. L. Nyborg, R. K. Gould, F. J. Jackson, and C. E. Adams, "Sonically Induced Microstreaming Applied to a Surface Reaction," *J. Acoust. Soc. Am.* 31, 706 (1959).
6. B. E. Noltingk, "The Effects of Intense Ultrasonics in Liquids," *Handbuch der Physik*, Vol. XI/2, S. Flugge, ed. (Springer-Verlag, Berlin, 1962).
7. M. del Duca, E. Yeager, M. Davies, and F. Hovorka, "Isotopic Techniques in the Study of the Sonochemical Formation of Hydrogen Peroxide," *J. Acoust. Soc. Am.* 30, 301 (1958).

Typical of recent developments in the use of ultrasonic cavitation is an application to soldering aluminum and other metals that form surface oxide layers. Campbell<sup>8</sup> describes an apparatus designed for this purpose. In this application, the solder is melted over the metal where a bond is desired. A tip which is excited to a high amplitude oscillation at an ultrasonic frequency is introduced into the pool of molten solder. Cavitation is induced in the liquid layer of solder, and the subsequent cleaning action removes the oxide layer from the metal, allowing the solder to bond to the metal. The particles of oxide float to the surface of the molten solder where they can be removed after the solder has solidified. Mr. Campbell is of the opinion that this process is superior to any of the present conventional methods of soldering aluminum.

The irradiation of molten metals with high-energy sound waves has been shown to improve grain structure and reduce the gas content in the solidified metal. A review of the work done in this field has been given by Hiedemann.<sup>9</sup> An extremely wide frequency range has been utilized in research on liquid metals, and little differences are noted with respect to this parameter. There is no convincing experimental evidence that cavitation is directly involved in these experiments, although the grain structure is believed to be due to the simultaneous formation of

---

8. C. Campbell, "Ultrasonic Soldering of Aluminum," *Electronic Progress* 2, 4 (Raytheon Manufacturing Co., Waltham, Mass., 1958).
9. E. Hiedemann, "Metallurgical Effects of Ultrasonic Waves," *J. Acoust. Soc. Am.* 26, 831 (1954).

solidification nuclei throughout the volume of the liquid phase of the metal.

Solutions of long-chain high polymers can be modified in a cavitation field. The progress of the alteration is easily monitored by the viscosity of the liquid, and many investigations have been made of different aspects of this phenomenon. A review of the literature in this field is included in a paper by Roberts, Yeager, and Hovorka.<sup>10</sup>

A phenomenon which depends on cavitation in liquids which has no direct use, but which has been widely examined, is sonoluminescence. As its name implies, this phenomenon consists of the radiation of light from a region of high acoustic activity. Several theories have been advanced to explain the light emission, among them electrical discharges and the intense temperatures attained by the contents of a cavity at collapse. Meyer and Kuttruff<sup>11</sup> have performed an interesting experiment in which it was demonstrated that the flashes of light occur at the instant of collapse of cavities formed in the liquid. The intensity of the luminescence has been shown to depend on the gases dissolved in the liquid as well as on the acoustic parameters. Meyer and Kuttruff also showed that the luminescence depends strongly on the liquid; for example, they demonstrated that the intensity of light emitted from cavitation in

---

10. W. Roberts, E. Yeager, and F. Hovorka, Ultrasonic Research Lab., Western Reserve Univ., Cleveland, Ohio; Tech. Rept. No. 18 (1957).

11. E. Meyer and H. Kuttruff, "Zur Phasenbeziehung zwischen Sonolumineszenz und Kavitationsvorgang bei periodischer Anregung," Z. Physik 11, 325 (1959).

mercury was several times that for water. Sonoluminescence has been proposed for use as a measure of the intensity of cavitation.

#### The Concept of Acoustic Cavitation

The basic features of acoustic cavitation in liquids are the formation of cavities filled with a mixture of the vapor of the liquid and gases and the subsequent growth and collapse of these cavities. The energy necessary for the process derives from the acoustic wave motion in the liquid. A pure liquid is unstable with respect to its gaseous phase when the pressure is lowered to the pressure of saturated vapor corresponding to the temperature of the liquid. The pure liquid can, however, be subjected to pressures considerably low than the saturated vapor pressure without transforming into the gaseous phase if there is an absence of a "critical nucleus." In the pure liquid, this nucleus can be regarded as a fluctuation in the liquid density which takes the form of a bubble of the vapor phase which is large enough for the external pressure to be balanced by the vapor pressure in the bubble and the effective pressure due to surface tension.<sup>12</sup> In an impure liquid, there are many possibilities for the presence of nuclei whose strengths are considerably less than those calculated for a pure liquid. The strength of a nucleus will be examined in the next section.

The fact that a pure liquid under tension will not spontaneously form a two-phase system can be easily demonstrated. Although the two-

---

12. N. A. Roi, "The Initiation and Development of Ultrasonic Cavitation," Soviet Phys.-Acoustics 3, 3 (1957).

phase system represents a state of lower energy than the initial strained liquid state, the pure liquid system would need to pass through states of higher energy than the initial state in order to reach the two-phase equilibrium. Consider a volume of liquid under tension. Let  $v$  represent the difference in the volume of the strained liquid and the volume the liquid would assume in the unstrained state. The strain energy stored in the liquid system can be written  $E_s = K(v)^2$ , where  $K$  is a constant. If a spherical empty cavity were to form in the liquid, the stored energy in the entire system would be written:

$$E_s = K\left(v - \frac{4\pi R^3}{3}\right)^2 + 4\pi R^2 \sigma ,$$

where  $R$  is the radius of the cavity interface and  $\sigma$  is the surface tension. Then

$$\frac{dE_s}{dR} = 8\pi R[-RK\left(v - \frac{4\pi R^3}{3}\right) + \sigma] ,$$

which is positive as  $R \rightarrow 0$ . The formation of a small cavity in the strained liquid system, therefore, requires that additional energy be added to the system to form the cavity.

The amount of gas in the cavity is very important with respect to the subsequent behavior of the cavity in an acoustic field. This effect has led Blake<sup>13</sup> to describe two distinct types of cavitation, gaseous

13. F. G. Blake, Jr., "The Onset of Cavitation in Liquids," Tech. Memo. No. 12, Acoustics Research Lab., Harvard Univ. (1949).

and vaporous. Flynn<sup>14</sup> has made the distinction more precise by defining cavitation in terms of the dynamics of cavity motion. On the one hand, a cavity might undergo periodic motion whether harmonic or not. Such motions are characteristic of gas-filled bubbles in acoustic fields of relatively moderate amplitude. Cavity motion of this type is called "stable cavity" motion. On the other hand, the cavities are often observed to collapse and disappear entirely after one or more acoustic periods. Cavity motion of this type is characteristic of vapor-filled cavities, although Flynn has calculated that gas-filled cavities may also act in this manner. A cavity that behaves in this manner is called a "transient cavity."

The physical manifestation of acoustic cavitation differs widely over the range of significant parameters: acoustic pressure and frequency, gas content, ambient pressure, and the state of purity of the liquid. Stable cavities are visible as bubbles or fog-like masses of bubbles. Detailed descriptions of the events characteristic of stable cavity formation can be found in the publications by Blake,<sup>\*</sup> Willard,<sup>15</sup> and Mohr.<sup>16</sup> Transient cavities appear as very brief silvery flashes when viewed with strong side lighting against a dark background. The

---

14. H. G. Flynn, "Physics of Acoustic Cavitation in Liquids," Physical Acoustics, Vol. 1B (Academic Press, W. P. Mason, ed., in press).

\* F. G. Blake, Jr., Reference 13, cited on p. 7.

15. G. Willard, "Ultrasonically Induced Cavitation in Water: A Step-by-Step Process," J. Acoust. Soc. Am. 25, 667 (1957).

16. W. Mohr, "Über Schwingungskavitation bei kurzen Schallimpulsen," Acustica 7, 267 (1957).

size of these depends mostly on frequency, being smaller the higher the frequency. There is no noise radiation except when the cavity collapses. A large pressure spike is observed for each event, and the collapse can be identified outside the container as a sharp snap.

The life history of a transient cavity has been recorded photographically by Ellis.<sup>17</sup> One series of photographs shows the growth and collapse of a cavity in degassed water in a 10 kc/s acoustic standing-wave field. These photographs show that expanding bubbles remain relatively spherical whereas during the collapse phase they become quite unsymmetrical. Data obtained photographically by Knapp and Hollander<sup>18</sup> of the growth and collapse of hydrodynamically induced cavitation show a similar history of the radius of the cavity as a function of time. With the exception of the loss of sphericity near the end of the collapse, the data agree quite closely with the predictions of the theory of the dynamics of cavity motion which will be outlined in a following section.

The asymmetry and breaking up of the cavity during collapse is due to the "Taylor instability" of accelerated liquid surfaces. Taylor's original theory<sup>19</sup> has been developed further by Binnie<sup>20</sup> for the case of

---

- 17. A. T. Ellis, "Techniques for Pressure Pulse Measurements and High-Speed Photography in Ultrasonic Cavitation," Cavitation in Hydrodynamics, London, H. M. S. O., 8-1-8-32 (1956).
- 18. R. T. Knapp and A. Hollander, "Laboratory Investigations of the Mechanism of Cavitation," Trans. Am. Soc. Mech. Engrs. 70, 419 (1948).
- 19. G. I. Taylor, "The Instability of Liquid Surfaces When Accelerated in a Direction Perpendicular to Their Planes," Proc. Roy. Soc. (London), Ser. A, 201, 192 (1950).
- 20. A. M. Binnie, "The Stability of the Surface of a Cavitation Bubble," Proc. Cambridge Phil. Soc. 49, 151 (1953).

a cavitation bubble. He shows that  $4\sigma/R$  is a critical value of the inward acceleration of the cavity surface -  $\frac{d^2R}{dt^2}$ . When this value is exceeded the liquid surface will break up into many randomly shaped cavities. For the average cavitation conditions, this limit will be exceeded when the cavity collapses from a radius larger than a few microns.

For the remainder of this study, the word cavitation is meant to apply to transient cavities unless otherwise stated. Inasmuch as the hallmark of a transient cavity is the collapse of the cavity in the liquid, accompanied by large radial interface velocities, it will be the investigation of this phenomenon to which attention will be directed.

#### The Strength of a Nucleus

A simple calculation can be made to show the static strength of a spherical bubble in a liquid. This strength can be called the limit for mechanical stability of the bubble. At the beginning it can be assumed that the bubble contains a certain amount of gas, and vapor of the liquid at the saturation vapor pressure. The pressure  $P$  external to the bubble is given by

$$P = P_v + \bar{M}RT/V - 2\sigma/R . \quad (1-1)$$

In this equation  $P_v$  is the saturation vapor pressure,  $M$  the moles of gas in the bubble,  $\bar{R}$  the gas constant,  $T$  the absolute temperature,  $V$  the volume of the bubble,  $\sigma$  the interfacial tension per unit transverse length at the bubble surface, and  $R$  the radius of the bubble. The maximum negative pressure  $P$ , for which Eq.(1-1) represents stable equilibrium,

occurs at a radius  $R^*$ , the solution of  $\frac{\partial P}{\partial R}\Big|_{R^*} = 0$ . The value of the critical radius  $R^*$  is

$$R^* = [9M\bar{T}/(8\pi\sigma)]^{1/2} . \quad (1-2)$$

The pressure corresponding to this radius is the critical external pressure  $P^*$ :

$$P^* = P_v - \frac{8}{9} [2\pi\sigma^3/(M\bar{T})]^{1/2} . \quad (1-3)$$

For values of  $P < P^*$ , no stable equilibrium radius exists and  $R$  will increase without limit.

Since  $M\bar{T} = 4\pi R_o^3/3 (P_o + 2\sigma/R_o - P_v)$ , where  $R_o$  and  $P_o$  are the initial values of the bubble radius and external pressure, the last equation can be written:

$$P^* = P_v - \frac{8}{9} \left[ \frac{3\sigma^3}{2R_o^3(P_o - P_v + 2\sigma/R_o)} \right]^{1/2} . \quad (1-4)$$

For relatively small bubbles, i.e., those having strengths in excess of a few atmospheres, the pressure due to surface tension is larger than  $P_o$  and  $P_v$ ; thus, the latter quantities can be neglected. If  $2\sigma/R_o \gg P_o - P_v$ , Eq.(1-4) can be written (for water,  $\sigma = 80$  dyne/cm):

$$P^* = P_v - 0.77 \sigma/R_o . \quad (1-5)$$

If it is assumed that the nucleus is a solid sphere which is not wetted by the liquid, i.e., a zero contact angle, the critical pressure required to separate the liquid from a solid sphere of radius  $R_o$  is:

$$P^* = P_v - 2\sigma/R_o . \quad (1-6)$$

Again, for values of  $P < P^*$ , no stable equilibrium radius exists, and the radius of the spherical cavity will increase without limit.

This result shows that the static strength of a small gas-filled cavity is less by a factor of 2.6 than the strength of a cavity formed by a spherical non-wetted solid of the same radius.

The static strength of a spherical nucleus is thereby shown to lie within the range defined by Eqs.(1-5) and (1-6), but the dynamic strength of the nucleus can be expected to be different. The solution of this problem lies in the consideration of the dynamics of cavity motion in an acoustic field. This problem has been attacked with various degrees of sophistication. By far the most complete discussion of the problem has been given recently by Flynn,<sup>\*</sup> whose work should form the basis for any serious consideration of the dynamics of cavity motion.

All the studies of the dynamics of cavity motion have several points in common. At the outset, an equation of motion for the cavity interface is derived. This equation is nonlinear, and analytic solutions have not been found. Since the equation is nonlinear, the nature of the solutions depends on the initial conditions. The initial velocity of the cavity is usually taken to be zero. The initial radius of the cavity is usually taken to be a parameter which is varied to obtain a family of solutions. The acoustic pressure is commonly expressed as  $-P_a \sin \omega t$ . The choice of this particular phase relation at time  $t = 0$  appears to be arbitrary. The equation of motion with the initial conditions is solved numerically by either an analog or a digital computer.

---

\* H. G. Flynn, Reference 14, cited on p. 8.

Different assumptions have been made in the derivation of the equations of motion. Flynn has reviewed the assumptions made by several authors.

All of the equations of motion include terms which represent the inertia of the liquid in which the cavity is situated. These terms are commonly derived for an incompressible liquid. Equations derived from this assumption have solutions which indicate that the cavity interface velocity near the end of the collapse phase exceeds the speed of sound in the liquid. The incompressible assumption does not hold in this case. Flynn has introduced an approximation of the compressibility of the liquid into his equation of motion used to predict collapse velocities.

The effect of gas inside the cavity has been treated in several different ways. Noltingk\* ignored the effects of gas entirely in his calculations. Some investigators have assumed that a constant mass of gas remains in the cavity. The mass of gas in the cavity is calculated from the equilibrium equation for the pressure in the initial spherical bubble. The gas is usually assumed to behave like an ideal gas, although the deviations from ideal gas behavior are considered by Flynn.

Other differences in the equations of motion depend on the manner in which the heat conduction between the contents of the cavity and the surrounding liquid is considered. In many cases this phenomenon is ignored. The calculations of Flynn show that the heat conduction has a pronounced effect on cavity motions, particularly during the collapse phase. In particular, he points out that the initial compression of the gas is isothermal, while the final stages of collapse are adiabatic.

---

\* B. E. Noltingk, Reference 6, cited on p. 3,

Two assumptions common to all derivations of the equations of motion deal with the surface tension of the cavity and the acoustic pressure. The usual equilibrium surface tension coefficient is assumed to hold under dynamic conditions, even for very small cavity radii, and the cavity radius is assumed to be very small with respect to a wavelength.

The solutions of the equations of motion of spherical cavities in water have been presented by several authors. The work of the two authors already mentioned is particularly noteworthy. Noltingk has calculated the motion of a cavity under the assumptions that there is a vacuum inside the cavity and that the liquid is incompressible. These solutions show that the cavity initially increases in size to a maximum radius during the tension phase of the acoustic wave. During the compression phase the cavity collapses. The maximum radius achieved by the cavity during expansion is taken to be indicative of the magnitude of the collapse velocity. The maximum radius of the cavity is shown to be inversely proportional to the frequency, and to be an increasing monotonic function of the acoustic pressure. The maximum value of the cavity radius is shown to be independent of the initial cavity radius  $R_o$  for  $R_o > R_c$ . For  $R_o < R_c$ , the maximum cavity radius is approximately equal to  $R_o$ ; in other words, the cavity grows rapidly under acoustic tension only for  $R_o \geq R_c$ . The calculation was performed for the special case described by these parameters: ambient pressure  $P_o = 1$  bar, acoustic pressure  $P_a = 4$  bars, and (for water)  $\sigma = 80$  dyne/cm. The critical value of  $R_o$  was found to be  $R_c = 0.2 \mu$ .

A threshold behavior was indicated only in the parameter  $R_o$ , a situation which is similar to the case of the static strength of a bubble of radius  $R_o$ . Following the form of Eq.(1-5), the critical negative pressure should be proportional to the pressure due to the surface tension of the initial cavity. The proportionality constant can be calculated from the values of the ambient and acoustic pressures and the size of the critical radius. On this basis the critical pressure becomes

$$P_v^* = P_v - 0.75 \sigma/R_o , \quad (1-7)$$

where  $P_v^*$  is the critical pressure required for the growth of the initial cavity.

The fact that the coefficients in Eqs.(1-5) and (1-7) are nearly identical indicates that the dynamic strength of a spherical vapor cavity in the liquid can be expected to be approximately the same as its static strength.

Flynn shows the radius-time history of air-filled cavity motions for several different acoustic pressures. He concludes that acoustic pressures of 1 bar or more are sufficient to increase the initial cavity radius by a factor of two during the expansion phase of the cavity motion. He argues that the inertial pressure term will dominate the gas pressure term during collapse if the collapse begins from a radius greater than about twice the initial radius. He concludes that this dominance will result in a sufficiently large collapse velocity to prevent further oscillation of the cavity.

The cavity motions calculated by Flynn result from acoustic pressure amplitudes of 10 bars to 100 bars do not collapse during the first acoustic compression phase. The solutions show that the cavities tend to oscillate about an expanded radius for one or more periods of the exciting signal before they collapse. The radius from which the cavities eventually collapse is shown to be larger for the higher acoustic pressures, and the time of collapse is less. This shows that the higher acoustic pressures will cause larger collapse velocities.

Since Flynn does not estimate the collapse velocity that would be necessary to explain experimental observations of cavitation, it is not possible to determine a definite threshold relationship from his analysis of cavity motion. The only threshold that can be inferred from his results is that the acoustic pressure must be greater than the ambient pressure.

When one interprets these threshold relationships, it must be remembered that they are not sufficient conditions. The actual magnitudes of the velocity of collapse of a cavity depend on all of the parameters considered in the analysis. The detection scheme employed will be of significance when the threshold is observed experimentally. For example, if cavitation events were to be observed optically, it would be necessary to take into account the fact that the maximum cavity radius is approximately inversely proportional to the frequency. There would be a danger then that the threshold would be determined more by the resolving power of the optics used than by the physics of cavitation.

The lack of an extremely sharp threshold has been observed by Moi<sup>\*</sup>. He defined a cavitation index based on the average height of the sound pulse received from a region of cavitation. He plotted this index as a function of the peak acoustic pressure and found a gradual increase in the cavitation index with increased acoustic amplitudes, above a certain minimum amplitude.

The solutions of the cavity dynamics problem which have been cited neglected an important phenomenon which can be of overriding importance in the case of gassy liquids. This is the growth of a cavity by a net influx of gas, a phenomenon called rectified diffusion. A theory to explain this type of cavity growth was given by Blake,<sup>†</sup> and elaborated further by Rosenberg,<sup>21</sup> and by Hsieh and Plesset.<sup>22</sup> According to this theory, a small bubble filled with gas is assumed to pulsate in phase with the pressure amplitude of the acoustic field. The bubble resonance frequency must be larger than the driving frequency for this phase relationship to occur. If the bubble was initially in equilibrium with its surroundings, gas will tend to diffuse out when the bubble is compressed and in when the bubble is expanded. Since the surface area of the bubble is larger when the bubble is expanded, there will be a net

---

\* W. Moi., Reference 16, cited on p. 8.

† F. G. Blake, Jr., Reference 13, cited on p. 7.

21. M. D. Rosenberg, "Pulsations and Growth of Gas-Filled Bubbles in Sound Fields," Tech. Memo. No. 25, Acoustics Research Lab., Harvard Univ. (1952).
22. D.-Y. Hsieh and M. S. Plesset, "Theory of Rectified Diffusion of Mass into Gas Bubbles," J. Acoust. Soc. Am. 33, 206 (1961).

influx of gas over one acoustic cycle. The cavitation threshold for rectified diffusion is defined as that acoustic pressure necessary to cause an initially very small bubble to grow to the point where it can become a cavitation nucleus. This theory predicts threshold values that are less than one atmosphere for cavitation in gassy liquids.

### Nucleation Theories

Thus far it has been seen that the tensile strength of a liquid is limited by a nucleus of some sort. The strength of a nucleus of spherical shape has been discussed. It is now necessary to discuss the various possibilities for the origin of the nuclei in liquids. It is appropriate to consider first the theories that apply to pure liquids.

Blake<sup>23</sup> has outlined four theories based on the kinetic theory of liquids. Three of these, due to Frenkel, Fürth, and Döring, either are not directly applicable to acoustic cavitation or represent oversimplifications. The theory proposed by Fisher<sup>24</sup> is a more refined treatment, and will be outlined here. As in the other theories, the probability of the formation of a nucleus in unit time in a unit volume of liquid is taken to be proportional to  $\exp(-W_{cr}/kT)$ . The work of formation  $W$  of the nucleus is alleged to be:

$$W = 4\pi R^2 \sigma - \frac{4}{3} \pi R^3 P . \quad (1-8)$$

---

23. F. G. Blake, Jr., "The Tensile Strength of Liquids: A Review of the Literature," Tech. Memo. No. 9, Acoustics Research Lab., Harvard Univ. (1949).

24. J. C. Fisher, "The Fracture of Liquids," J. Appl. Phys. 19, 1062 (1948).

The critical radius  $R^*$  occurs when  $\frac{\partial W}{\partial R} = 0$ . When this condition is applied to Eq.(1-8), the value of  $R^*$  is found to be  $2\sigma/P$ . When this value of the critical radius is substituted into Eq.(1-8) the work of formation of the critical nucleus is found to be

$$W_{cr} = \frac{16\pi\sigma^3}{3P^2} .$$

A cavity which exceeds the critical radius will increase without limit for a given  $P$ , and cavities with smaller radii will contract and disappear.

The major difference between this theory and the others mentioned lies in the choice of the proportionality constant for the exponential probability function. This constant was derived from the theory of absolute reaction rates given by Turnbull and Fisher<sup>25</sup> and is to an order of magnitude of the form  $(NkT/h) \exp(-\Delta f_o^*/kT)$ , where  $N$  is the number of molecules in the liquid and  $\Delta f_o^*$  is the free energy of activation for the motion of an individual molecule past its neighbors at the cavity surface. The rate of formation of critical nuclei becomes:

$$\frac{dn}{dt} = NkT/h \exp\left[-(\Delta f_o^* + \frac{16\pi\sigma^3}{3P^2}) \frac{1}{kT}\right] . \quad (1-9)$$

Since the formation of the first critical nucleus leads to the fracture of the liquid it is possible to assume that the pressure at which one cavity is formed in  $t$  seconds represents the magnitude of the

25. D. Turnbull and J. C. Fisher, "Rate of Nucleation in Condensed Systems," *J. Chem. Phys.* 17, 71 (1949).

liquid strength  $P^*$ . The rate of nucleus formation is then written as  $1/t$ , and the pressure required to produce one critical cavity in  $t$  seconds per mol of liquid becomes:

$$P^* = - \left[ \frac{16\pi}{3} \frac{\sigma^3}{kT \ln(NkTt/h) - \Delta f_o^*} \right]^{1/2}. \quad (1-10)$$

The quantity  $\Delta f_o^*$  is assumed to be the activation energy for diffusion. This energy is known to be less than 10 kcal/mol for liquids. It can be seen that  $I^*$  varies little with  $\Delta f_o^*$  as  $\Delta f_o^*$  varies between 0 and 10 kcal/mol, and for this reason  $\Delta f_o^*$  can be neglected. At  $T = 300^\circ K$ ,  $\Delta f_o^* = 0$ , one obtains  $P^* = -1740$  bars for a waiting time  $t = 10^{-15}$  seconds; and  $P^* = -1100$  bars for  $t = 10^{16}$  seconds. Since the liquid strength varies so little with such immense changes in waiting time, it is reasonable to assume  $t = 1$ . Equation (1-10) can then be simplified to:

$$P^* = - \frac{16\pi}{3} \left[ \frac{\sigma^3}{kT \ln(NkT/h)} \right]^{1/2}. \quad (1-11)$$

The value of the liquid strength for water computed from this formula is  $P^* = -1320$  bars, which corresponds to a critical nucleus with a radius of  $10^{-7}$  cm. This result shows the extreme difficulty one must overcome if it is hoped to obtain a sample of liquid pure enough to allow the theoretical liquid strength to be measured.

It will be pointed out in the next section that experiments have shown that the strength of liquids is considerably lower than the values computed from Eq.(1-11). The first approach to an explanation of this fact that will be outlined considers the possible presence of impurities

in the form of solid matter which is not wetted by the liquid. This case has been treated by Fisher<sup>\*</sup> in a manner analogous to the above calculation for the strength of a pure liquid. The work necessary for the formation of a spherical cavity near the surface of a solid body is written:

$$W = 2\pi R^2(1-m)\sigma_L + \pi R^2(1-m^2)(\sigma_S - \sigma_{SL}) - \frac{\pi R^3}{3} (2-3m+m^2) \frac{1}{P} , \quad (1-12)$$

where  $\sigma_L$ ,  $\sigma_S$ , and  $\sigma_{SL}$  are respectively the surface tensions at the liquid-vapor, solid-vapor, and solid-liquid boundaries;  $m = (\sigma_{SL} - \sigma_S)/\sigma_L = \cos \alpha$ , where  $\alpha$  is the wetting angle.

The work of formation of a critical nucleus and the corresponding radius are:

$$W_{CR} = 16\pi\sigma_L^3\phi/(3P^2) , \quad (1-13)$$

$$R^* = \left[ \frac{4\sigma_L - 2m(1+m)\sigma_S}{2-m} \right] P ,$$

$$\text{where } \phi = \frac{(2+m)(1-m^2)}{4} .$$

The derivation of the critical pressure required to separate the liquid from an imperfectly wetted solid particle parallels the derivation of Eq.(1-11). In the present case the work of formation of a critical nucleus is given by Eq.(1-13). The critical pressure is given by Fisher as;

$$P^* = - \left[ \frac{16\pi}{3kT} \frac{\sigma_L^3 \phi}{\ln(NkT/h)} \right]^{1/2} . \quad (1-14)$$

\* J. C. Fisher, Reference 24, cited on p. 18.

This expression differs from Eq.(1-11) by the factor  $\phi^{1/2}$ , and in addition N is now considered to be the number of molecules in contact with the surface of the solid body.

Since  $\phi \rightarrow 0$  as  $\alpha \rightarrow 0$ , it can be seen from Eq.(1-14) and the definition of  $\phi$  that if the wetting angle is zero the strength of the liquid with respect to separation from the solid body is also zero. If it is assumed that bodies of varying degrees of wettability are in the liquid as cavitation nuclei, any threshold can be explained. Thus, it would be desirable in any threshold measurement to eliminate foreign particles.

It is frequently assumed cavitation nucleus is a free bubble of gas in the liquid. Relatively large bubbles will rise to the surface of the liquid; their rate of travel under Stokes' law is about  $20\ 000 R_o^2$  cm/sec where the liquid is water.<sup>26</sup> Smaller bubbles will be dissolved rapidly due to the fact that the gas pressure in the bubble is greater than the equilibrium pressure of the gas over the free surface because of the surface tension. Approximate calculations by Kurtze<sup>27</sup> give the lifetime of a bubble as

$$\tau = R_o^3 / (3D\beta) \text{ seconds} , \quad (1-15)$$

where D is the diffusion constant for gas in the bubble and  $\beta$  is the ratio of the number of gas molecules per unit volume that are in solution in the liquid and free in the bubble respectively. Representative

26. F. E. Fox and U. F. Herzfeld, "Gas Bubbles with Organic Skin as Cavitation Nuclei," J. Acoust. Soc. Am. 26, 984 (1954).

27. G. Kurtze, Nachr. Akad. Wiss. Göttingen, Math.-Phys. Kl. 1 (1958).

values for air dissolved in water indicate  $D = 2 \times 10^{-5} \text{ cm}^2/\text{sec}$  and  $\beta = 0.02$ . Equation (1-15) indicates that a bubble of  $1\mu$  radius should dissolve in 0.01 sec. It appears that large bubbles will rise out of the liquid and small ones will dissolve.

Nevertheless, there are two experimental facts which lead one to suspect that the cavitation nuclei are stable bubbles containing gas. It is generally known that the strength of a liquid increases when the liquid is degassed; see for example Galloway.<sup>28</sup> In addition, qualitative experiments show that water which is subjected to a pressure of 1000 bars over a period of several minutes will become substantially stronger. The boiling point of such water has been shown to increase by more than 100°K.<sup>29,30</sup> In addition, Harvey<sup>31</sup> has shown that the static strength of water can be substantially increased by pressurization. These experiments cannot be explained if one assumes that solid particles alone are responsible for the cavitation nuclei.

One hypothesis which has been advanced to explain the apparent stability of gas bubble nuclei is the formation of a single-molecular layer, or skin, on the bubble surface which impedes the diffusion of

- 28. W. I. Galloway, "An Experimental Study of Acoustically Induced Cavitation in Liquids," *J. Acoust. Soc. Am.* 26, 849 (1954).
- 29. D. C. Pease and L. R. Blink, "Cavitation from Solid Surfaces in the Absence of Gas Nuclei," *J. Phys. Colloid. Chem.* 51, 556 (1947).
- 30. E. N. Harvey, Barnes, McElroy, and Whitely, "Removal of Gas Nuclei from Liquids and Surfaces," *J. Am. Chem. Soc.* 67, 156 (1945).
- 31. E. N. Harvey, W. C. McElroy, and A. H. Whitely, "On Cavity Formation in Water," *J. Appl. Phys.* 18, 162 (1947).

gas.<sup>\*</sup>,<sup>32,33</sup> By this hypothesis, cavitation occurs when the skin breaks. The threshold is determined by the breaking strength of the film and the size of the bubbles. A skin of this type might, for example, be a single-molecular layer of fatty acid molecules adsorbed on the bubble surface.

Kurtze,<sup>†</sup> has developed the concept advanced by Harvey<sup>\*\*</sup> that gas bubbles can be stabilized in surface cracks in solids. According to this view, crevices in the surface of a small suspended solid particle are filled with gas, the curvature of the gas-liquid interface being convex to the gas. Fisher<sup>††</sup> has pointed out that extremely large pressures are required to force the liquid to the bottom of such a crack. Even in a liquid with no dissolved gas a bubble in the form of a small vapor cavity will always exist at the bottom of these cracks. The suggestion has been made by Flynn<sup>\*\*\*</sup> that a possible way to remove these stabilized air bubbles is by cavitation itself. The bubble will be drawn out of the crevice during the tension cycle of the acoustic wave and form a cavitation nucleus. Since the very large pressures generated within the contents of the cavity near the end of the collapse phase can

\* F. E. Fox and U. F. Herzfeld, Reference 26, cited on p. 22.

32. M. Strasberg, "Undissolved Air Cavities as Cavitation Nuclei," Cavitation in Hydrodynamics, London, H. M. S. O. 6-1-6-13 (1956).

33. R. B. Lindsay, "Acoustics and the Structure of Liquids," Sci. 120, 409 (1945).

† G. Kurtze, Reference 27, cited on p. 22.

\*\* E. N. Harvey, Reference 31, cited on p. 23.

†† J. C. Fisher, Reference 24, cited on p. 18.

\*\*\* H. G. Flynn, Reference 14, cited on p. 8.

dissolve the gas, it may be possible to destroy the nucleus in this manner. Evidence of this phenomenon is presented in Chapter III.

More recently (1959) Sette<sup>34</sup> and (1962) Sette and Wanderlingh<sup>35</sup> have advanced the hypothesis that cavitation nucleation can result from high energy elementary particles passing through the liquid. This theory has some similarity with Seitz's theory of nucleation in bubble chambers.<sup>36</sup>

According to this theory, cosmic-ray neutrons in the 10 Mev energy range enter the liquid and interact with oxygen atoms. The oxygen atoms are ionized and are given an energy in the 2 or 3 Mev range. These oxygen recoil nuclei are ionizing particles which during their life in the liquid may deposit energy at a rate of the order of a few thousand Mev per cm. It is assumed that the energy deposited in a length equal to the diameter of the resulting vapor cavity must be sufficient to provide the energy of formation of that cavity. It is estimated by Sette that the rate of energy deposit is sufficient to create vapor cavities in the liquid with a radius of about  $5 \times 10^{-5}$  cm. According to Eq.(1-5) this corresponds to a cavitation threshold of 1.2 bars. Sette presents considerable experimental data on the cavitation threshold at 1 Mc/s in distilled water which indicate a threshold of 1.1-1.6 bars peak acoustic pressure.

---

- 34. D. Sette, "Sonic Cavitation and Ionizing Radiation," Proc. III Intern. Congr. Acoust., Stuttgart, 1959, V. I. Elsevier Publ. Amsterdam, 330 (1961).
- 35. D. Sette and F. Wanderlingh, "Nucleation by Cosmic Rays in Ultrasonic Cavitation," Phys. Rev. 125, 409 (1962).
- 36. F. Seitz, "On the Theory of the Bubble Chamber," Phys. Fluids 1, 2 (1958).

In a recent paper, Messino, Sette, and Wanderlingh<sup>37</sup> have reported that the cavitation threshold can be materially lowered by dissolving a uranium salt in water. A 5%-by-weight solution of uranyl nitrate in distilled water was examined for its cavitation threshold in the apparatus described in previous papers by these authors. The threshold was found to be lowered from 1.6 bars to 0.55 bars. This effect was explained on the assumption that large cavitation nuclei are created by U<sup>235</sup> fission fragments which have larger mass and higher specific ionizing power than oxygen nuclei. The fission is assumed to be induced by cosmic neutrons by the same mechanism which creates the oxygen recoil nuclei.

Lieberman<sup>38</sup> demonstrated that the cavitation threshold could be lowered by exposing the liquid to an artificial source of high energy particles. The cavitation was produced in pentane and acetone in his experiments, and the neutrons from his source had energies of about 4 Mev.

#### Theories Which Do Not Consider Nuclei

It is rather widely accepted that some sort of nucleus is necessary to explain the low experimental values of the cavitation threshold in liquids. Several theories which have been proposed do not consider a

---

37. D. Messino, D. Sette, and F. Wanderlingh, "Effects of Uranium Salts on Sound Cavitation in Water," J. Acoust. Soc. Am. 35, 926 (1963).
38. D. Lieberman, "Radiation-Induced Cavitation," Phys. Fluids 2, 466 (1959).

nucleus of any type. These theories have been reviewed by Blake,<sup>\*</sup> but a few will be mentioned here to indicate the relative lack of success of this approach.

A second-order approximation to the equation of state for fluids which takes into account deviations from ideal behavior is the van der Waal's equation:  $(p + a/V^2)(V - b) = RT$ . The term  $a/V^2$ , where  $V$  is the molal volume, represents the effect of intermolecular attractive forces. This term has been called the intrinsic pressure. One theory proposes that this pressure should be the theoretical tensile strength of the liquid. The intrinsic pressure can be calculated from critical-point data for water, and it is found to be nearly 10 000 bars. Temperley<sup>39</sup> has argued that the theoretical strength is not the intrinsic pressure, but the pressure at the position of the minima of the van der Waal's isotherms,  $(\frac{\partial P}{\partial V})_T = 0$ . At room temperature this gives a value of about 900 bars for water.

Briggs, Johnson, and Mason<sup>40</sup> have proposed a theory based on Eyring's theory of viscosity, plasticity, and diffusion.<sup>41</sup> Using this theory the authors derive another expression for computing the intrinsic pressure  $a/V^2$ . Anticipating that the result will be too large, they

\* F. G. Blake, Jr., Reference 23, cited on p. 18.

- 39. H. N. V. Temperley and L. G. Chambers, "The Behavior of Water Under Hydrostatic Tension," Proc. Phys. Soc. (London) 58, Part 1, 420 (1946).
- 40. L. B. Briggs, J. B. Johnson, and W. P. Mason, "Properties of Liquids at High Sound Pressures," J. Acoust. Soc. Am. 19, 664 (1947).
- 41. H. Eyring, "Viscosity, Plasticity, and Diffusion as Examples of Absolute Reaction Rates," J. Chem. Phys. 4, 283 (1936).

introduce a factor beta which is of order 1000 when the applied pressure is negative and of order one when the pressure is positive. Blake<sup>\*</sup> finds no physically plausible basis for the introduction of the beta factor and concludes that the theory should be rejected.

Thorndike<sup>42</sup> has computed the cavitation threshold purely on the basis of energy density considerations. He sets the energy density in a rarefactional half-wavelength of the acoustic field equal to the surface energy per cm<sup>2</sup> of a spherical rupture in the liquid. Aside from the fact that his approach is somewhat phenomenological, it does not even include the ambient hydrostatic pressure. Since both theoretical and experimental evidence indicate that the acoustic pressure should be at least as large as the hydrostatic pressure, this theory cannot be taken seriously.

A theory assuming that coreless irrotational vortex motion is the mechanism responsible for cavitation has been advanced by Dean.<sup>43</sup> Free vortex motion is specified because the pressure P in a free vortex goes to  $-\infty$  as  $1/r^2$  as  $r \rightarrow 0$ . This theory can be rejected because cavitation is often observed in acoustic fields where free vortex motion is nonexistent.

<sup>\*</sup> F. G. Blake, Jr., Reference 23, cited on p. 18.

42. A. M. Thorndike, "Experiments of Cavitation in the Range 10 kc to 50 kc," O. S. R. D. Section C-4, N. D. R. C., Univ. of Cal., San Diego, Pub. Bd. Rept. No. 81495.

43. R. B. Dean, "The Formation of Bubbles," J. Appl. Phys. 15, 446 (1944).

### Experimental Cavitation Thresholds

A great many papers have been devoted to the investigation of the dependence of the threshold of acoustic cavitation on the state of the liquid, the acoustic frequency, the time of irradiation, etc. The measured acoustic amplitudes necessary to initiate "cavitation" have been frequently inconsistent. This circumstance is due to different concepts of what cavitation is, different procedures used by different experimenters, and to the fact that the exact state of the liquid has not always been carefully controlled. It should be noted that such control is generally very difficult to accomplish in practice.

Acoustic cavitation thresholds have been measured at several different frequencies in the range extending from 20 kc/s to 3 Mc/s. In the usual case, cavitation thresholds were measured at a single frequency. Only in a paper by Esche<sup>44</sup> was an effort made to measure experimentally the frequency dependence of the threshold of acoustic cavitation. In this work, nine different experimental arrangements were utilized to determine the threshold at nine different frequencies from dc to 3.3 Mc/s. The water was described as distilled, filtered, and de-aerated. The experimental apparatus used by Esche is listed in Table I.

The results of Esche's experiment along with those of several others are plotted in Fig. 1. A similar presentation of cavitation

---

<sup>44</sup>. K. Esche, "Untersuchung der Schwingungskavitation in Flüssigkeiten," Akust. Beihefte 4, 208 (1952).

TABLE I  
The experimental apparatus used by Esche

Frequency c/s	Method of excitation	Sound field	Position of pressure maximum	Method of observation	Determination of pressure
0	static	—	surface of glass tube	optical	barometer
$10^2$	electro- magnetic	radial resonance of a cylindrical volume of fluid	free liquid	oscillation amplitude	—
$1.5 \times 10^3$	—	—	surface of aluminum container	acoustical and optical	hydrophone
$3 \times 10^3$	—	—	—	—	—
$1.5 \times 10^4$	magneto- strictive	focused progressive waves	—	acoustical	calculated from radiated power and focal diameter as determined by a hydrophone
$1.75 \times 10^5$	—	—	—	—	—
$3.65 \times 10^5$	—	—	—	—	—
$5 \times 10^5$	piezo- electric	—	—	acoustical and optical	focal diameter determined by Schlieren optics
$3.3 \times 10^6$	—	—	—	—	—

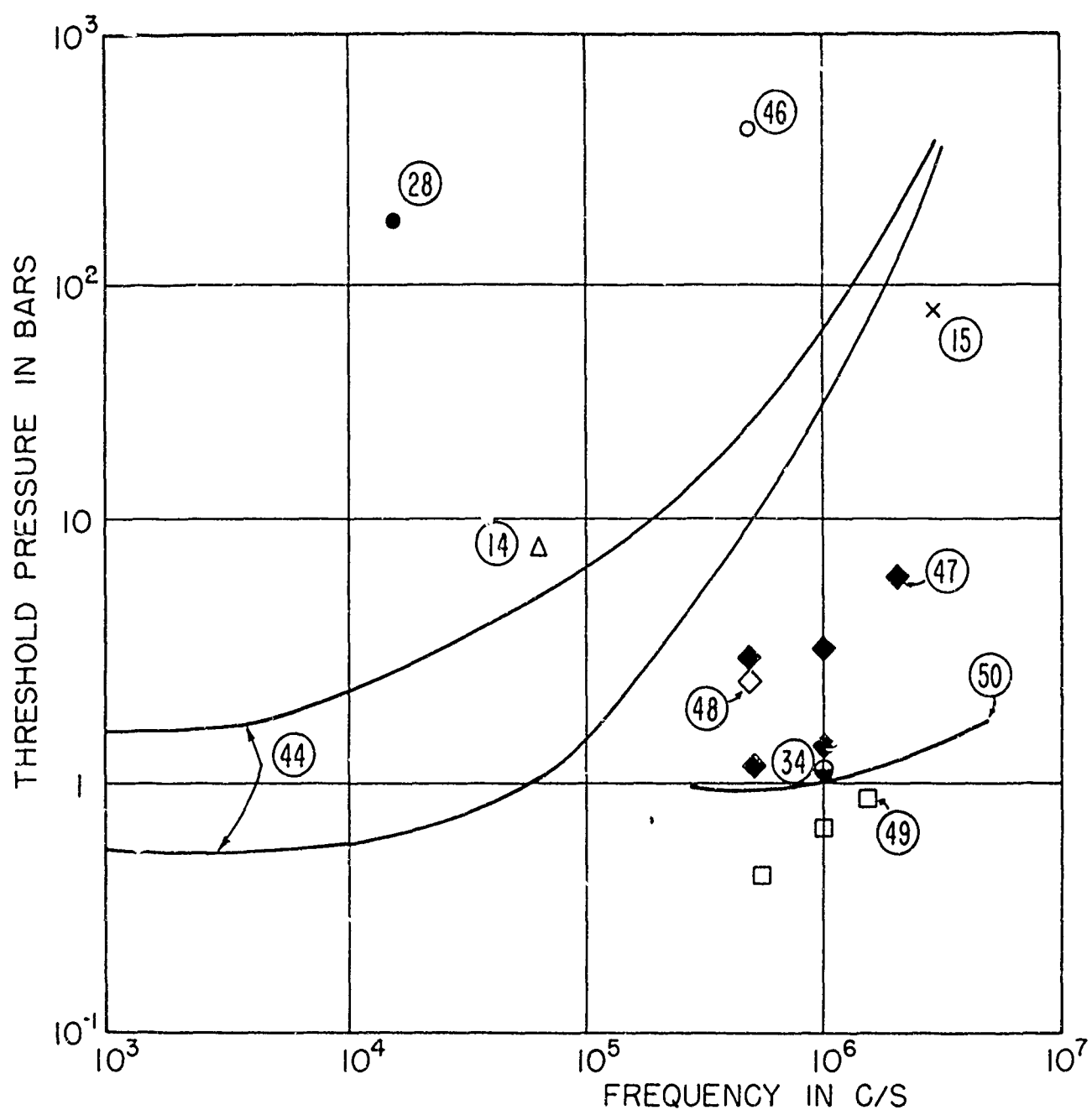


FIGURE 1

EXPERIMENTAL CAVITATION THRESHOLDS

(1) INDICATES REFERENCE SOURCE

threshold data has been given by Sirotyuk.<sup>45</sup> The solid lines are the upper and lower limits of Esche's data. The source of these data is denoted by the reference number located near each point on the figure. In each case except Sette's, the water was degassed apparently to the limits attainable by the experimenters. The disparity in the experimental results is plainly evident.

There are several important factors which were not considered by Esche. It is quite likely that the critical nuclei for acoustic cavitation are small bubbles of gas stabilized in the liquid, but no special means were provided in Esche's experiment for monitoring the gas content of the liquid under examination. This deficiency is enhanced by the fact that a different sample of liquid was used to obtain each point on the frequency curve. The same problem existed with respect to solid particle contamination. Perhaps a more serious problem was the fact that the time which each element of liquid remained in the region of maximum pressure depended on the apparatus. At the two lowest frequencies, standing waves were used, and an element of liquid subjected to the maximum pressure was likely to remain in that position for the duration of the measurement. At the higher frequencies, however, focused progressive acoustic waves were used, and the streaming through the focal region due to radiation pressure would have caused a given element of liquid to be subjected to the maximum pressure for a relatively short duration.

---

45. M. G. Sirotyuk, "Ultrasonic Cavitation," Soviet Phys. - Acoustics 8, 201 (1963).

Proof that the threshold is influenced by the length of time an element of liquid remains in a region of high pressure was presented by Willard.<sup>51</sup> In his experiment cavitation could not be produced in water even with an intensity of  $15 \text{ kW/cm}^2$  at 5 Mc/s in a focused progressive acoustic wave field. Streaming through the focus was estimated to be as high as 10 m/sec. When a reflector was introduced on the opposite side of the focus from the projector, however, so as to form a standing-wave field, cavitation was detected at  $4 \text{ kW/cm}^2$ . In addition, direct evidence of the dependence of the strength of liquids on the irradiation time has been reported by several authors. Esche himself showed an increase in the cavitation threshold with decreased irradiation time. These measurements, of course, were made with the same apparatus previously described, and are evidently distorted due to streaming through the focus. Similar results have been reported by Lange<sup>52</sup> and by Briggs, Johnson, and Mason.\*

The effect of the viscosity of the liquid on its cavitation threshold has been determined by several authors. Connolly and Fox<sup>53</sup> varied the temperature of water with various dissolved air contents, assuming that the primary factor affected by the temperature change was the viscosity. They found very little dependence, the cavitation threshold

---

51. G. W. Willard, "Focusing Ultrasonic Radiators," *J. Acoust. Soc. Am.* 21, 360 (1949).
52. Th. Lange, "Methoden zur Untersuchung der Schwingungskavitation in Flüssigkeiten mit Ultraschall," *Akust. Beihefte* 2, 75 (1952).
- \* L. B. Briggs, J. B. Johnson, and W. P. Mason, Reference 40, cited on p. 27.
53. W. Connolly and F. E. Fox, "Ultrasonic Cavitation Thresholds in Water," *J. Acoust. Soc. Am.* 26, 843 (1954).

changing only a few percent over a temperature range of 5° to 45°C.

Briggs, Johnson, and Mason<sup>\*</sup> measured cavitation thresholds with liquids of various viscosities. Their results show a change in the cavitation threshold by a factor of less than three over a range of viscosities from 0.007 poise to 8.0 poise, the threshold increasing with increased viscosity. On the basis of these data, it appears that the viscosity of the liquid is not a very significant parameter with respect to the cavitation threshold.

The effect of hydrostatic pressure on the cavitation threshold has been carefully measured by Galloway.<sup>†</sup> He found that the threshold was directly proportional to the hydrostatic pressure for liquids that were air-saturated. The cavitation threshold was 1 bar peak acoustic pressure at 1 bar hydrostatic pressure. Galloway has further proposed that this experimental fact be used to calibrate hydrophones. The voltage developed by the hydrophone when the air-saturated water in which it is immersed begins to cavitate is taken as the sensitivity in volts per bar.<sup>54</sup> The description of cavitation given by Galloway fits the definition of a transient cavity. One must evidently be careful in this calibration procedure to distinguish between the cavities formed by rectified diffusion and the transient-cavity collapse.

---

\* L. B. Briggs, J. B. Johnson, and W. P. Mason, Reference 40, cited on p. 27.

† W. I. Galloway, Reference 28, cited on p. 23.

54 "W. I. Galloway, A Simple Calibration Technique for Low-Sensitivity Transducers," J. Acoust. Soc. Am. 25, 1127 (1953).

Galloway has also measured the pressure dependence of the cavitation threshold on hydrostatic pressure for water that is in several stages of degassing. With water that is undersaturated with dissolved air, he finds that the cavitation threshold is independent of the hydrostatic pressure from 1 bar down to 0.05 bar.

The dependence of the cavitation threshold on the state of the liquid has been dealt with by several authors, but this information is almost completely devoted to the gas content of the liquid and no specific information is given about the solid-particle contamination. This is unfortunate in view of the possibility of explaining the cavitation threshold on the basis of solid particles which are not wetted by the liquid. It is often assumed that because the liquid is distilled solid particles cannot be present, but anyone who has dealt with the problem of purifying water knows that this is not true.

The most complete information about the threshold of cavitation as a function of the amount of dissolved gas is given by Galloway.\* His experiments were carried out at 26.3 kc/s in a 12-liter spherical glass boiling flask. The sphere was excited in the seventh radial mode by a resonant magnetostriction transducer. Cavitation events were detected either by a probe hydrophone located at the second pressure maximum, or visually. The two methods were reported to give equivalent results. The threshold was defined as that pressure necessary to create one cavitation event per second.

---

\* W. I. Galloway, Reference 28, cited on p. 23.

The spherical resonator containing the liquid sample was connected to another glass sphere which could be evacuated. The degassing was accomplished by connecting the two spheres with the latter evacuated while simultaneously cavitating the liquid. The amount of dissolved gas could be calculated at any stage by measuring the partial pressure of the air in equilibrium over the liquid, and by applying Henry's law.

The test liquids were distilled water, benzene, synthetic sea water, and an aqueous solution of dioxane. The cavitation threshold was found to depend on the amount of dissolved gas. The data are given in Fig. 2: Curve 1 is for water and Curve 2 is for benzene. The cavitation threshold of the liquid at 22°C at atmospheric pressure is given on the ordinate. The abscissa represents the following quantities: The top scale represents the air concentration in mols per liter of water; the bottom scale represents the equilibrium pressure of the air above the liquid. The results show that the threshold increases linearly down to an equilibrium air-saturation pressure of about 10 mm Hg, where it tends to a limit of about 200 bars for water and 140 bars for benzene. The figure for water was the limiting pressure available for Galloway's apparatus, and is the highest reported value available for such a relatively low frequency. This is the point plotted in Fig. 1 that is credited to Galloway.

The work of Connolly and Fox\* gives another insight into the effect of the degree of saturation of the liquid on its cavitation threshold. In these experiments the threshold of tap water was measured

---

\* W. Connolly and F. E. Fox, Reference 53, cited on p. 32.

at a frequency of 1 Mc/s. The water was first saturated with air at 30°C and then cooled by steps to 0°C rapidly enough so the total amount of air in the sample changed negligibly by diffusion. The cavitation threshold was measured at five temperatures intermediate to the limiting temperatures. Since the gas solubility increases with decreasing temperature, the percentage of saturation decreased as the temperature decreased. The cavitation threshold was found to increase from about 2 bars at 30°C to about 4.5 bars at 0°C. Whereas in Galloway's experiment\* the degree of saturation of the water was altered by the elimination of air from the liquid, the degree of saturation in this experiment was altered by changing the temperature. The change in the cavitation threshold as a function of the liquid saturation can be compared for the two experiments. It is found that the temperature decrease has slightly more effect than the removal of gas,

#### Statement of the Problem

On the basis of this brief look at the history of acoustic cavitation theories and experiments, several problems emerge. In addition, the pertinent variables which must be controlled and the degree to which they should be controlled become apparent. We hope that much of the existing cavitation threshold data that are seemingly at variance can be codified by paying careful attention to the more important variables.

---

\* W. I. Galloway, Reference 28, cited on p. 23.

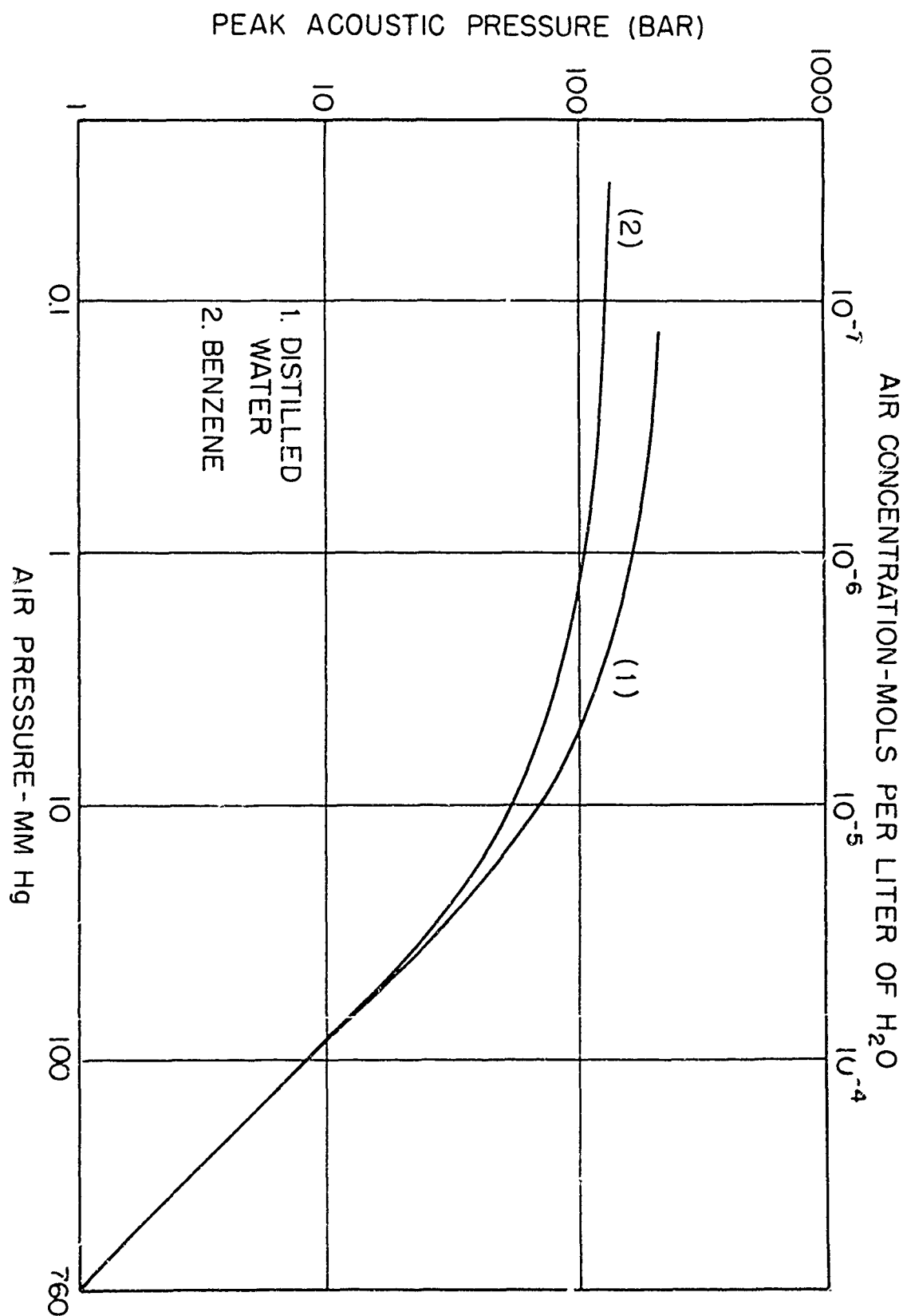


FIGURE 2  
CAVITATION THRESHOLDS (FROM GALLOWAY, REF. 28)

The main topic of investigation is the frequency dependence of the threshold of acoustic cavitation. It is impossible to make a statement about the importance of frequency on the cavitation threshold on the basis of the data in Fig. 1.

The most important factor in the uncertainty of the existing data is the lack of control over the state of the liquid under test. Only in a few cases are quantitative figures given about the state of the liquid, and consequently it has not been possible for different experimenters to repeat experimental conditions. The two most relevant factors which must be determined to define the condition of the test liquid appear to be the gas content and the solid-particle contamination. The first of these two has been excellently controlled by a few authors, as has been mentioned; the latter, however, has been almost universally ignored. In our own experiments we intend to establish experimental conditions so that these parameters can be quantitatively determined. In addition, control over the hydrostatic pressure and temperature of the liquid will be maintained.

Another factor which undoubtedly contributes to the disparity among the various published results is the geometry of the acoustic field. Published values of cavitation thresholds have been obtained by the use of plane progressive waves, focused progressive waves, and plane and focused standing waves. In addition, cavitation has been obtained at or near solid boundaries as well as in the volume of the fluid itself. In this work we intend to produce the cavitation in a focused standing-wave field in the volume of the liquid well removed from solid boundaries.

The liquid sample as well as the geometry of the acoustic field in the sample will be the same at all frequencies of observation.

We shall also seek to avoid confusion by adopting a consistent operational definition of what a cavitation threshold is. It has been seen that the physical manifestation of cavitation differs over the range of possible experimental conditions. Noltingk\* suggests, "The satisfactory way of establishing a threshold is by making quantitative measurements over a range of acoustic intensities; qualitative estimates whether or not an effect occurs are really only justified when that effect never occurs in a small way." This advice has not always been followed by the experimenters who have been concerned with cavitation thresholds.

A final point concerns the manner in which the magnitude of the acoustic field is measured and expressed. The information of interest in a cavitation threshold measurement is the peak acoustic pressure. Many authors have chosen instead to quote their results in terms of the acoustic intensity which obtains at the threshold of cavitation. The intensity is calculated from the geometrical focusing properties of the wave system and the measured power input to the system. Some authors have measured pressure directly and then converted to intensity by assuming that the usual plane wave acoustic impedance holds in their experiment. This procedure is not only indirect, but subject to error for two reasons. First, the cavitation region is often at a focal point and the plane wave acoustic impedance is not appropriate. Second, the

---

\* B. E. Noltingk, Reference 6, cited on p. 3.

liquid, and particularly a gassy liquid, becomes generally filled with minute air bubbles near the cavitation threshold and the characteristic specific acoustic impedance of the medium will be changed. For these reasons, we shall always measure and report our cavitation thresholds as a function of peak acoustic pressure.

## Chapter II

## EXPERIMENTAL APPARATUS

The specifications for the experimental apparatus were drawn up in Chapter I. The requirements as set forth are best realized by a standing-wave acoustic system. Specifically, the radially symmetric resonant modes of a spherical volume of water are employed. This configuration offers many advantages over other possible acoustic systems. The focus of the system is always at the center of the sphere for any of the radially symmetric modes, and the pressure at the focus is 17 dB higher than the pressure at the second pressure maximum. The pressure distribution is symmetric about the center so there can be no acoustic streaming anywhere in the spherical system. The boundary conditions for a radially symmetric standing wave are simple, e.g., uniform velocity over the external surface. This situation makes radially symmetric standing waves relatively easy to establish.

It is useful to examine the concept of a radially symmetric standing wave. In general, a uniformly distributed acoustic pressure must be applied to the external surface of the spherical volume of liquid to maintain the standing wave. If the liquid in which the standing wave is established is lossless, it is not necessary to add power to the system to maintain the wave motion. The pressure and the velocity at any radius in the sphere will be in quadrature. The magnitude of the pressure that must be applied to the external surface is found to be zero at a set of frequencies called the resonance frequencies.

43

If a thin elastic shell is placed around the volume of the liquid the pressure will not be zero at the boundary of the liquid because a certain pressure is required to expand the shell. The pressure that must be applied to maintain the standing waves is found to be zero on the external surface of the shell at a new set of resonance frequencies. The resonance frequencies of a spherical volume of liquid surrounded by a thin elastic shell are computed in Appendix A.

A system composed of water enclosed by a thin glass shell is almost, but not quite, lossless. Power must be continuously added to the system through the external surface of the shell. A small pressure that is in phase with the velocity is applied at the glass surface. This pressure must be of uniform amplitude and phase over the external surface if the standing wave is to be truly radially symmetric. The magnitude of this pressure can be estimated from the Q of the resonant modes. The Q's of the modes were measured and found to be approximately 5000. The magnitude of the pressure distributed uniformly over the external surface of the sphere will be about  $10^3 \mu$  bars for a 10-bar focal pressure (see Eq. (B-5) of Appendix B).

If the external surface of the sphere is not driven at every point, but only over a total surface area A, the pressure applied over the surface A must be increased by a factor equal to the ratio of the total external surface area to the area A. This assumes that the disturbing effect of the transducers is not great enough to alter the uniform velocity distribution by a significant amount.

As A is decreased, there must be some point at which the pressure applied over this area becomes large enough to distort the velocity at the surface of the sphere in the region of the transducer. It is intuitively obvious that the area A should be divided into equal fractional areas which are distributed uniformly over the external surface of the sphere to minimize the effect of the distortion.

At least two experimenters have used radially symmetric standing-wave modes in water as a means of producing cavitation in the water. Galloway\* operated at the sixth radially symmetric resonant mode in a 12-liter spherical glass flask. This mode was excited by a single magnetostriction transducer attached to the surface of the glass shell. There was no mention of any difficulty encountered with this type of excitation. An almost identical apparatus was used by Lieberman.<sup>†</sup> Lieberman extended the use of his apparatus to include the fifth and seventh modes as well as the sixth. He reports extreme difficulty in establishing undistorted modes. By adjusting the water level at the top of the sphere he was able to achieve good results at one mode, but further adjustment was necessary when the frequency was switched to another mode.

In an attempt to resolve this difficulty, a two-liter flask was fitted with a single piezoelectric driver of a type to be discussed shortly. The spatial pressure distribution in the water was measured with a probe hydrophone. It was found that undistorted radial modes

---

\* W. I. Galloway, Reference 13, cited on p. 23.

† D. Lieberman, Reference 38, cited on p. 26.

25

could not be excited with one driver located on the external surface of the sphere without adjusting the height of the water in the neck of the flask for each mode. In addition, no amount of adjustment would enable an undistorted mode to be excited above the tenth mode.

There are two cogent reasons for keeping the distortion of the resonant standing wave to a minimum. Any distortion will decrease the acoustic pressure at the focus of the system; but very little less in the focusing properties of the spherical standing wave can be tolerated because of the extremely high acoustic pressure required for cavitation. In the second place, the distortion of the standing wave can shift the position of the focus; yet it is absolutely necessary to know where the pressure maximum is located so that the pressure at that point can be measured.

The distortion would be zero if the entire external surface could be covered with one continuous transducer, but this construction would be difficult, to say the least. It was decided to try a spherical array of transducers to determine if a necessary condition for establishing undistorted modes might be satisfied by using a discrete number of transducers.

At the outset, an array of twelve uniformly spaced transducers was cemented to the external surface of a two-liter flask. Each transducer had a circular face with a diameter of 1.5 inches. The transducers were located at the points of tangency between the spherical surface and a circumscribed pentagonal dodecahedron. Probing of the spatial pressure distribution revealed that undistorted radial modes were established

from the third through the 120th. With the pressure probe located at the focus, the pressure response for a radial mode was always at least 10 dB higher than for any non-radially symmetric mode with an adjacent mode frequency. Most important of all, the distortion of the radial modes was not appreciable for any height of water in the neck of the flask.

During the early part of the experiments this resonator was broken. A replacement was constructed with eight transducers located at the points of contact between the spherical surface and an inscribed cube. The differences in the performance of these two resonators will be discussed in the section Performance of the Resonator. A photograph of the entire experimental apparatus is included as Fig. 3. The spherical resonator with its transducers is shown in the photograph of the experimental apparatus in Fig. 4. A schematic diagram of the entire apparatus is given in Fig. 5. The remainder of this chapter is devoted to a description of this equipment.

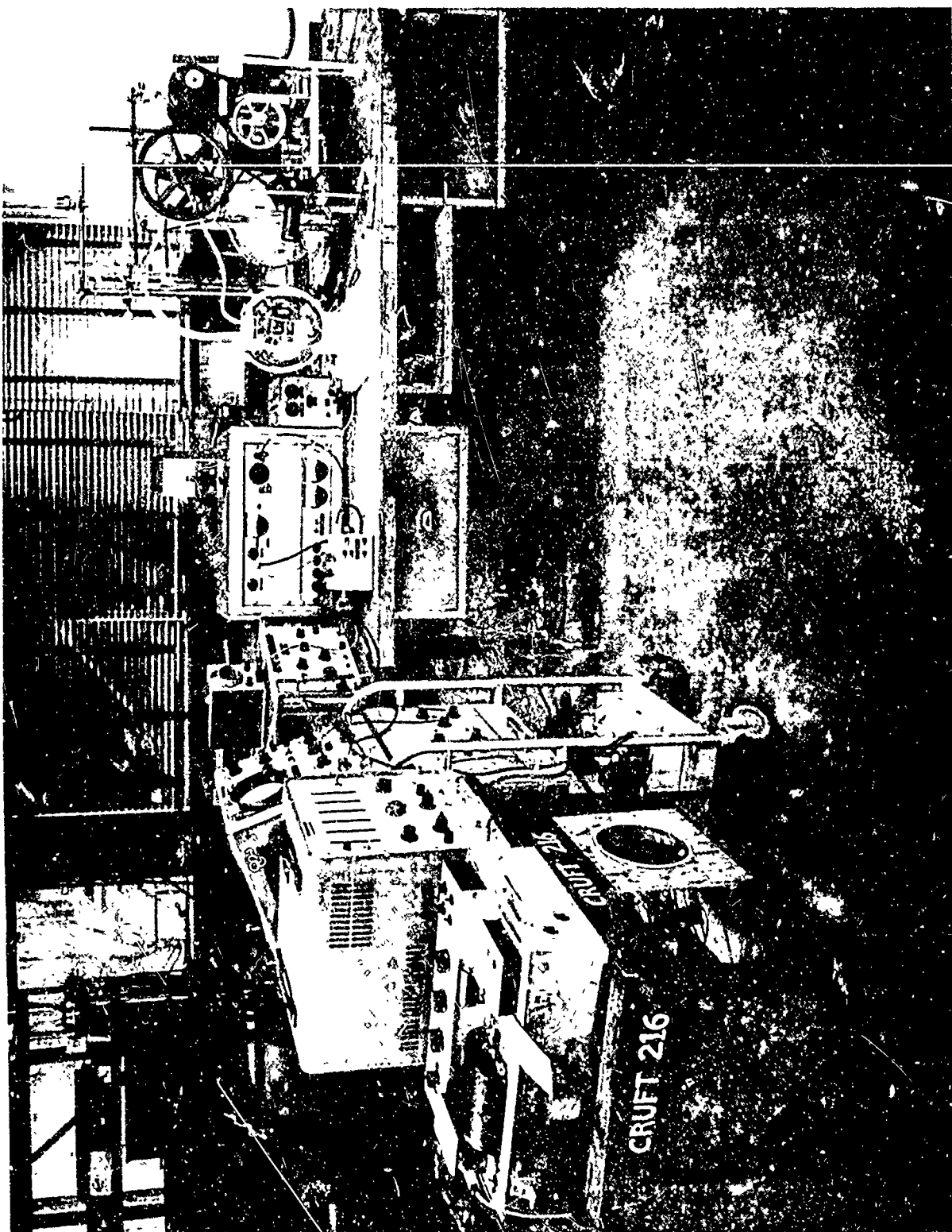
#### The Resonator

The presence of the glass shell surrounding the water affects both the modal frequencies and the radial surface velocity that must be supplied at a resonance frequency to establish a given acoustic pressure at the focus. It is necessary to know both of these quantities for all the modes in order that proper transducers can be designed for the purpose of exciting the radial modes. These calculations are carried out in Appendix A.

The size of the glass shell is determined by the frequencies of operation and by the driving velocities available. The sphere is one

AD 600 420

FIG. 3 PHOTOGRAPH OF THE EXPERIMENTAL APPARATUS



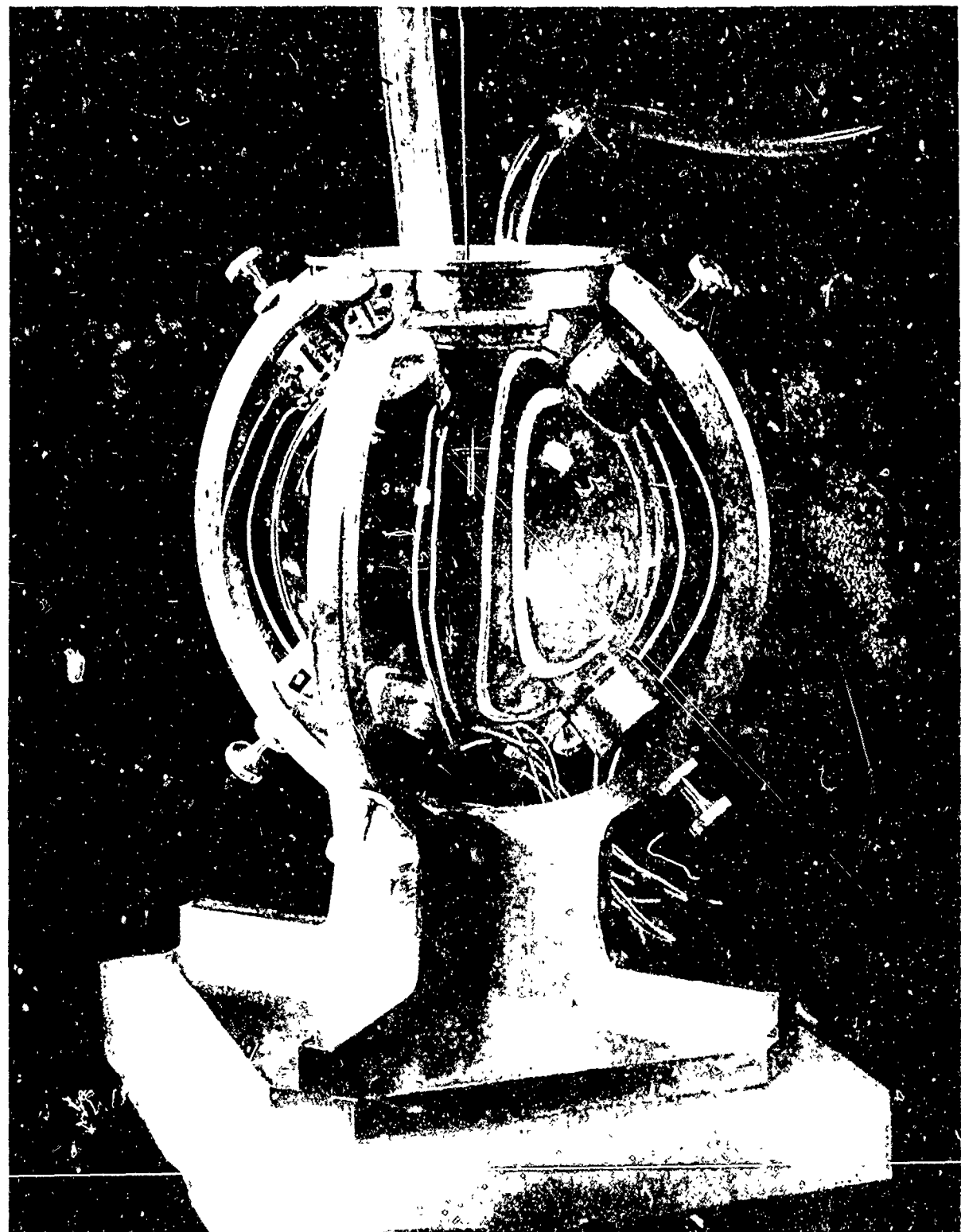
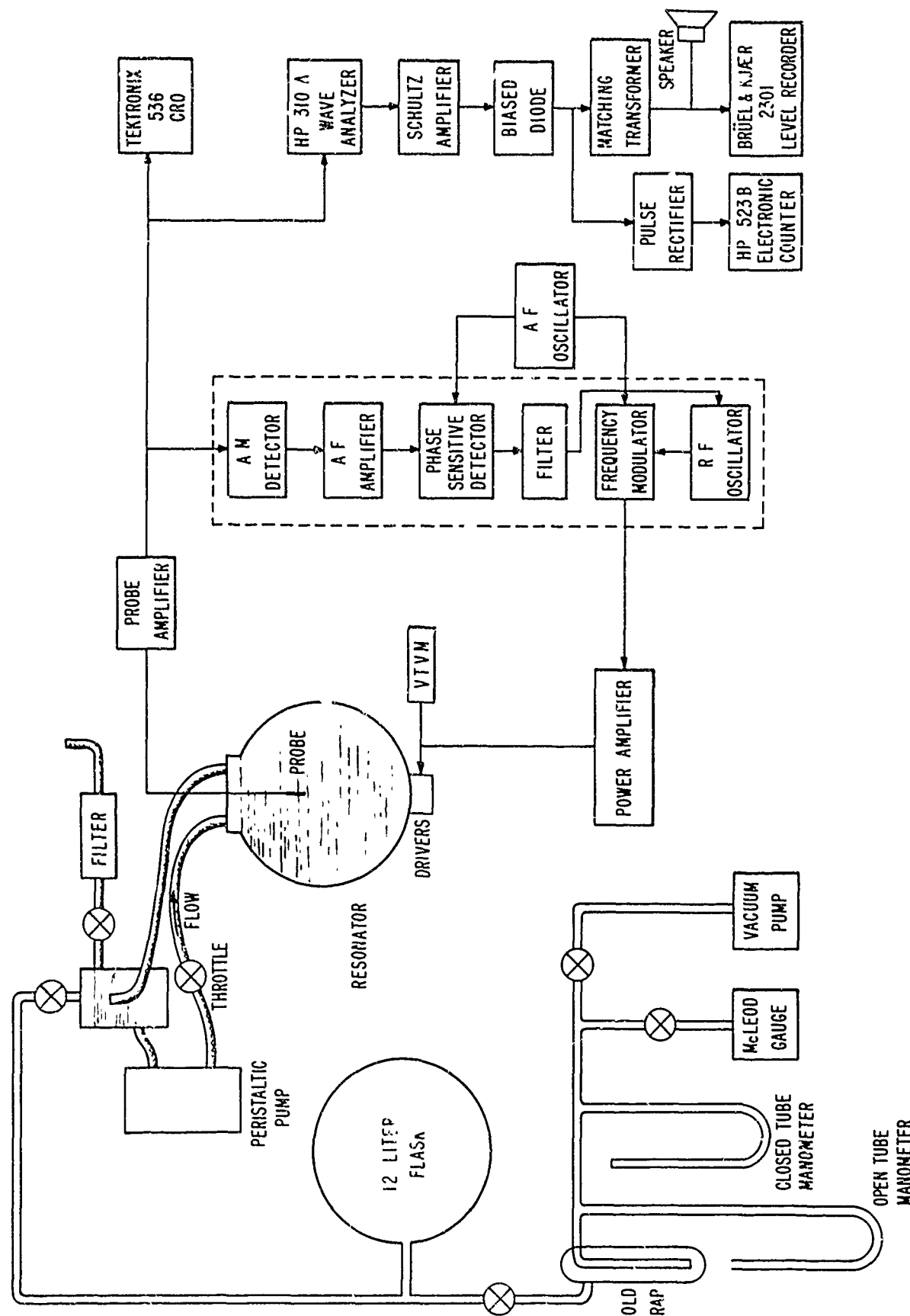


FIG. 4 PHOTOGRAPH OF THE SPHERICAL RESONATOR  
AND DRIVER TRANSDUCERS



SCHEMATIC DIAGRAM OF THE EXPERIMENTAL APPARATUS

FIGURE 5

wavelength in diameter at the lowest radially symmetric resonance frequency. This is not the only consideration, however. It is shown in Appendix A that the velocity at the external surface of the sphere at a modal frequency is inversely proportional to the radius for a given pressure at the focal point. On the basis of the transducer calculations in Appendix B it was decided that at frequencies of approximately 20 kc/s, and for a maximum variational pressure of 10 bars at the focus, the radius of the sphere would be about 10 cm. A two-liter sphere has a radius of 7.8 cm. The resonance frequency of the third radially symmetric mode of a two-liter sphere is about 27 kc/s. The choice of the two-liter sphere limits the acoustic pressure at the focus to about 10 bars at 27 kc/s. If a larger sphere had been used, greater pressures at the focus would be possible at 27 kc/s, but then difficulties at the high end of the frequency scale appear. It was desired to obtain acoustic pressures of the order 200 bars at 1 Mc/s. With a 200-bar peak pressure at the focus, the average peak pressure throughout the volume of the sphere will be about 40 bars. Calculations show that a plane acoustic wave of this amplitude would form a shock wave in about 50 wavelengths. The two-liter sphere is large enough so there will be 50 wavelengths from the surface to the center at 1 Mc/s. For this reason, the two-liter sphere was judged to be the largest acceptable size.

A standard two-liter pyrex round-bottom boiling flask was used because of the chemical resistance of glass to water, visibility, and the low mechanical losses in glass. If the spherical shell is to be suitable for operation at 1 Mc/s, its radius should be uniform within

less than one quarter wavelength at this frequency. For water this is 0.38 mm. Several flasks were examined, and at least one was found for which this tolerance was just met.

The neck of the flask was removed just above the point where it meets the spherical surface. This cut was ground plane and perpendicular to the line through the center of the neck and the center of the sphere. A lucite cap was fabricated to fit on this joint and attached permanently by an epoxy.\* The lucite cap was fitted with threads and an "O" ring seat. A lucite top was screwed into the cap which made an airtight seal against the "O" ring.

In the center of the top, a hole and threaded packing gland were made to accept the 1/16 inch diameter shaft of the probe hydrophone. A 1/16 inch "O" ring around the probe shaft is compressed by a brass gland nut to form an airtight seal which allows vertical motion and some lateral motion of the probe hydrophone. On opposite sides of the hydrophone packing gland two lucite nipples screwed into the top allow for the connection of Tygon tubing through which the water is circulated.

#### The Transducers

The transducers must be capable of producing large velocities at the external surface of the resonator. The frequency range of operation extends from 27 kc/s to 1 Mc/s, or more than 5 octaves. The coupling coefficients of piezoelectric ceramics are constant over this frequency

---

\* Emerson and Cuming, Inc.; Eccobond 45.

range and the mechanical losses are small. For these reasons piezoelectric ceramics are good electromechanical transducers for this application.

On the basis of the calculations in Appendix A it was discovered that a ceramic thin enough to be below self-resonance over this frequency range could not produce the velocities that are required to drive the resonator to sufficient pressure amplitudes. The transducer velocities could be increased by operating the transducer at a self-resonance at each frequency at which the cavitation is to be produced.

The first model of a multiresonant transducer which was tested consisted of a half-wave bar of ceramic tuned to the lowest frequency, 27 kc/s. According to theory, it should be possible to excite this bar at all of its higher odd-order modes. Such a bar was tested to see if this was practical. Motional admittance circles were measured at the fundamental mode and the first five higher-order modes. The electro-mechanical coupling coefficients of the bar transducer were found to be 0.510, 0.499, and 0.486 at the fundamental mode of vibration and at the first two odd-order modes, respectively. The coupling coefficients of the bar at the first two even-order modes were 0.084 and 0.080, respectively. The equivalent series mechanical resistances of the odd-order modes, beginning with the fundamental mode, were 9.6, 54.3, and 256 dyne-sec/cm. The mechanical resistances increase approximately as the square of the mode number. Thus 25 times more power input is required at the second odd-order resonance frequency, which is the fifth resonance of the bar, than is required at the fundamental frequency to produce a given velocity.

It might be expected that the increase of the losses with increasing mode number is due to the mechanical losses in the piezoelectric ceramic. If a low-loss material such as brass were used to make up the majority of the transducer with just sufficient piezoelectric material to excite the modes of the composite structure, these losses could be minimized. In the design of the conventional "sandwich" transducer the piezoelectric material is usually placed in the center of the composite bar, which is operated at half-wave resonance. It is not possible to excite the even order modes of such a bar, but both even- and odd-order modes can be excited if the piezoelectric ceramic is placed at the end of the bar.

The analysis of such a composite transducer is carried out in Appendix B. The considerations which led to the final dimensions are also given there. The results specify a 0.1 inch thick piezoelectric ceramic disk and a 0.70 inch long brass cylinder. The diameter of each element is 1.5 inch. The resulting composite transducer has a fundamental frequency of about 82 kc/s. The ceramic element itself is resonant at about 1.2 Mc/s, placing an upper limit on the useful frequency range of the transducer.

Up to this point the transducers and the resonator have been treated as separate systems. A consideration of the composite system is simplified by two facts. In the first place the two systems are not closely coupled. The velocity of only 12% of the external surface of the resonator is constrained to be equal to the transducer velocity. The velocity over the free surface of the resonator will be higher than

CII

the transducer velocity at frequencies where the impedance at the interface between the transducers and the resonator is different from zero. In the second place the dissipation in the transducers can be expected to be much greater than the dissipation in the resonator. The dissipation in the transducers is due to the losses in the ceramic, the losses that occur in the cemented joints, and the losses in the transducer mountings.

The energy stored in the resonator modes can be expected to be larger than the energy stored in the transducer modes because of the larger volume and acoustic pressure of the former standing-wave system. Since the power dissipated in the resonator can be expected to be much less than the power dissipated in the transducers, the Q's of the resonator modes will be much larger than the Q's of the transducer modes. This observation is confirmed by measurements of the completed system. The resonator Q's are larger by a factor which ranges from 50 to 500.

The resonance frequencies of neither system will be altered very much when they are considered as a composite system because of the weak coupling between them. The amplification of the transducer velocity will occur over relatively broad bands of frequencies centered at the transducer resonance frequencies. Several resonator modes will occur within the bandwidth of a transducer mode. The transducers will deliver an essentially constant velocity to the resonator over the bandwidth of the resonator mode because of the disparity of the Q's. The resonator modes occurring within the bandwidths of the transducer modes will be characterized by higher focal pressures in the resonator than could be achieved by a non-resonant piezoelectric ceramic transducer.

The ceramic elements for the transducers are PZT-4 disks, 0.1 inch thick and 1.5 inch in diameter.\* The backing metal is brass. A thin brass shim 1.5 inch in diameter is ground to match the curvature of the glass flask and is fitted between the transducer and the glass wall. Several different methods of cementing the brass shim and backing cylinder to the ceramic were tried. It is necessary to make electrical contact to the silvered surfaces of the ceramic disk through the cemented joint. Even a thin layer of cement between the electrode of the ceramic and the brass pieces will be too much, because the dielectric constant of the ceramic is about 1200, whereas that of most cements is about 5.

Originally a conductive silver-filled epoxy was used to cement the transducers together.<sup>†</sup> These bonds were satisfactory electrically, but they seemed to fail in fatigue. Eastman 910<sup>\*\*</sup> was finally employed. This cement has a very low viscosity, and it sets under the action of shear strain, there being no solvents to evaporate. The surfaces of the brass pieces were first roughened with coarse emery paper. Then a smooth layer of cement was applied to the brass surfaces, taking care that there were no air bubbles in the cement. The three pieces were placed side by side in the correct order on a "V" block. A 1.5 inch diameter brass cylinder about 1 inch long with a convex end whose radius of curvature matched the radius of curvature of the shim was placed in the V next to the shim with the curved surfaces adjacent. The "v" block was positioned

---

\* Clevite Corp., Electronic Components Div., part no. 24100-4

† Emerson and Cuming, Inc.; Eccobond 56C.

\*\* Distributors, Armstrong Cork, Inc.

SC

just below the jaws of a large vise so the components of the transducer were between the jaws. The vise was closed on the components of the transducer as rapidly and as hard as possible, immediately forcing out most of the cement from the joints. The accompanying high rate of shear strain in the cement caused it to set almost instantaneously. The high spots on the rough surface of the brass pieces are in electrical contact with the silvered electrodes on the surface of the ceramic.

The assembled transducers were tested by measuring their input impedance at the fundamental resonance frequency of 82 kc/s. The input impedance of the ceramic element alone would have been  $480 \Omega$  capacitive reactance. Only those transducers whose input impedance at resonance was  $50 \Omega$  or lower were accepted. If a transducer had a higher input impedance than  $50 \Omega$  it was broken apart by applying an 800 V rms (higher than applied during the experimental measurements) signal at 50 kc/s. This caused some carbonization of the cement and made it possible to remove the brass pieces from the ceramic with a sharp blow in a direction across the joint. The surfaces were cleaned and the transducer was recemented. None of the transducer joints made in this way failed during the course of these experiments.

Each transducer was lapped to the glass flask with Carborundum (240 mesh) and water at the point where it was to fit on the glass surface. A miscalculation was made while laying out these points, resulting in the upper and lower sets of four transducers being farther apart than anticipated. The error did not seem to be seriously detrimental to the operation of the resonator, however.

The transducers are held in an aluminum frame, which can be seen in Fig. 4. The transducers are attached to the glass by a thin film of Dow Corning silicone stopcock grease, care having been taken to assure that no air bubbles were left trapped in the grease. The brass backing piece of each transducer is drilled at its center to half its thickness from the back. A 1/8 inch thick Corprenex<sup>\*</sup> plug is inserted at the bottom of this hole. A formica dowel fits into the hole and against the Corprenex plug. The other end of the dowel is held firmly in the end of an adjusting screw that is threaded into the aluminum frame. The adjusting screws are tightened slightly against the Corprenex pads to insure a constant compression across the greased joints between the brass shims and the glass surface. The adjusting crews are secured with locknuts.

The eight transducers are wired electrically in parallel. The inner brass shim is the ground connection on each transducer and the brass backing piece is the other electrode. The outer electrodes are insulated from the aluminum frame by the formica dowels.

#### Performance of the Resonator

The performance of the assembled resonator and its drivers is best explained by the tabulation in Table II. The first column is the number assigned to the particular resonance of the composite system used for experimental measurements. The eighth column shows the actual mode number of the resonant system to which this corresponds.

---

\* Trade name of a cork-neoprene mixture manufactured by Armstrong Cork, Inc.

TABLE II  
Resonator performance characteristics

Operational Mode No.	Frequency Calculated (Appendix A)	Frequency Measured	Q	Driving Sensitivity Bar/Volt	Input Impedance Ohms	Power for 100 Bar at Focus Watts	Mode Shape		
							Mode No.	dB re Focal Pressure First Node	Antinode
1	27 050	27 000	1500	0.020	1500	16 000	3	-14	-30
2	45 850	46 000	2000	0.105	1000	900	5	-17	-38
3	81 850	81 900	2992	0.495	250	400	9	-15	-34
4	184 800	184 800	4200	0.930	100	115	20	-13	-30
5	352 500	353 300	6600	1.15	58	131	39	-14	-24
6	691 080	691 000	10 000	2.60	45	33	78	-12	-25
7	—	1 162 000	11 000	8.39	34	4.05	130	-11	-20

The second column represents the predicted resonance frequencies of the system as calculated in Appendix A. Due to an uncertainty about the exact temperature of the water, and consequently the speed of sound, the calculated values were normalized to the measured values at the fourth operational mode, or the 20th mode of the resonant system. The very close agreement between the calculated values and the experimental values presented in the third column was very helpful in locating the modes the first time.

The measured Q of each mode is presented in column four. These Q's are apparently determined by losses at the boundary of the resonator. If the losses in the water alone are considered, the Q's would be about 50 times larger than the measured values.\* The losses by radiation to the air can be estimated, with the result that  $Q_n = 5400n$ , where n is the mode number. The measured Q's are less by a factor of approximately 10 than the values predicted on the basis of the power radiated into the air surrounding the resonator. It is apparent that the Q's are limited by the losses in the transducers, even though the transducers are loosely coupled to the resonator.

The Q's of the transducers cannot be increased by changing the area of their cross section because both the energy stored in the transducer and the power dissipated are proportional to the area of the cross section. The degree of coupling between the transducers and the resonator can be decreased by decreasing the area of contact between the two

---

\* D. Lieberman, Reference 38, cited on p. 26.

systems. This would increase the Q's of the resonator. The decreased coupling would require larger transducer velocities, however.

Some qualitative information can be obtained from the results of measurements made on the twelve-transducer resonator and the eight-transducer resonator. The latter system required about 50% less power to produce a given acoustic pressure at its focus. The Q's of this system were about 30% larger at all of the modes. It was found that the distortion of the standing-wave modes was larger for the eight-transducer resonator. The increased distortion evidently did not cause the focal pressure to be reduced by an amount as large as the increase in the focal pressure caused by the increased Q's. The coupling between the transducers and the resonator can be reduced by decreasing the area of the transducers. If a great many transducers of small cross section are used, it might be possible to maintain low distortion while at the same time achieving very large Q's. It must be remembered, however, that as the coupling is decreased, larger transducer velocities will be required. It is not possible to estimate how far one can go in the direction of decreasing the coupling between the two systems and continue to realize increased pressure sensitivity. A criterion would need to be set on the amount of distortion in the standing wave that could be tolerated.

In column five the driving sensitivity of the resonator is given in terms of the peak acoustic pressure at the focus in bars for a driving voltage of one volt peak. This information was obtained experimentally. The input impedance of the resonator at the various modes is given in column six. The impedance was measured with a variable

inductance connected across the transducer array, which was tuned for parallel resonance with the capacitance of the transducers. The information in column seven was calculated from that in columns five and six. The impedance and power information were used to determine the specifications for the power amplifier which drives the resonator.

Columns nine and ten show the distortion in the standing-wave modes of the resonator. The ninth column lists the relative magnitude of the pressure at the first pressure antinode with respect to the pressure at the focus in decibels. The theoretical value is -17 dB. Most of the values are within 4 dB of this theoretical value. The tenth column lists the relative magnitude of the pressure at the first pressure node with respect to the pressure at the focus in decibels. The theoretical value is minus infinity. The measurements for the first four modes are limited by noise in the measuring system. The pressure at these nodes is less than 3% of the peak pressure at the center of the sphere. The pressure at the first node of the remaining modes is less than 10% of the peak pressure at the focus.

#### The Power Amplifier

The data in Table II show that a power amplifier for driving the resonator when tuned with a parallel inductance should have a wide range of output impedances, a large dynamic range, high power output capability, and a wide frequency range. The results given by Esche\* indicated

---

\* R. Esche, Reference 44, cited on p. 29.

that cavitation thresholds occur at about 1 bar at 20 kc/s and increase to as high as 200 bars at 1.5 Mc/s. On the basis of the data in Table II and the results obtained by Esche, it was decided that the amplifier should be capable of 400 watts output over the frequency range extending from 20 kc/s to 1.5 Mc/s.

Figure 6 is a schematic of the power amplifier. The output stage comprises two 4X150 radial beam power tetrodes coupled to the load through a special output transformer. A  $200\ \Omega$  and a  $50\ \Omega$  output impedance are obtained from the secondary windings of this transformer. A  $1500\ \Omega$  output impedance is obtained by connecting the load across the primary winding which then acts as an autotransformer. A series coupling capacitor prevents the plate voltage of the output stage from being applied across the load in this mode of operation.

The output transformer is wound on a 3-inch ferrite toroid, with a  $6000\ \Omega$  primary winding and two identical  $50\ \Omega$  secondary windings.\* The toroid with its windings is mounted in an "O" ring sealed metal can. Before sealing, the can was filled at a temperature of  $100^{\circ}\text{C}$  with a special fluorocarbon liquid.<sup>†</sup> A calculation using the thermodynamic properties of this fluid indicates that the pressure of the liquid-vapor system at room temperature is less than one-tenth atmosphere. Both the liquid and vapor of this fluorocarbon have a voltage breakdown strength in excess of 6 kV/mil, so the transformer windings are adequately

---

\* The transformer, exclusive of its case, was supplied by Spectran, Inc., of Maynard, Massachusetts.

† Minnesota Mining and Manufacturing Co.; Fluorocarbon FC75.

insulated against the high voltages encountered. In addition, as the ferrite heats up the fluorocarbon vaporizes around the core, removing the heat generated. The external surface of the can is placed in an air stream provided by the same fan that cools the output tubes. The condensation of the fluorocarbon at the walls of the can completes an internal heat transfer cycle which protects the ferrite core. The resulting transformer is only 2.5 inches in diameter and 2 inches high, but it is capable of delivering 450 watts continuously over the entire frequency range.

The grids of the output tubes are biased for class AB<sub>2</sub> operation. Each grid is driven by a cathode-follower stage which is capable of supplying the grid current for AB<sub>2</sub> operation. The cathode followers are preceded by a voltage-gain stage, a phase-inverter stage, and finally by an initial voltage-gain stage. The amplifier can be driven to 400 watts output with a 1 V rms input signal. The half-power output points are 12 kc/s and 1.5 Mc/s.

A regulated -150 volt bias supply is located on the same chassis as the amplifier itself. A separate chassis (Fig. 7) contains a regulated 300 volt power supply which provides screen current for the output tubes and plate current for the tubes in the driver stage and in the power supply voltage regulators. A 1500 volt, 0.6 amp unregulated plate supply is located on the same chassis with the screen supply. The plate supply voltage is metered, as are the output tube cathode current and screen current. A toggle switch on the front panel next to the cathode current meter enables either or both cathode currents to be indicated on

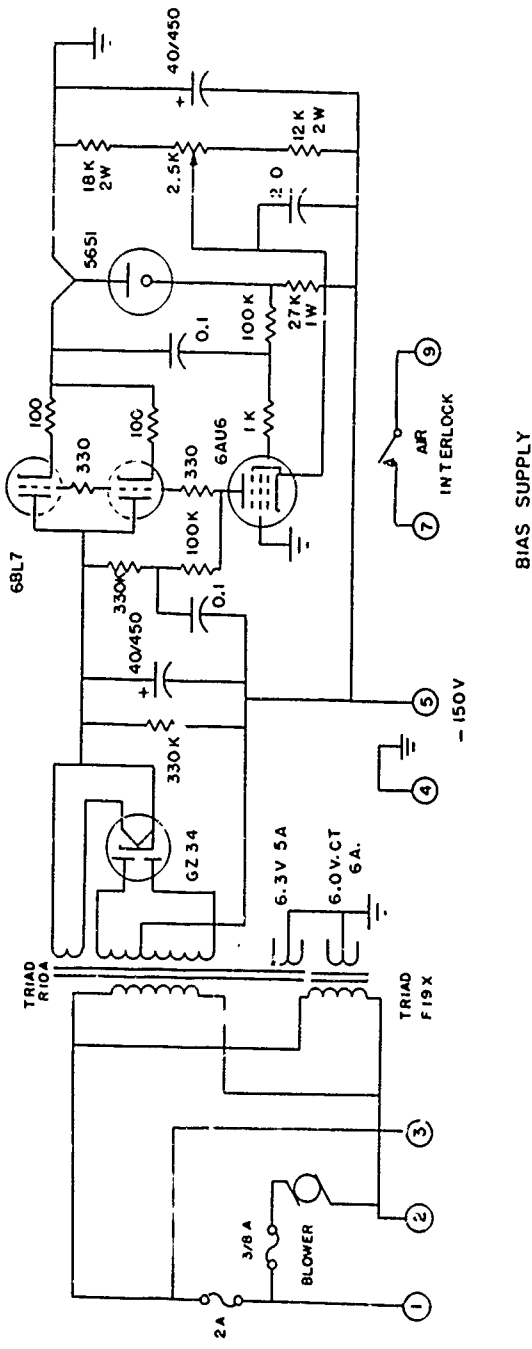
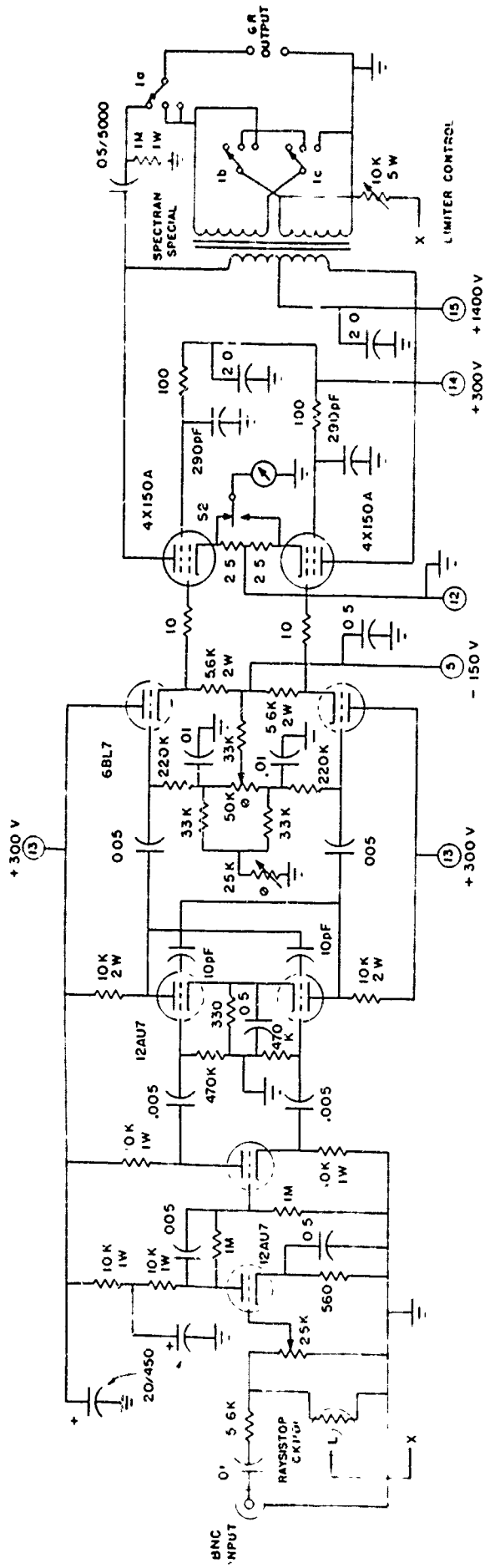


FIG. 6 POWER AMPLIFIER CHASSIS

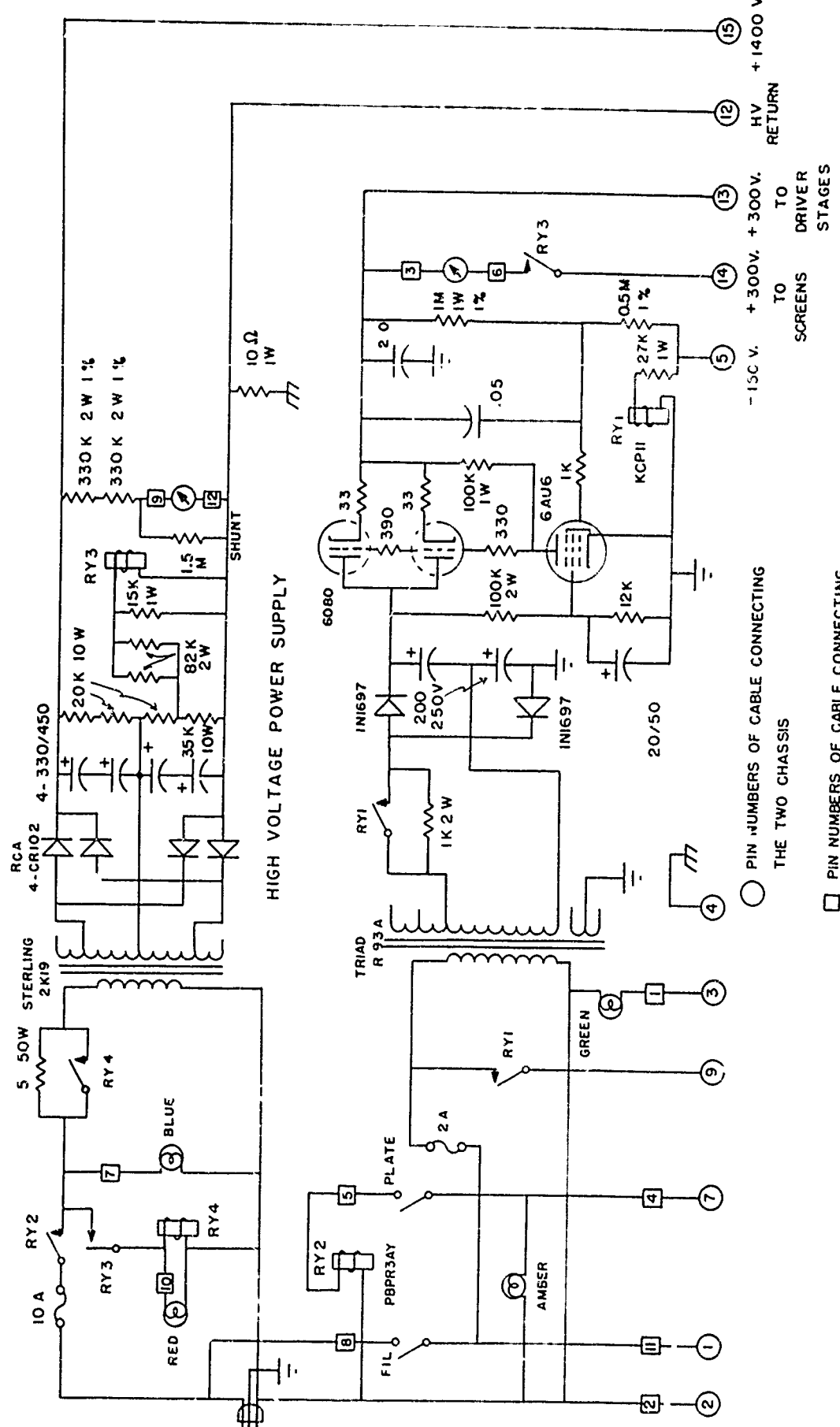


FIG. 7 POWER SUPPLY CIRCUITS

the meter. Screw adjustments next to the toggle switch allow the total no-load cathode current to be adjusted and the two currents to be balanced.

The output tubes are protected by relays in the various power supplies. When the amplifier is turned on, the relays supply filament current for two minutes, bias voltage, driver plate voltage, final plate voltage, and final screen voltage sequentially. In the event that any one of the above quantities fails to be supplied, all others higher in the sequence are immediately turned off. Each power supply is individually protected by a fuse.

The entire amplifier and all its appurtenances are mounted in a cabinet that measures 23×14×16 inches and weighs 95 pounds. It can be seen in the photograph of the apparatus.

#### Pressure Probes

It was necessary to construct a pressure probe that is rugged and small and has a reasonably flat response to 1 Mc/s. It was initially proposed to use a small thin-walled piezoelectric cylinder, 1/16 inch in diameter by 1/16 inch in length with a pressure release inner surface. For a cylinder of PZT-5,\* the fundamental radial resonance frequency would be 600 kc/s.

It was suggested that the fundamental resonance frequency could be increased by mounting the hollow cylinder rigidly on a central metal core.<sup>†</sup>

---

\* Clevite Corp., part no. 1-1010-5.

† F. V. Hunt, private communication, 10 December 1962.

The fundamental resonance frequency of this structure is calculated in Appendix C. It is found that the fundamental resonance of the cylindrical shell is raised by a factor of 2.4 by the solid core. The fundamental resonance frequency of the solid core cylinder will be 1.44 Mc/s, which will not interfere with the sensitivity of the probe in the frequency range of interest. The question of the sensitivity of this type of probe hydrophone must be considered. A search of the literature disclosed no analysis of this type of hydrophone, so the analysis is included in Appendix C.

Very surprisingly, the analysis shows that constraining the inner walls of the cylinder can increase the receiving sensitivity of the device over that which is obtained with a pressure release inner boundary.

With this encouragement several probes were made, using the PZT-5 cylinders mentioned. The construction of these probes is illustrated in Fig. 8. The inside diameter of each ceramic cylinder was honed slightly to remove the roughness. The central brass core was made separately for each cylinder, about 1/2 mil undersize. The core and ceramic cylinder, whose inner and outer surfaces are silvered, were then sweat soldered at a temperature of 100°C with a low-temperature solder. A #22 conductor Teflon-coated wire was soldered to the brass core, and the wire passed through the 1/16 inch o.d. stainless steel tube. The brass core was cemented to the tube with epoxy. After the small epoxy tip on the outside end of the brass core had been applied to serve as insulation, the entire tip of the probe was covered with a silver film by evaporation under vacuum. The silver serves both as an electrical connection from

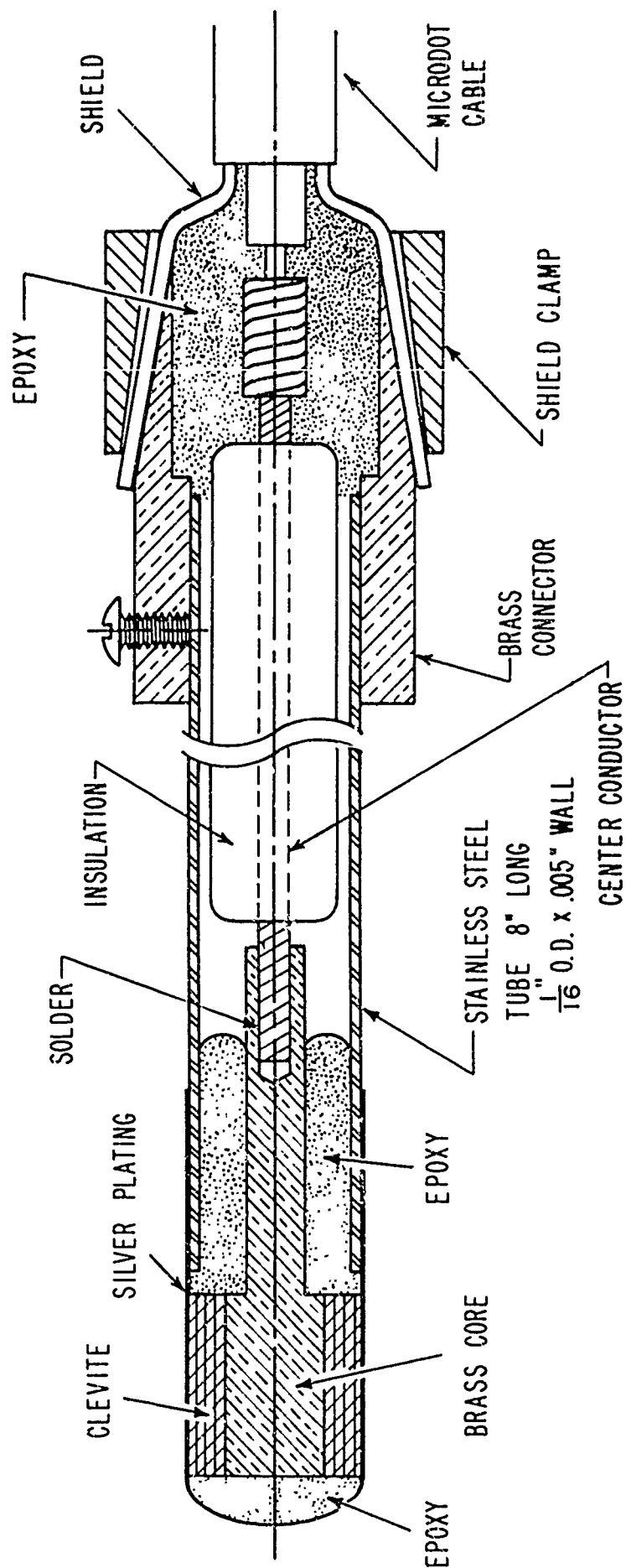


FIG. 8 CONSTRUCTION OF THE PRESSURE PROBES.

the steel tube to the external electrode of the ceramic and as an electrostatic shield for the outside end of the brass core.

The probes have a capacitance of about 200 pF measured at the electrical connector, about half of which is due to the capacitance of the lead and the capacitance between the steel tube and internal conductor. The theoretical sensitivity for these probes as calculated in Appendix C is -128.2 dB//1 V/ $\mu$ bar. Taking the shunt capacitance of the leads and amplifier input impedance into account, the theoretical sensitivity of the probes is -134.2 dB//1 V/ $\mu$ bar. This agrees very well with the measured values, as will be shown.

One other probe was constructed. This was for use at 500 kc/s and above, where the 1/16 inch probe diameter is one half wavelength or more. For this probe no special reason existed for achieving high sensitivity. To construct the probe, one of the 1/16 inch cylinders was shattered. A small piece, about 1/32 inch square, was selected, and a #30 enameled wire was soldered to each face. The chip was suspended 1 inch from the end of a stainless steel tube of the same size used for the larger probes. The chip was then dipped in a dilute epoxy solution to insulate it, a silver surface was evaporated over the chip, and electrical contact established between one of the leads and the silver coating. The sensitivity of this probe was determined to be -149.1 dB//1V/ $\mu$ bar by comparison measurements with the 1/16 inch probes at 350 kc/s.

Since the primary objective of these measurements is to determine threshold pressure levels, a very careful calibration of the probe hydrophones is required. The most accurate method of calibration is by free-

field pressure reciprocity. It is not practical to calibrate in air at frequencies around 1 Mc/s, so it was decided to calibrate in water. The calibrations were performed in a tank of water which measured 30×30×50 inches. Short pulses of sound were used to enable the direct sound path to be distinguished from sound paths reflected at the boundaries of the tank. The apparatus used in making the calibrations is illustrated in Fig. 9.

The oscillator is set at the frequency for which the calibration is desired. The transistor gate is adjusted to provide pulse widths as long as possible, but short enough so that the first reflection (from the water surface) does not interfere with the direct path transmission. The trigger delay is adjusted to equal the direct path travel time from the driver to the receiver. The oscilloscope is triggered just before the direct path transmission reaches the receiver. The sweep rate on the oscilloscope is adjusted to fill the screen with the direct path pulse. The pulse repetition rate on the transistor gate is set just high enough so the oscilloscope presentation appears to be a steady-state signal. No difficulties with overlap of pulses were encountered with this pulse repetition rate. Under these conditions the height of the received voltage pulse is determined. By setting the trigger delay to zero, the transmission current pulse height is displayed on the oscilloscope and measured. The receiving circuit is calibrated by the insertion voltage method as illustrated in Fig. 9. This circuit is built into the probe amplifier.

Since the probes are rather insensitive, it is not possible to use them for both the driver and receiver. Consequently, two standard

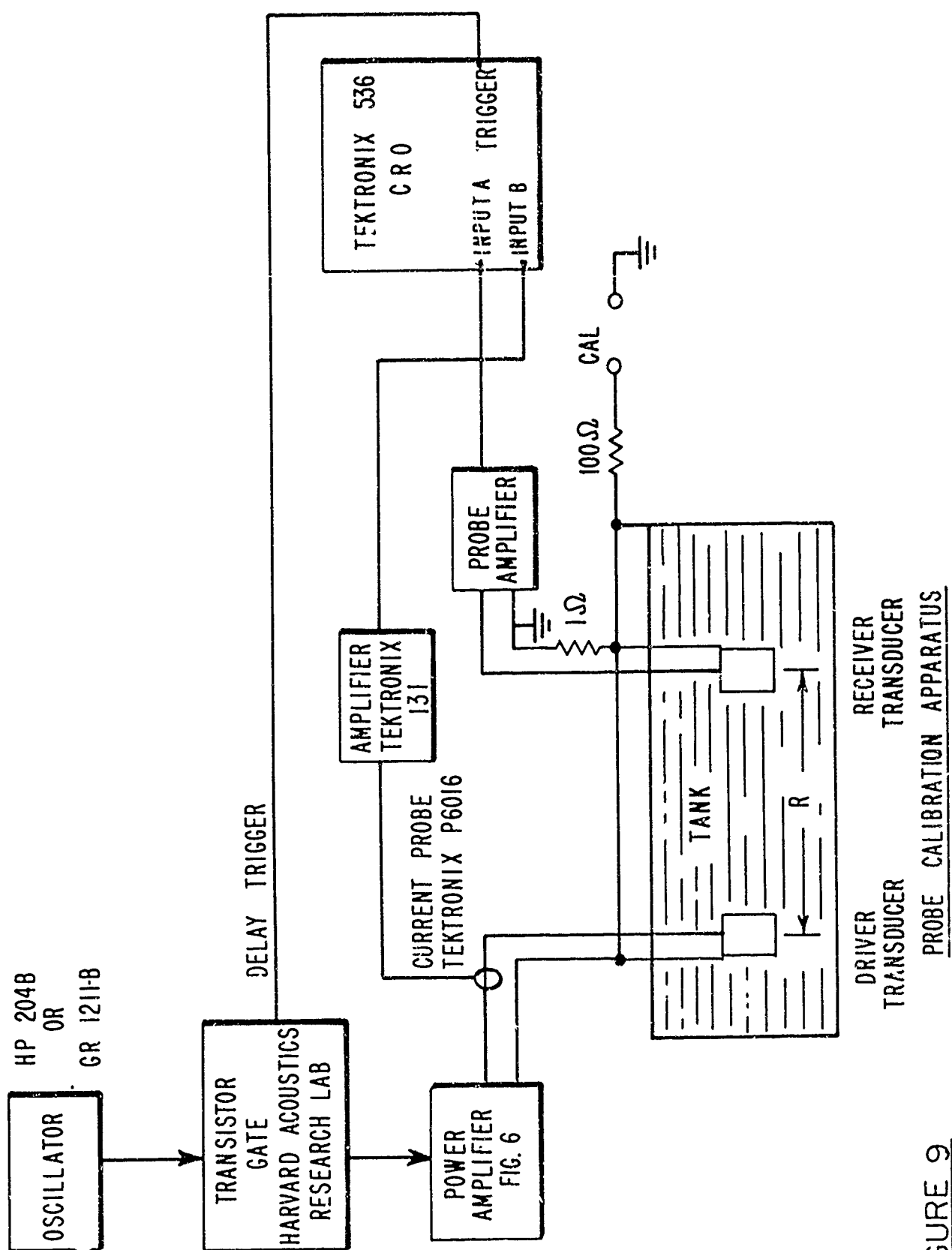


FIGURE 9

hydrophones were used in conjunction with the probes. A USRL standard transducer type 5A was used over the frequency range extending from 20 kc/s to 150 kc/s, and a USRL type E8 was used from 150 kc/s to 1.5 Mc/s. Calibrations were supplied for each of these transducers, but they were recalibrated as a check.

If one is to obtain an absolute pressure calibration of a reversible hydrophone by the free-field reciprocity technique it is necessary to employ two additional reversible hydrophones. With these three hydrophones three measurements are made, and it is possible to omit only one of the three from the role of transmitter for all of these measurements. Since it was not desired to drive the probes (the current necessary to achieve a good signal-to-noise ratio would destroy the probes), two additional piezoelectric transducers were constructed. These consisted of a 0.1 inch thick, 1.5 inch diameter piezoelectric ceramic disk backed by a 0.12 inch thick Corpren<sup>e</sup> pad for isolation of the disk from the mounting. The disk was sealed into a 1.75 inch circular recess 0.5 inch deep in a brass housing. An epoxy\* sealing compound was poured into the recess around the disk, leaving the outside surface of the ceramic exposed. A four-foot length of Microdot cable was attached to the disk and passed through an 18 inch long hollow brass tube which was threaded into the brass housing. The housing and the external electrode of the ceramic were connected to the shield of the Microdot cable. The shielded conductor of the cable was soldered to the surface of the ceramic next to

---

\* Emerson and Cuming, Inc.; two parts catalyst 15 to one part Eccobond 40 by weight.

the Corpren. The hollow brass tube with the cable passing through it was filled with epoxy to seal the entrance to the brass housing, and to suppress radial resonances in the tube.

These transducers were found to be so directive at the calibration frequencies that they did not radiate as a simple source. To reduce the directivity of the transducers, the radiating surface was decreased. A 1 cm diameter circular groove was cut in the external electrode at the center of the radiating faces of the transducers. A narrow path was cut on the electrode from the central radiating area to the point where electrical contact was made with the cable. The directivity of the modified transducers was small enough so they adequately simulated simple sources at the distances employed for the calibrations. The sensitivities of these hydrophones were -108.1 and -108.5 dB/1 V/ $\mu$ bar.

The two reversible piezoelectric transducers, along with each standard hydrophone in turn, were used as three passive, linear, reversible hydrophones. The sensitivities were measured over the applicable frequency range for each standard transducer. The results for the type E8 transducer were very gratifying. The sensitivity determined by this procedure agreed with USRL's calibration to within  $\pm 0.2$  dB over the entire frequency range. The estimated accuracy of reading the pulse heights on the oscilloscope is 2 parts out of 50, or 4%. This corresponds with the observed deviation. The calibrated sensitivity of the type 5A transducer was 1.2 dB greater than the USRL calibration over the applicable frequency range. Thus, 1.2 dB was added to the USRL calibration for this hydrophone.

The calibration of the probes was carried out directly by transmitting with the appropriate standard transducer and receiving with the probe to be calibrated. The free-field reciprocity relation is:

$$S_t S_r = \frac{2R}{\rho f} \frac{E_r}{I_t} ,$$

where  $S_t$  and  $I_t$  are the receiving sensitivity and driving current, respectively, of the transmitting hydrophone, and  $S_r$  and  $E_r$  are the receiving sensitivity and output voltage, respectively, of the receiving hydrophone.  $R$  is the distance between the acoustic centers of the two hydrophones;  $\rho$  is the density of the medium; and  $f$  is the frequency of the acoustic wave. The distance  $R$  was determined at each frequency by measuring  $E_r$  for  $I_t$  constant at different separation distances,  $X$ , of the geometric centers of the two transducers. A carriage over the top of the tank was provided for this purpose. A plot of  $E_r^{-1}$  as a function of  $X$  was made at 10-cm intervals in  $X$  between 20 cm and 120 cm. The data were extrapolated to  $E_r^{-1} = 0$  at  $X_0$ . To obtain  $R$  the value of  $X_0$  was then added to any of the values of  $X$  for which  $E_r$  and  $I_t$  had been measured.

With  $R$  determined the only unknown in the reciprocity relation is the probe sensitivity. The sensitivities of four of the six probes constructed were flat from 20 kc/s to 1.2 Mc/s within  $\pm 0.4$  dB. The other two had low sensitivities at several frequencies and were discarded. The sensitivities of the four good probes were: -135.1, -138.2, -135.6, -136.6 dB//1 V/ $\mu$ bar. The theoretical sensitivity as calculated in Appendix C and corrected for shunt capacitance is -134.2 dB//1 V/ $\mu$ bar.

### Automatic Frequency Control System

Most of the power supplied to the transducer array which drives the resonator is dissipated in the transducers. The power dissipated in the water itself can be estimated from the measured Q of the system. The definition of Q has the form

$$Q = \frac{2\pi \times \text{energy stored}}{\text{energy dissipated per cycle}} = \frac{\omega E_s}{W} , \quad (2-1)$$

where  $E_s$  is the time average of the energy stored in the system and W is the power input.

The energy stored in a volume element dV is

$$dE_s = \frac{p^2}{2\rho c^2} dV , \quad (2-2)$$

where p is the peak acoustic pressure in the volume element.

For a radially symmetric mode, the pressure<sup>55</sup> and volume element are

$$p(r) = P_0 \frac{\sin kr}{kr} ; \quad dV = 4\pi r^2 dr . \quad (2-3)$$

If the effect of the glass envelope on the resonance frequency is neglected, the outside surface is a pressure release surface at resonance. Then for the nth radial mode,  $k_n = n\pi/R = \omega_n/c$ , where R is the radius of the spherical volume of water. With the change of variable

---

55. P. M. Morse and H. Feshbach, Methods of Theoretical Physics, Vol. II, p. 1470 (McGraw-Hill Book Co., New York, 1953).

ic

$x = k_n r$ , the energy stored in the  $n\pi$  mode is, from Eqs.(2-2) and (2-3),

$$E_s = \frac{2\pi P_o^2}{\rho c^2 k_n^3} \int_0^{n\pi} \sin^2 x dx = \frac{R^3 P_o^2}{\rho c^2 n^2 \pi} . \quad (2-4)$$

From Eqs.(2-1) and (2-4) the power dissipated in the water is

$$W = \frac{P_o^2 R^2}{\rho c n Q} . \quad (2-5)$$

For the third operational mode at 82 kc/s ( $n = 9$ ; see Table II) and a peak acoustic pressure at the focus of 100 bars, the power dissipated in the resonator can be found from Eq.(2-5) to be 20 watts. Such a rate of energy dissipation is sufficient to raise the ambient temperature in the water by several degrees. The change in the velocity of sound which accompanies this temperature rise is more than sufficient to detune the resonant system. For example, it was found that after the driving frequency had been adjusted to resonance, the acoustic pressure at the focus would decrease by 6 dB in less than four minutes at an acoustic pressure of 10 bars because of the resonance-frequency shift. At higher acoustic pressures less time was required for the system to detune itself.

Much of the experimental data had to be collected during continuous operation for several hours. It was obvious, therefore, that some device was called for which would continuously return the driver for peak response at a particular resonance mode no matter how the frequency of that mode might vary in time.

The schematic of the apparatus (Fig. 5) shows the elements of this automatic frequency controller. A radio-frequency oscillator is provided

that will operate at any one of a series of approximate modal resonance frequencies selected by a switch. An audio-frequency oscillator is arranged to produce frequency modulation of this rf oscillation at a rate of about 14 c/s. The modulation index is adjusted so that the total frequency swing is less than one half of the bandwidth of the resonator mode. The frequency-modulated rf signal is amplified in the power amplifier and applied to the driver transducer array.

The probe hydrophone is located at one of the secondary pressure antinodes of the radial standing wave in the spherical resonator. If the mean oscillation frequency does not coincide with the resonance frequency of the selected mode, the frequency modulation will cause an amplitude modulation of the probe output at the audio frequency. This amplitude modulation is in phase with the frequency modulation if the rf oscillator is tuned below the resonance frequency of the mode, and it is out of phase with the frequency modulation if the rf oscillator is tuned above the resonance frequency of the mode. If the rf oscillator is tuned to the exact resonance frequency of the mode, there will be no amplitude modulation of the pressure field.

The amplitude-modulated signal from the probe is amplified by the probe amplifier and delivered to a linear rectifier. The audio frequency component of the output of the linear rectifier is further amplified and then compared with the signal from the af oscillator in a phase-sensitive detector. The output of the phase-sensitive detector is a full-wave-rectified af wave that is positive if the two inputs to the detector are in phase and negative if the signals are out of phase.

This rectified output is then filtered, and the resulting dc voltage is applied to a frequency controlling circuit in the rf oscillator. If the applied voltage is positive, indicating that the rf oscillator frequency is too low, the frequency of the rf oscillator is increased. A negative control voltage has the opposite effect. Separate frequency trimmers for each mode are located on the rf oscillator so the approximate mode frequencies can be pre-set.

Most of the elements of the automatic frequency control are located on one chassis, as indicated by the dashed lines in Fig. 5. This chassis can be seen just in front of the power amplifier in the photograph of the apparatus in Fig. 3. A schematic of the automatic frequency controller is given in Fig. 10.

Examination of Fig. 10 from left to right shows first the amplitude modulation detector. Next is a low-pass filter with a different time constant for each rf oscillation frequency. The 2N404 is the audio-frequency amplifier. The phase-sensitive detector follows. The full-wave rectified signal from the phase-sensitive detector is shunted by the 50  $\mu$ F capacitor. The frequency modulation and control is accomplished by applying the af signal and the frequency control signal to the biasing circuit of the Semicap.\* The capacitance of the Semicap is part of the tank circuit of the oscillator. The oscillator is of standard Colpitts type. A different tank circuit and feedback circuit is used at each frequency. The table lists the values of the inductance,

---

\* A variable capacitance diode manufactured by International Rectifier Corp.

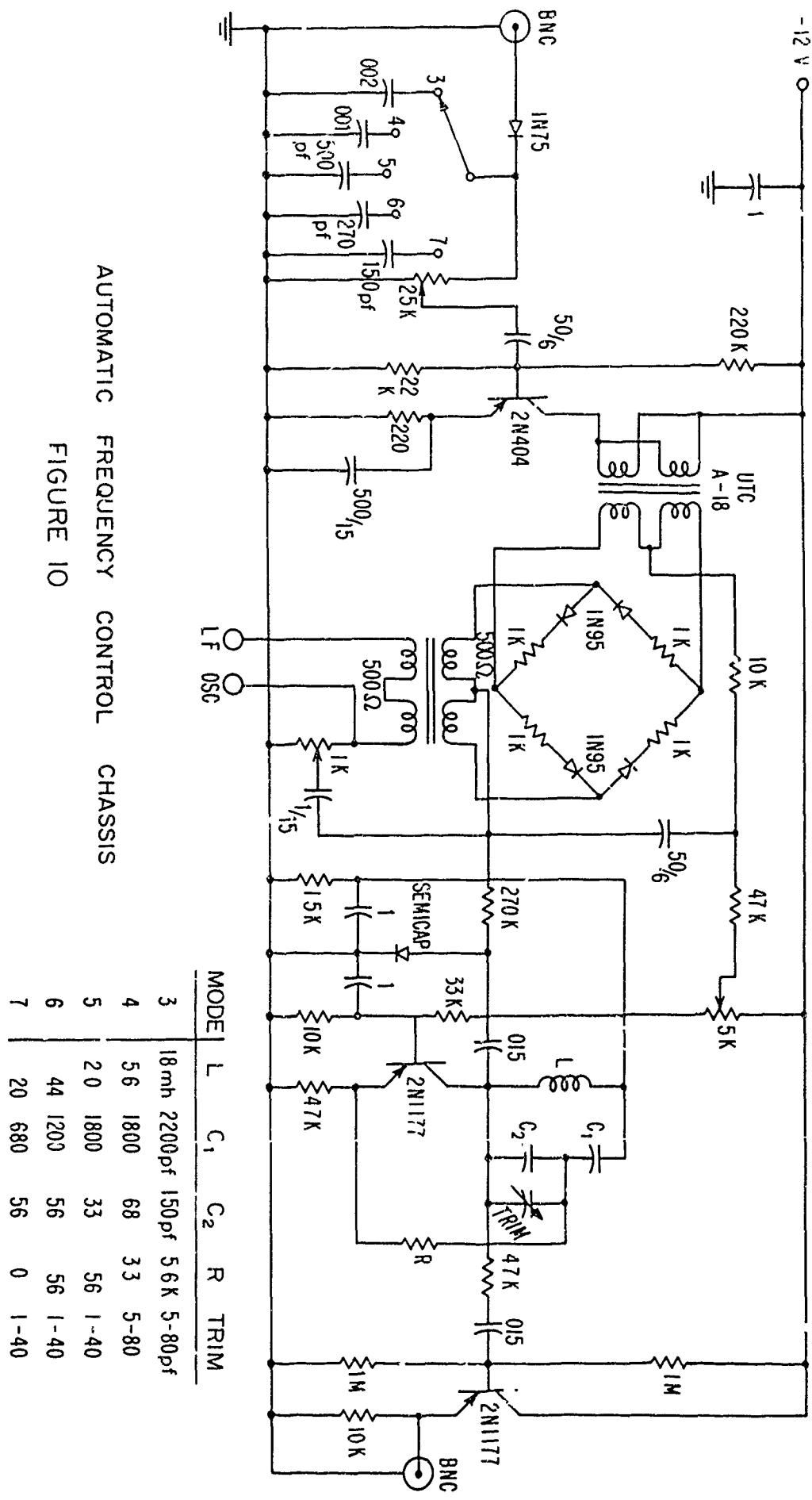
feedback capacitance divider, trimmer, and feedback resistor that are switched in at each operational mode. An emitter follower isolates the tank circuit from the input of the power amplifier.

#### The Probe Amplifier

The pressure probes must be terminated in a high-impedance, low-input-capacitance amplifier. The bandwidth must cover at least 10 kc/s to 2 Mc/s, with a gain of 40 dB. A schematic of the amplifier built for this purpose is shown in Fig. 11. The amplifier itself is located behind the resonator in the photograph of the apparatus.

A 1-ohm voltage insertion calibration resistor is connected at the input to this amplifier. A 100-ohm resistor connected in series with the calibration terminal provides a 40 dB attenuator for the calibration voltage. The 1-ohm calibration resistor is followed by a capacitance voltage-divider attenuator. The voltage divider provides for 0, 20, 40, and 60 dB attenuation of the probe hydrophone signal. The attenuator is followed by a variable-cutoff high-pass network. This network was used while calibrating the probes to improve the signal-to-noise ratio. The attenuator and high-pass filter are located in a shielded box inside the amplifier chassis.

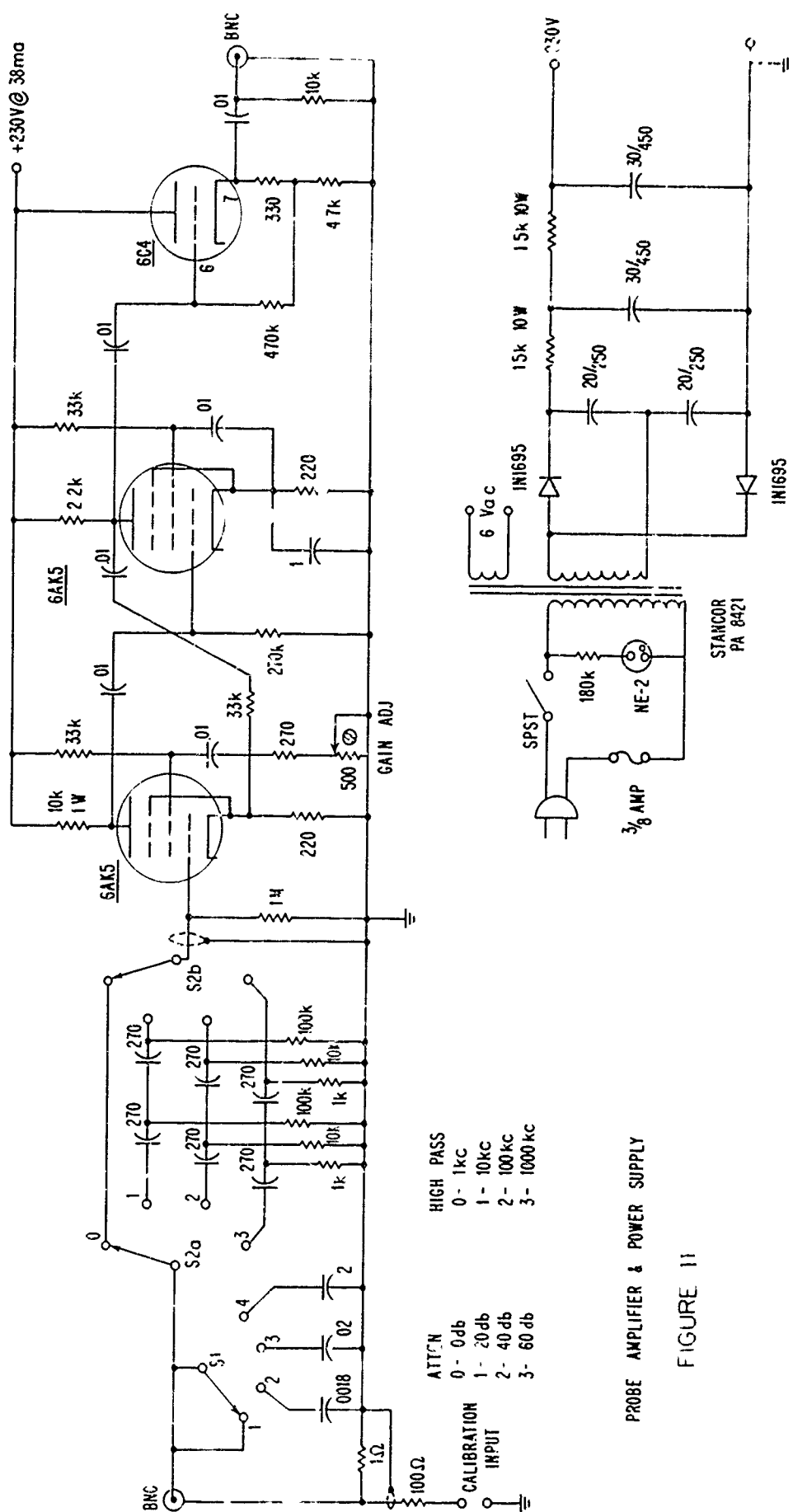
The amplifier itself consists of two cascaded pentode stages with negative feedback. The load impedance of these stages is kept low to increase the bandwidth. The gain of the amplifier is adjusted by varying the amount of negative feedback. The amplifier stages are followed by a cathode-follower output. The amplifier has a self-contained power supply.



## AUTOMATIC FREQUENCY CONTROL CHASSIS

**FIGURE 10**

MODE	L	C <sub>1</sub>	C <sub>2</sub>	R	TRIM
3	18mh	2200pf	150pf	56K	5-80pf
4	56	1800	68	33	5-80
5	20	1800	33	56	1-40
6	44	1200	56	56	1-40
7	20	680	56	0	1-40



## PROBE AMPLIFIER & POWER SUPPLY

The amplifier can be adjusted to 40 dB of gain with the pressure probes connected to the input. The bandwidth extends from 1 kc/s to 5 Mc/s. The output impedance is approximately 500 ohms, and the amplifier can deliver 20 volts rms into a high-impedance load.

#### Cavitation Detection Circuit

The remainder of the electronic elements in the schematic diagram of the apparatus are devoted to the detection and recording of cavitation events. It was observed that under some conditions cavitation at its threshold could not be detected visually. The collapse of a transient cavity produces a pressure pulse in the liquid which has an extremely short time duration as it passes the probe. The frequency distribution of the energy in the pulse is therefore continuous over a wide range of frequencies.

Under certain conditions small air bubbles exist in the liquid. The nonlinear oscillations of these bubbles in the acoustic pressure field radiate sound. The radiation from the oscillating bubbles may be expected to contain all integral harmonics of the forced oscillation and the free oscillation and the sum and difference frequencies of these.\*

An experiment was conducted to test the validity of these ideas. Three small air bubbles were formed in the focal region of the resonator by applying an acoustic pressure of 0.6 bar at 27 kc/s. The diameter of these bubbles was estimated to be 1 mm. The linear resonance frequency

---

\* H. G. Flynn, Reference 14, cited on p. 8.

of these bubbles should be about 5 kc/s. Once the bubbles were formed the acoustic pressure was lowered to 0.3 bar. The bubbles were driven at a frequency higher than their resonance frequency, so they came to stable equilibrium at the first pressure node. The reason for this equilibrium position is discussed in Chapter V. The spectrum density of the pressure oscillations in the water was examined with the wave analyzer. Bandwidths of 3000 c/s, 1000 c/s, and 200 c/s were used. No difference in the measured spectrum density was observed with the different bandwidths. The amplitude of the first fourteen harmonics decreased by 9 dB per octave. Above the fourteenth harmonic the system noise was greater than any signals from the bubble radiation. It was possible to detect line components of the spectrum at several non-harmonic frequencies between the first and sixth harmonic frequencies of the driving signal, but the magnitude of these components was at least 30 dB less than the adjacent harmonics of the driving signal.

It was concluded that the indication of the collapse of the cavities could be satisfactorily separated from nonlinear bubble oscillations by measuring the energy of the probe signal contained in a 3000 c/s bandwidth centered between the sixth and seventh harmonics of the driving frequency.

The instrument used for the detection of transient cavity collapses was a Hewlett-Packard Model 310A wave analyzer. The output of the probe amplifier is sampled through a 3 kc/s wide band centered between the sixth and seventh harmonic of the fundamental acoustic frequency when possible. Since the analyzer cannot be tuned to frequencies

64

higher than 1.5 Mc/s, it was necessary to sample at frequencies closer to the fundamental acoustic frequency when cavitation at the higher frequencies was being examined.

The output of the wave analyzer was amplified by a Shultz type of voltage amplifier which was built at the Harvard Acoustics Research Laboratory. The output of the Shultz amplifier was applied to a diode which was biased to pass only signals greater than +1.5 volts. The gain of the Shultz Amplifier was always adjusted so the system noise level was just below this value.

A pm speaker was attached to the diode through a matching transformer to provide an aural indication of cavitation events. A Brüel and Kjaer Type 2301 level recorder with a linear potentiometer was connected across the voice coil of the speaker. This recorder has a calibrated time base, and it was used to obtain time histories of the cavitation events. A Hewlett-Packard Model 532B electronic counter was used to measure the total number of events. When used as a totalizer this instrument has a direct-coupled input and requires a positive dc pulse to record one event. The pulses from the wave analyzer were observed to cause some high-frequency ringing in the matching transformer. The time resolution of the totalizer was high enough to detect each positive-going swing of this ringing as an additional event. In order to avoid these spurious counts it was necessary to rectify the "event" signal with an additional diode and to use a filter with a time constant (about 5 ms) long with respect to the period of this ringing (about 80 kc/s). Under these circumstances the resolution of the totalizer was reduced to about 200 events per second.

Water Control Apparatus

The elements on the left-hand side of Fig. 5 comprise the filtering, circulating, and degassing systems. The resonator is connected to this system by two Tygon tubes. One of these tubes runs from the top of the resonator to an enclosed glass reservoir located above the resonator. This is the water return line when the system is recirculating. This tube is thick-walled and will not collapse under a vacuum. It connects to a glass input tube in the reservoir which curves upward upon entering the reservoir. This deflection of the stream prevents air bubbles from the resonator from recirculating by entering the exit tube of the reservoir. From the exit of the reservoir a thin-walled Tygon tube passes through a peristaltic pump\* and back to the other connection on the top of the resonator. This tube is thin-walled so the pump can collapse it. Since it also collapses when the system pressure is lowered below about .5 atmosphere, it is not possible to use the pump for circulating when the system is under a high vacuum. A hose clamp is placed on the output end of the pump for controlling the flow rate. Rates from zero to sixteen cubic centimeters per second are possible. The water is added to the system through a filter holder† connected to the top of the reservoir through a stopcock and a length of Tygon tubing.

---

\* The peristaltic pump is a Randolph Model 610 designed to operate at 575 rpm with 1/2 inch i.d. tubing. The speed has been reduced to 65 rpm and 3/8 inch i.d. tubing is used. This modification changes the flow rate from 16 liters per minute to 1 liter per minute.

† Millipore Filter Corp., Type XX5002500.

*✓*

The vacuum system is connected to the water system through a stop-cock located on the top of the reservoir. This system consists of a 12-liter glass vessel which can be evacuated through a liquid-nitrogen cold trap by a Cenco Megavac vacuum pump. An open-tube mercury manometer is used to measure pressures from atmospheric down to 10 mm Hg. A closed-tube mercury manometer is used to measure pressures from 35 mm Hg to 5 mm Hg. A Stokes McLeod gage is used from 5 mm Hg to 5 $\mu$  Hg. The exact position of these elements and the valves between them are indicated in Fig. 5. The function of the water control apparatus will be described in the following Chapter.

## EXPERIMENTAL PROCEDURE AND OBSERVATIONS

Two types of experiments were undertaken in this study. The basis of the first set of experiments was the study of the effect of several parameters on the cavitation threshold in water. The parameters considered were the acoustic frequency, acoustic pressure, ambient pressure, amount of dissolved air in the water, and the size of the solid particles suspended in the water. For this set of experiments the threshold of cavitation was considered to be that acoustic pressure required for the first detectable evidence of cavity formation in the volume of the water. The nature of this initial cavity varied over the range of some of the parameters, and will be discussed in this chapter.

In the second type of experiment the characteristics of cavitation in water at acoustic pressures above the threshold were considered. This type of experiment has been able to reveal some important characteristics of the cavitation mechanism itself. The elucidation of the cavitation mechanism in turn illuminates the problem of the cavitation threshold.

In each of the two types of experiment a wealth of qualitative information has been gathered that cannot be adequately expressed graphically, or in any of the other familiar forms used to express quantitative information. Since the qualitative effects of cavitation are so intimately bound to exact experimental procedure, the two cannot be separated. It is the purpose of this chapter to describe as closely as possible the observations that were made during the course of the investigation.

Threshold Measurements

The parts of the apparatus which contain the water specimen, including the reservoir, Tygon tubing, and the resonator, were initially flushed with a mixture of hot water and Alconox. The system was then flushed with 5 gallons of distilled water to remove the Alconox. Each time a new sample of water was introduced, the system was evacuated to a pressure of 10 microns of Hg. The water was admitted to the system through the filter holder. When filtered water was desired, the appropriate filter was in place during the filling operation. The evacuation of the system preparatory to filling served to remove the suspended impurities in the air inside the apparatus and provided a pressure differential across the filter to overcome its flow resistance.

The water was degassed to a certain extent by the filling operation. It was necessary to circulate the water for several hours with the space over the water surface in the reservoir open to the atmosphere when the water was to be saturated with dissolved air. The upturned inlet pipe in the reservoir created a fountain effect which aided the saturation process.

For those measurements which called for degassed water, the 12-liter flask was evacuated to a pressure slightly less than the desired equilibrium air saturation pressure. The valve between the 12-liter flask and gages was closed at this point and the vacuum pump was allowed to continue pumping out the cold trap and gages. When the pressure reached  $5 \mu\text{Hg}$ , the valve to the pump was closed. The valve between the reservoir and the atmosphere was closed, and the valve between the

3

reservoir and the partially evacuated 12-liter flask was opened. Approximately 2 cc of water evaporated from the water in the reservoir to fill the 12-liter flask with vapor at the equilibrium vapor pressure. The air that came out of solution from the water also flowed into the 12-liter flask until equilibrium was established.

To speed up the degassing of the water the resonator was driven at the second operational mode (46 kc/s) with a 100 V rms signal. The result was quite spectacular. Initially the entire volume of water in the resonator became filled with air bubbles rising to the top and then up through the Tygon tubing to the reservoir. This process was accompanied by a steady hissing noise. Both the noise and the amount of bubbles remained nearly constant for about 5 minutes when the pressure in the 12-liter flask was less than one-half bar. After an additional 10 minutes the hissing and bubble formation nearly ceased.

During the initial stage the water was so filled with bubbles that no well-defined radial standing wave could be detected with the probe hydrophone. As the degassing operation drew near completion, however, fewer bubbles were formed. Spherical concentric shells of bubbles remained in the resonator, although these bubbles did not make the hissing sound. An examination of the spatial pressure distribution with the probe revealed that the radial mode had been established, and the surfaces or sheets of bubbles were located at the pressure nodal surfaces. A frequency analysis of the electrical signal from the probe showed, of course, a large component at the driving frequency if the probe was not at a pressure node. All of the integral harmonics of the

.90

driving frequency were present and their amplitudes decreased at about 9 dB per octave with increasing frequency. When the signal to the resonator was turned off, these bubbles floated to the surface of the water in the reservoir and escaped.

At this point the water was tested for the completeness of the degassing by reapplying the acoustic field. If no new bubbles formed in the water, even with an increased driving voltage, the dissolved air was assumed to be in equilibrium with the water at the partial pressure of the air over the water interface in the reservoir. The valve between the reservoir and the 12-liter flask was closed. Next, the valve between the 12-liter flask and the evacuated gages and cold trap was opened. The volume of the trap and gages was negligible with respect to the volume of the 12-liter flask, so the pressure measured by the gages was the total pressure in the flask. The water vapor in the flask flowed into the liquid nitrogen cold trap and condensed. The removal of the water vapor from the 12-liter flask by the cold trap was a relatively slow process, and it was necessary to wait several hours for the process to be completed. When the water vapor was removed, the pressure indicated by the gages was the partial pressure of the air in the 12-liter flask. Since the valve between the flask and the water in the resonator was closed when the partial pressure of the air in the two systems was in equilibrium, the final pressure indicated by the gages was the equilibrium air saturation pressure.

At this point the water sample was ready for the threshold measurements. Any one of the seven frequencies employed in this experiment

was chosen for the first measurement, and the subsequent frequencies were chosen in random order. If one of the two lowest frequencies was chosen, the power amplifier was driven directly by an oscillator set at the modal frequency. For any of the other five frequencies, however, the automatic frequency control was used.

The pressure probe was placed at the center of the sphere and the desired frequency selected by a switch on the oscillator chassis. The frequency trimmer was adjusted to bring the oscillator frequency to the correct modal frequency as indicated on the electronic counter. A fine adjustment of the oscillator trimmer was made to bring the pressure response at the focus to within about 2 dB of its maximum, as observed in the probe output voltage indicated on the C.R.O. The modulation index was increased from zero sufficiently so that an amplitude modulation of about 10% could be seen on the probe output voltage. The gain of the control circuit was then increased from zero sufficiently to cause the amplitude modulation to disappear. The disappearance of the amplitude modulation indicated that the control system was locked to the exact modal frequency. If the modulation index had been set too high, an amplitude modulation of twice the frequency of the modulation frequency would remain. In this event the modulation index was decreased until the amplitude modulation disappeared.

After the control circuit was locked to the resonance frequency of the mode, the probe was moved around at the region of the center to find the point of maximum response, and this response was noted. The probe was then withdrawn from the center to a point where the probe voltage

was at least 15 dB down from that which obtained at the focus, and this response was noted. At the lower frequencies the probe was left at the outer edge of the central pressure maximum. At higher frequencies it was left at one of the secondary pressure maxima. It was always well removed from the region in which cavitation occurred. The difference in the voltage from the probe at the center and at the outside point was applied to the readings of the probe voltage taken during the threshold measurement to establish the pressure at the focus. The probe positioning was carried out at an acoustic pressure well below the threshold value.

With the completion of the tuning, the wave analyzer in the cavitation detection circuit was set at a non-harmonic frequency well above the driving signal frequency. The power amplifier voltage gain was then increased in 1 dB steps as indicated by a VTVM connected to the output of the power amplifier. Each new pressure level was maintained for one minute before proceeding to the next level.

During this stage a sharp eye was kept on the focal region, and attention was directed to the loudspeaker. Visual observation was aided by a focused beam of light from a 100-watt projector lamp passing through the focal region at right angles to the direction of view. The cavities formed in the water were of two kinds. The physical manifestation of each kind also differed according to the acoustic frequency. At this point it becomes necessary to discuss the two types of cavities for which the thresholds of formation have been determined.

Initially, the discussion will be concerned with the formation of air bubbles in the focal region. The ranges of the various parameters

for which air bubbles were formed will be presented in Chapter IV. In general, air bubbles were formed only in gassy water.

At 27 kc/s, 46 kc/s, and 82 kc/s very small bubbles appeared throughout the focal region. They did not all appear at once, or in the same place, but they all seemed to have about the same initial size. This size was estimated to be about 50 to 100 microns. After the first bubble appeared, and in the span of about 30 seconds, there could be as many as ten or twenty of them. These bubbles drifted towards the center of the focal region where they coalesced. The single bubble that was thus formed at the center gradually increased in size with time. It had a very clear spherical surface. This bubble seemed to grow even when no new small bubbles were being added to it. After a period of time, which could be as long as one minute, this bubble suddenly developed a frosted appearance and began to dance around, executing an erratic and rapid motion about the center of the sphere. This behavior was observed to begin when the bubble radius was about equal to the resonance size at the driving frequency.\* After a few seconds of this behavior, this bubble was rapidly ejected from the center radially outward. It slowed down and came to rest at the nearest pressure node. As it came to rest its surface became smooth and clear again. The acoustic pressure in the resonator was observed to drop sharply by as much as 4 dB during the short period of erratic motion about the center of the sphere. The pressure returned to its normal value upon the ejection of the bubble from the center.

---

\* See Eq.(5-3), page 115.

1/1

There was no noise generation detectable during any of the phases of this cycle except during the short period of time the bubble gyrated about the center. This phase of the bubble cycle was accompanied by an audible rushing sound. The noise could be heard with the unaided ear as well as detected by the probe hydrophone.

Once the bubble had come to rest at the node and the acoustic pressure had returned to normal a new bubble formed at the center at the same rate at which the first one had formed. This bubble was ejected in time, as were succeeding ones. Some of the bubbles deposited at the first pressure node coalesced. This process usually occurred at the top of the spherical nodal surface because the bubbles moved along that surface until they reached its top. When the bubble on the top of the nodal surface became large enough its buoyancy would become great enough to allow the bubble to escape to the surface.

The size of the bubbles observed was larger for low frequencies and high equilibrium air saturation pressures. At acoustic pressures above the threshold the process proceeded as described but at an increased rate. In fact, if the pressure was as large as twice the threshold, the flow of bubbles formed continuous paths and even sheets. The phenomenon then resembled the "streamers" described by Blake<sup>56</sup> and the "trees" described by Noltingk.\*

---

56. F. G. Blake, Jr., "Apparatus and Techniques for a Study of Cavitation," Tech. Memo. No. 11, Acoustics Research Lab., Harvard Univ. (1949).

\* B. E. Noltingk, Reference 6, cited on p. 3.

..5

As the frequency of the acoustic wave was increased the size of the individual bubbles decreased. At frequencies above 183 kc/s, the motion of the bubbles was hard to detect because of their small size. The formation process of the bubbles could not be observed, but they became visible at the pressure nodal surfaces. This provided a dramatic demonstration of the standing-wave field in the resonator. At 1.16 Mc/s as many as twenty concentric spherical shells of bubbles were formed at the center of the resonator when the water was saturated with dissolved air. These shells were separated by one half wavelength, or 0.63 mm. The diameter of the bubbles themselves appeared to be about one-fifth of their separation, or a radius of about 60 microns. These bubbles coalesced at the tops of the spherical shells and floated to the surface as more bubbles were formed.

There was no audible hiss accompanying bubble formation at the higher acoustic frequencies. Harmonic frequencies of the driving signal were detected in the water when the bubbles were formed. The highest frequency to which the wave analyzer could be tuned, 1.5 kc/s, limited the number of harmonics that could be measured. In the case of bubble formation at 1.16 Mc/s it was not possible to measure any of the harmonic frequencies.

The second type of cavity motion which was observed is typical of the motion described in Chapter I as a transient cavity. This type of cavity motion looked much like a small comet whose lifetime was very brief. The head of the comet was hemispherical and bright in the reflected light of the illumination lamp. The diameter of the comet increased towards the tail. The tail was less clear and bright than the

head, and had a jagged appearance. The axis of the comet was always radial, with the head towards the center. The head was not always located at the exact center of the resonator, but at random positions within the focal region. The rate of occurrence of these events depended on the acoustic pressure and on the flow velocity through the focal region. The dependence on the latter variable will be discussed later. The size of the comets occurring at any one acoustic pressure was similar. An audible snap could be heard for each occurrence and a short burst of noise in the water could be detected in a narrow frequency band centered at any frequency above the fundamental driving frequency. This type of disturbance will be referred to as a cavitation event.

At the lowest acoustic frequency for which cavitation was produced, 27 kc/s, these cavitation events were quite spectacular. The total length of the comet-shaped cavity was as large as 3 cm and the maximum diameter near the tail was as large as 1 cm. The dimensions of the cavities were approximately inversely proportional to the square of the acoustic frequency. At the resonator mode near 353 kc/s the cavitation events were barely discernible to the eye, and at 1.16 Mc/s it was not possible to see the cavitation events at all. This situation made the use of the aural detection scheme absolutely necessary.

The foregoing physical description of the cavitation event is apparently in agreement with the observations of other experimenters. Lieberman,\* for example, describes a typical cavity occurring at an

---

\* D. Lieberman, Reference 38, cited on p. 23.

acoustic pressure near the threshold for cavitation at an acoustic frequency of 26.3 kc/s: "It appeared to the eye as an instantaneously formed elongated cavity about one inch long, directed outward from the center of the sphere."

It is of interest to determine why the cavity has this characteristic shape. A series of photographs was taken of cavitation in degassed water at an acoustic frequency of 82 kc/s. The focal region of the resonator was illuminated by an intense focused light beam directed perpendicular to the line of observation. A black panel behind the resonator enhanced the definition of the cavities. A photograph taken with a steady illumination and an exposure of 1/12 second showed five of the elongated cavities. Without altering the acoustic pressure or frequency, and keeping the same exposure time, a set of photographs was then taken with illumination from a stroboscope operating at 40 flashes per second. Some of these photographs showed nothing, while others showed one or two widely separated individual cavities. These cavities were approximately spherical, with rather deep surface corrugations.

Finally, a set of photographs was taken with the stroboscope set at 417 flashes per second. The acoustic parameters and the exposure time remained unchanged. In each photograph four or five sets of cavities could be seen. Each set of cavities appeared to be a row of four or five individual cavities. The lengths of these rows of cavities were approximately equal to the lengths of the individual elongated cavities observed with the steady illumination. The lengths of the rows of cavities were not all the same. This was apparently due to the fact that

all of the rows were not directed in the same radial direction from the center of the sphere. The depth of focus of the lens system was less than the length of the elongated cavities. Only the cavities in rows that were in planes nearly perpendicular to the lens axis were in focus.

Two of the photographs are shown in Fig. 12. The acoustic parameters were:  $P_a = 10$  bars;  $f = 82$  kc/s. The exposure time of each picture was  $1/12$  sec. Photograph (a) was taken with a  $1 \mu\text{sec}$  flash occurring 40 times per second, while photograph (b) was taken with a  $1 \mu\text{sec}$  flash occurring 417 times per second.

The cavity nearest the center of the sphere in each row was usually the smallest, although the individual cavities were all about 1 mm in diameter. The outermost cavity was usually the largest cavity in its row. It had a very definite shape, sometimes appearing to be several cavities. In a few cases several very small bright cavities, whose diameters were approximately  $50 \mu$ , could be seen at the end of a row.

It is appropriate to mention at this point that objects appearing at the center of the sphere are magnified by a factor of about 1.5 by the spherical water interface. This magnification and the magnification of the lens system were calibrated at the same time by photographing the pressure probe at the center of the sphere.

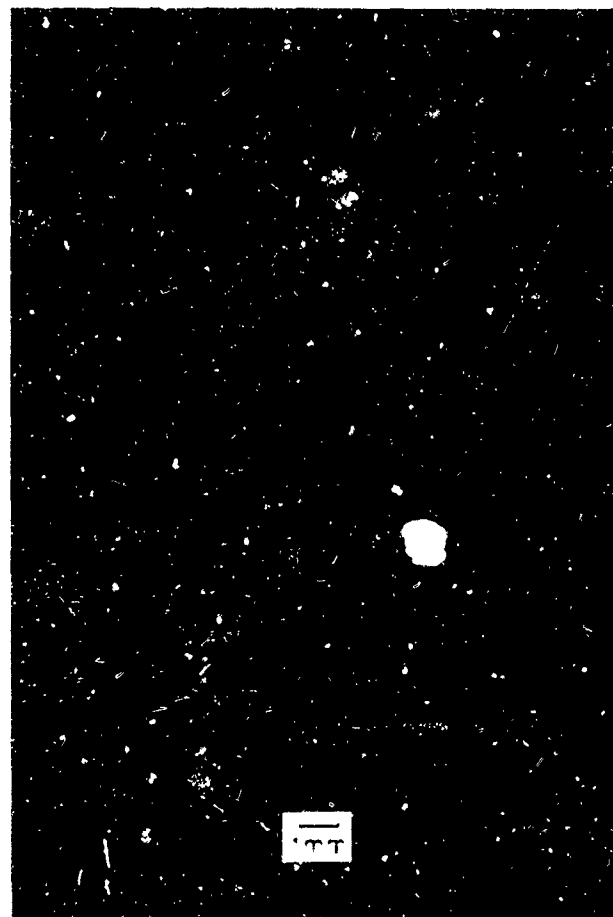
The interpretation of these results is straightforward. A spherical cavity is formed, which moves radially outward. The cavity size increases for a time, after which it begins to collapse. The collapsing cavity breaks into several smaller cavities which disappear. The time scale of the entire process is of the order of 10 ms, or about 800

acoustic periods. The mechanism of this type of cavity behavior in an acoustic standing wave is discussed in Chapter V.

The procedure which was followed for determining the cavitation threshold will now be outlined. The acoustic pressure was increased in 1 dB steps of 1 minute duration. When a cavitation event was detected either visually or by a audible snap from the loudspeaker, the pressure level was decreased by 1 dB. If no additional events occurred after a 10-minute wait the pressure level at which the event occurred was taken as the threshold. When an event did occur at the reduced pressure, the pressure level was further reduced by 1 dB for 10 minutes. When the experimental conditions were such that a bubble was formed, the acoustic pressure was decreased by a sufficient amount to allow the bubble to rise to the surface before the pressure was re-established at the reduced level. The lowest pressure for which an event was detected was taken to be the cavitation threshold. Often the threshold level was the same level at which the first event was detected. It was never necessary to lower the pressure at which the first event was detected by more than 4 dB to find the threshold.

The 10-minute waiting criterion was checked by waiting for periods of as much as one hour. It was found that the 10-minute wait was sufficient in 11 out of 12 cases checked. For the one instance when an event occurred outside the 10-minute interval the level was further reduced by 0.5 dB, and a 60-minute waiting time produced no new events.

Repeatability measurements showed that a given threshold value was measured 8 times out of 10 to within  $\pm 0.5$  dB. On the other two occasions

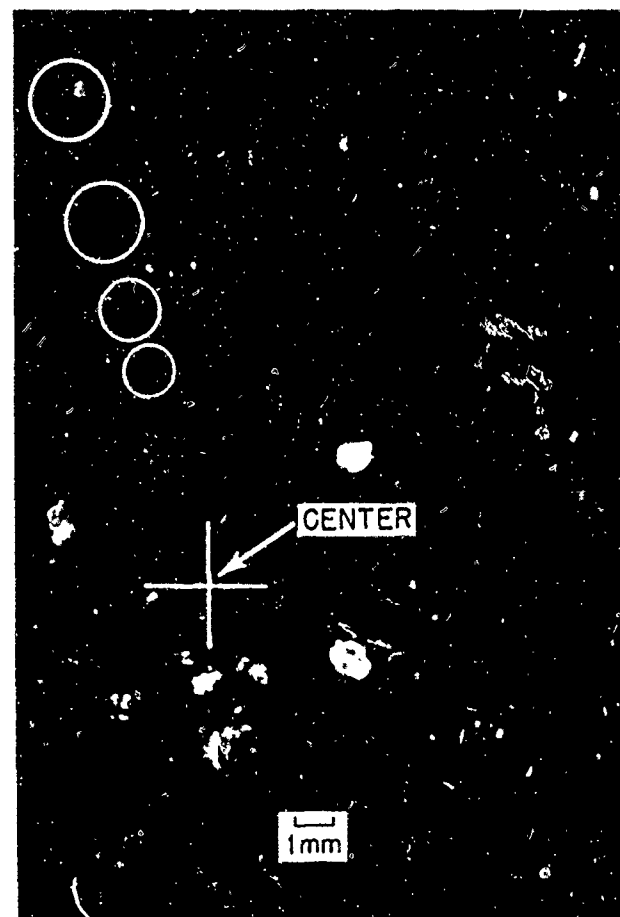


(a)

Exposure time = 1/12 sec.

40 flashes/sec.

Acoustic pressure  $P_a \approx 10$  bars      Frequency = 82 kc/s



(b)

Exposure time = 1/12 sec.

417 flashes/sec.

PHOTOGRAPHS OF TRANSIENT CAVITIES

FIGURE 12

the deviations from the mean of the 10 measurements were 0.6 dB and +0.7 dB. The probe sensitivities were estimated to be correct to  $\pm 0.4$  dB. Since the finite waiting time also introduced a small amount of error, it was estimated that the thresholds could be measured to an accuracy of  $\pm 0.5$  dB. Since the measurements were repeated to this precision by the threshold measuring procedure outlined above, this procedure was considered to be realistic.

#### Measurements Above Threshold

Upon the completion of the threshold measurements the effect of acoustic pressures greater than the threshold value was examined. At any of the frequencies used, a sample of water was found to cavitate more rapidly as the acoustic pressure was increased above the threshold. When the conditions of the experiment were such that air bubbles were formed at the threshold pressure, acoustic pressures above the threshold resulted in a more rapid generation of air bubbles in the focal region. The "trees" or "streamers" such as described in the previous section were formed at first. As the acoustic pressure was increased further, a point was soon reached where the volume of water became so filled with bubbles that the standing-wave pressure field was disrupted. The acoustic pressure in the sphere would fall about 20 dB and the bubbles would remain.

When the conditions of the experiment were such that the comet-like cavities were formed (transient cavities), the rate of occurrence of these cavitation events was observed to increase with increased acoustic

pressure. An increase of the acoustic pressure by a factor of two over the threshold value was sufficient to increase the rate of events to about 10 per second. The increased acoustic pressure also increased the size of the cavities somewhat, as well as the magnitude of the pressure pulse which accompanied the collapse of each cavity.

A time history of the cavitation events was made at several constant acoustic pressure levels. If the acoustic pressure level was less than about twice the threshold pressure the cavitation rate would proceed in time with a constant average for 5 hours or more. A distribution of the times between events was measured by recording each event on the Brüel and Kjaer level recorder. The distribution of observed waiting times will be examined in Chapter IV. It is found that the events are statistically independent.

At the acoustic pressures required to produce cavitation events it was noticed that a very slow upward flow of water through the focus was taking place. This flow stopped at much lower acoustic pressures. This flow was not considered to be due to acoustic streaming because it was always in the vertically upward direction for all resonator modes. There was no reason to suspect an asymmetry in the same direction in all of the modes, and the spatial pressure distribution had been found to be very symmetric in the vertical direction through the focus. However, the power dissipated in the water had already been observed to be of sufficient magnitude to detune the resonant modes prior to installation of the automatic frequency control. Since the power dissipated is proportional to the square of the pressure, most of the dissipation occurs

in the focal region. It was concluded, therefore, that the flow through the focal region was caused by convection currents. The flow could be observed visually by small particles in the water made visible by the Tyndall effect. The estimated flow velocity through the focus was about 1 mm/sec.

The possibility that the cavitation rate was determined by this flow velocity was examined by circulating the water with the peristaltic pump. The cavitation rate was indeed found to be a function of the flow velocity through the focus. At an acoustic pressure 1 dB above the threshold it was possible to obtain cavitation rates from 0.04 to 11.0 events/second by circulating the water at different flow velocities.

Many experimenters in the past have used a particular rate of cavitation as a criterion for the threshold. This criterion seems to be specious, or at least unreliable. Since most of these experiments were not carried out with radially symmetric standing waves there must have been acoustic streaming through the focal region of the apparatus.

The rate of cavitation was found to be proportional to the velocity of water flow through the focal region. At a constant flow velocity the cavitation rate would remain constant for a period of several hours. If the experiment was continued long enough, however, the cavitation rate would begin to decrease. In fact, it was possible to continue at a constant acoustic pressure and flow rate until the cavitation would cease altogether. When the cavitation had ceased, an increase of the acoustic pressure level would again produce cavitation which would proceed with a constant rate for a finite time. After a sufficient period of time this

10<sup>4</sup>

cavitation rate would also approach zero. Thus, the cavitation threshold of a sample of water could be increased by repeated cavitation at acoustic pressures above the initial threshold pressure.

This phenomenon suggested a new series of experiments. It appeared to be possible to measure the total number of cavitation events that could be produced in a sample of water by a particular acoustic pressure. To do this, the sample of water was initially subjected to an acoustic pressure 50% greater than the threshold value. The water was circulated at 10 cm<sup>3</sup>/sec during the measurements. The cavitation events that occurred were totalized on the electronic counter. The experiment was allowed to continue until the cavitation rate decreased to one-tenth of the initial cavitation rate. At this point the acoustic pressure was increased until the cavitation rate increased to the same initial rate that had been obtained at the first pressure level. The number of events at the new pressure level was counted until the cavitation rate decreased to one-tenth of the initial value.

After the acoustic pressure reached a value of about 10 times the initial threshold pressure, it was observed that further increases in the acoustic pressure had no effect on the cavitation rate. The measurements were terminated at this pressure. The results of these measurements are presented in Chapter IV.

Five different samples of water were examined for the number of cavitation events produced in them as a function of the acoustic pressure. They were: tap water, tap water filtered through a 1 micron filter, tap water filtered through a 0.45 micron filter, distilled water,

and distilled water filtered through a 0.45 micron filter. Each sample was degassed at a pressure of 100 mm Hg. Each sample was found to have the same cavitation threshold, but the total number of events produced in each sample was different. More than 300 000 events were produced in the tap water, while only about 30 000 events were produced in the distilled water. There was little difference in the filtered and unfiltered distilled water samples, but the 0.45 micron filtered tap water produced about one-fourth as many cavitation events as the unfiltered water.

For any of the samples it was found that the increase of the cavitation threshold by repeated cavitation was permanent. The tap water sample was allowed to remain for one week in the apparatus after its threshold had been increased by a factor of 4 by repeated cavitation. This increased threshold was the same at the end of the week as it had been just after the repeated cavitation measurement. This evidence that cavitation nuclei in water can be destroyed by cavitation appears to be at variance with observations of cavitation in ultrasonic cleaners. Typical observations of cavitation in a "clean" ultrasonic cleaner tank indicate that cavitation will proceed at a constant rate for an indefinite time. Indeed, there is no mention in the literature of the cavitation in an ultrasonic cleaner ever slowing down and stopping for an unexplained reason.

The main difference between the tap water in the experimental apparatus and the water in an ultrasonic cleaner arises because the water in the cleaner is open to the atmosphere. Accordingly, the sample of tap water that had been "strengthened" by cavitation was circulated

through the system while a jet of "room" air was directed on the fountain of water in the reservoir. This jet of air was obtained by pumping on the vacuum inlet of the reservoir with the water inlet valve open. After 30 minutes the water sample was judged to be fully saturated with dissolved "room" air. The inlet valve to the reservoir was closed and the water was degassed at a pressure of 100 mm Hg. The cavitation threshold was measured and found to be the same as the initial value that had been measured before the cavitation threshold had been increased by repeated cavitation. This appears to confirm the tentative conclusion that cavitation nuclei can be atmospheric dust particles.

It has been mentioned that as the acoustic pressures were increased, a point was reached where the cavitation rate was nearly independent of the acoustic pressure. This terminal cavitation rate could not be decreased by cavitating for long periods of time. It was conjectured that these cavitation events were possibly being nucleated by the cosmic-ray mechanism postulated by Sette.\* A paraffin shield was made to fit around the resonator. The walls of the shield were 3 cm thick. According to Sette's theory, cosmic-ray neutrons with energies of about 10 MeV are the nucleating agents. The paraffin shield has a thickness sufficient to reduce the average energy of incident neutrons of this energy by a factor of ten.

The effect of the paraffin shield was first examined on a sample of distilled water that had not been previously cavitated. The shield had no noticeable effect on the cavitation threshold of this sample.

---

\* D. Sette, Reference 34, cited on p. 25.

&lt;C&gt;

A sample of distilled water was then prepared for which the terminal cavitation rate had been reached by repeated cavitation. The acoustic pressure was adjusted to four times the initial threshold pressure, and the cavitation events were recorded on the level recorder. After about 30 minutes the paraffin shield was placed around the resonator. The cavitation was allowed to continue, at the same acoustic pressure, for another 30 minutes. After this period the shield was removed, and the cavitation was continued for an additional 30 minutes.

The effect of the shield was to reduce the cavitation rate by a factor of three during the time it was in place. The actual time history of the cavitation events during this experiment is shown in Fig. 22, Chapter V.

The collected observations which have been made of cavitation in water can be summarized as follows:

1. The cavities formed in water by an ultrasonic acoustic standing wave are characterized by two distinct kinds of motion. Transient cavities have a very short lifetime which is terminated by collapse. Stable cavities, or air bubbles, oscillate for an indefinite period. The kind of cavity motion depends mostly on the air content of the water.
2. Of the two kinds of cavity motion, only the transient cavity with its associated collapse fits our definition of cavitation. Under certain conditions air bubbles are formed, and their presence appears to preclude the formation of transient cavities. The minimum pressure required to produce either air bubbles or transient cavities can only be properly called the threshold of cavitation when the kind of cavity motion which occurs is specified.

3. The transient cavity appears to be an elongated crack because the cavity moves radially outward at relatively high speed from the center of the resonator.
4. A nucleus from which a cavity can be formed must exist in, or be convected into, a region of sufficient acoustic pressure to form a cavity.
5. At least one kind of cavity nucleus can be destroyed when a cavity is formed from it.
6. The cavitation nuclei can be supplied to the water by exposure to "room" air.
7. The cavitation threshold is independent of the size of the solid particles in the water for particles larger than  $0.45\mu$ . The total number of cavitation events that can be produced in a sample of water, however, is a function of the number of particles of size greater than  $0.45\mu$ .
8. There is a terminal rate of cavitation which remains after repeated cavitation of a sample of water. This terminal rate of cavitation is dependent on the convection velocity of the "strengthened" water through the focal region of the standing wave. At a constant convection velocity, this terminal rate of cavitation can be lowered by shielding the water with a paraffin screen.

These qualitative results will be used in Chapter V to help explain the quantitative results which are presented in Chapter IV. In addition, these observations will be taken into account in a discussion of the cavitation nucleus.

## Chapter IV

### EXPERIMENTAL RESULTS

#### Cavitation Thresholds

The experimentally determined cavitation threshold pressures are presented in this chapter. The thresholds were measured for distilled water and tap water as a function of acoustic frequency. The ambient hydrostatic pressure, equilibrium air saturation pressure, and the maximum solid particle size present in the water are all parameters that were varied in the experiment. The water was always at room temperature, which varied between 19.5°C and 22°C.

The cavitation threshold was found to vary smoothly as a function of frequency. As a result, it was possible to obtain an accurate representation of the frequency dependence of the threshold by measuring at frequencies separated by about one octave. The frequencies employed were: 27 kc/s, 46 kc/s, 82 kc/s, 183 kc/s, 353 kc/s, 690 kc/s, and 1.16 Mc/s. The precise frequencies varied about  $\pm 4\%$  from these nominal values because of small changes in the resonance frequencies caused by temperature fluctuations.

The maximum size of solid particles in the samples was determined by filtering the water through filters of known pore size. There was no measurable difference in the cavitation thresholds of the samples of water that had been filtered and those that had not been filtered. For the sake of uniformity, however, all of the samples used for threshold measurements were filtered through the smallest pore size filter, 0.45  $\mu$ .

The experimental cavitation threshold pressures for water as a function of frequency are plotted in Figs. 13 through 17. The same information is presented in tabular form in Table III. The ambient

TABLE III  
Experimental cavitation thresholds for water (in bars)

air saturation pressure (mm Hg)	frequency (kc/s)						
	27	46	82	183	353	690	1160
760	0.45*	1.2*	1.9*	2.8*	6.0	14.0	32.4
700	0.69*	1.8*	2.9*	4.1	6.7	15.2	34.5
250	3.1	3.5	4.1	4.5	6.8	15.2	35.0
100	8.1	4.9	4.2	4.8	7.2	16.0	35.0
10	-	12.1	6.2	5.0	7.2	16.0	35.0

\* indicates the formation of gas bubbles.

hydrostatic pressure was 1 bar in each case. The data in the figures represent the cavitation threshold pressures in samples of water with varying equilibrium air saturation pressures. The values of this parameter are, sequentially, 10 mm Hg, 100 mm Hg, 250 mm Hg, 700 mm Hg, and 760 mm Hg.

The data points on these figures are coded to indicate which kind of cavity motion was observed at the frequency and equilibrium air saturation pressure represented by the point. The open circles represent the threshold pressures required to form transient cavities, and

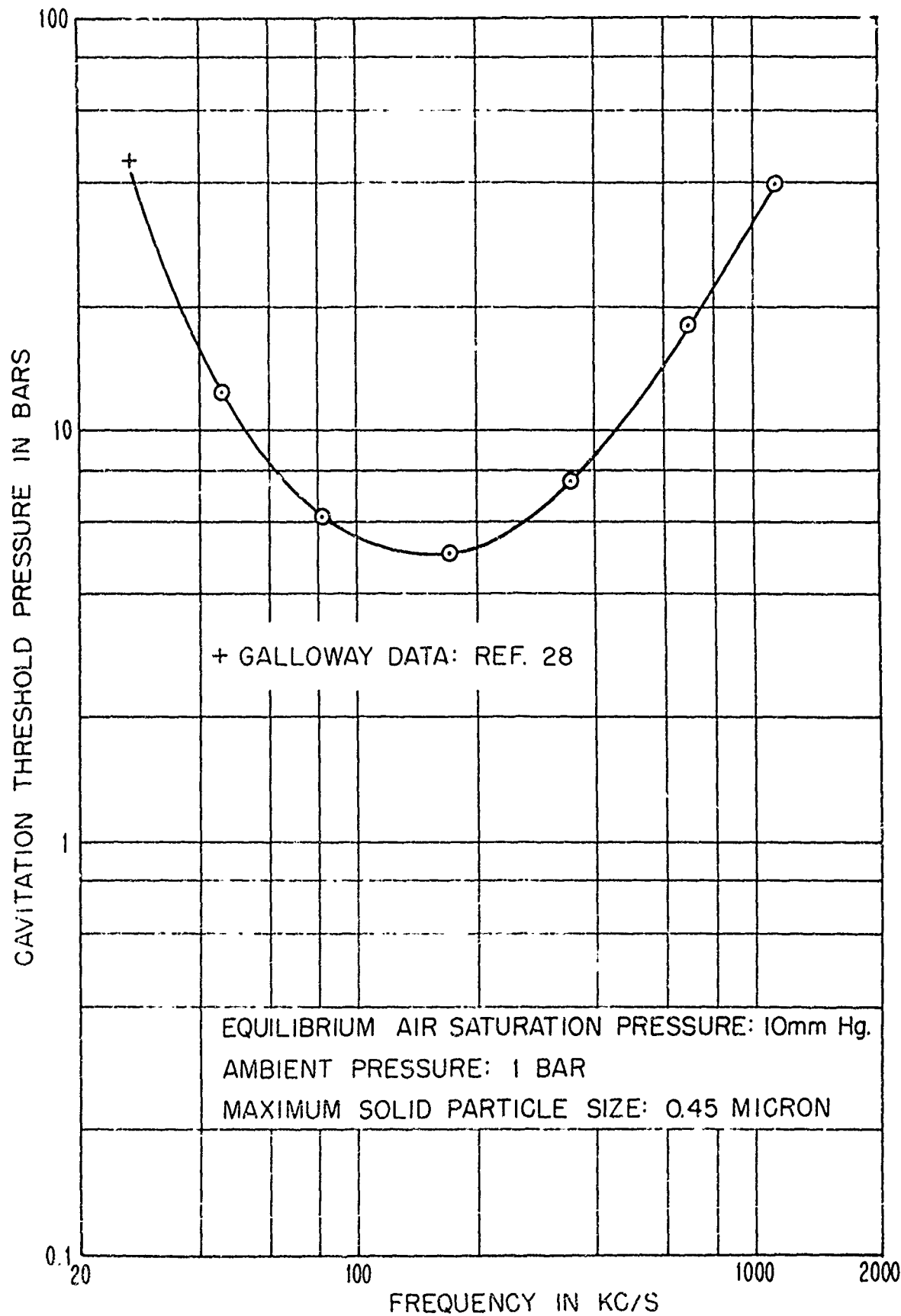


FIG 13 CAVITATION THRESHOLD FOR WATER

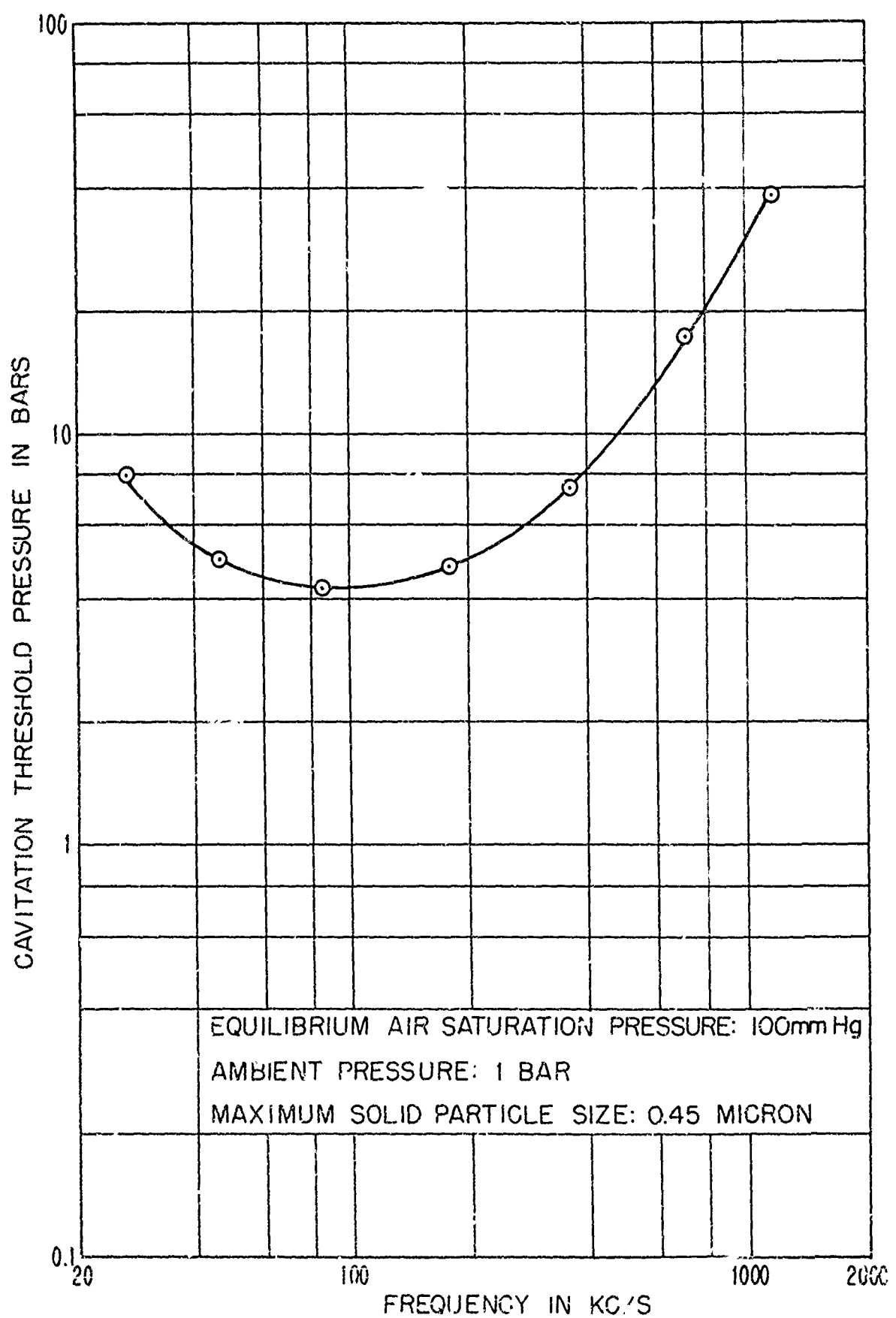


FIG. 14 CAVITATION THRESHOLD FOR WATER

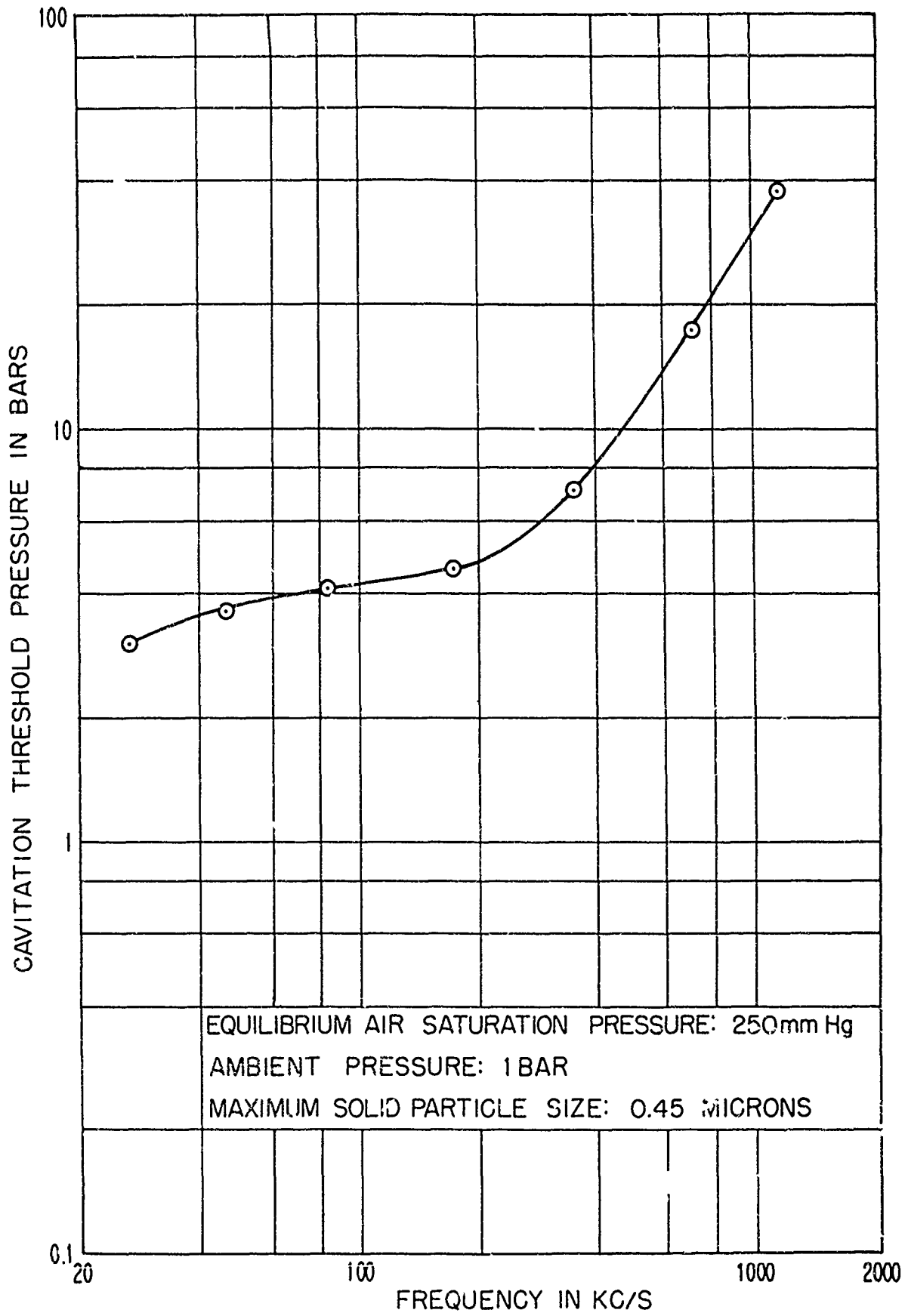


FIG. 15 CAVITATION THRESHOLD FOR WATER

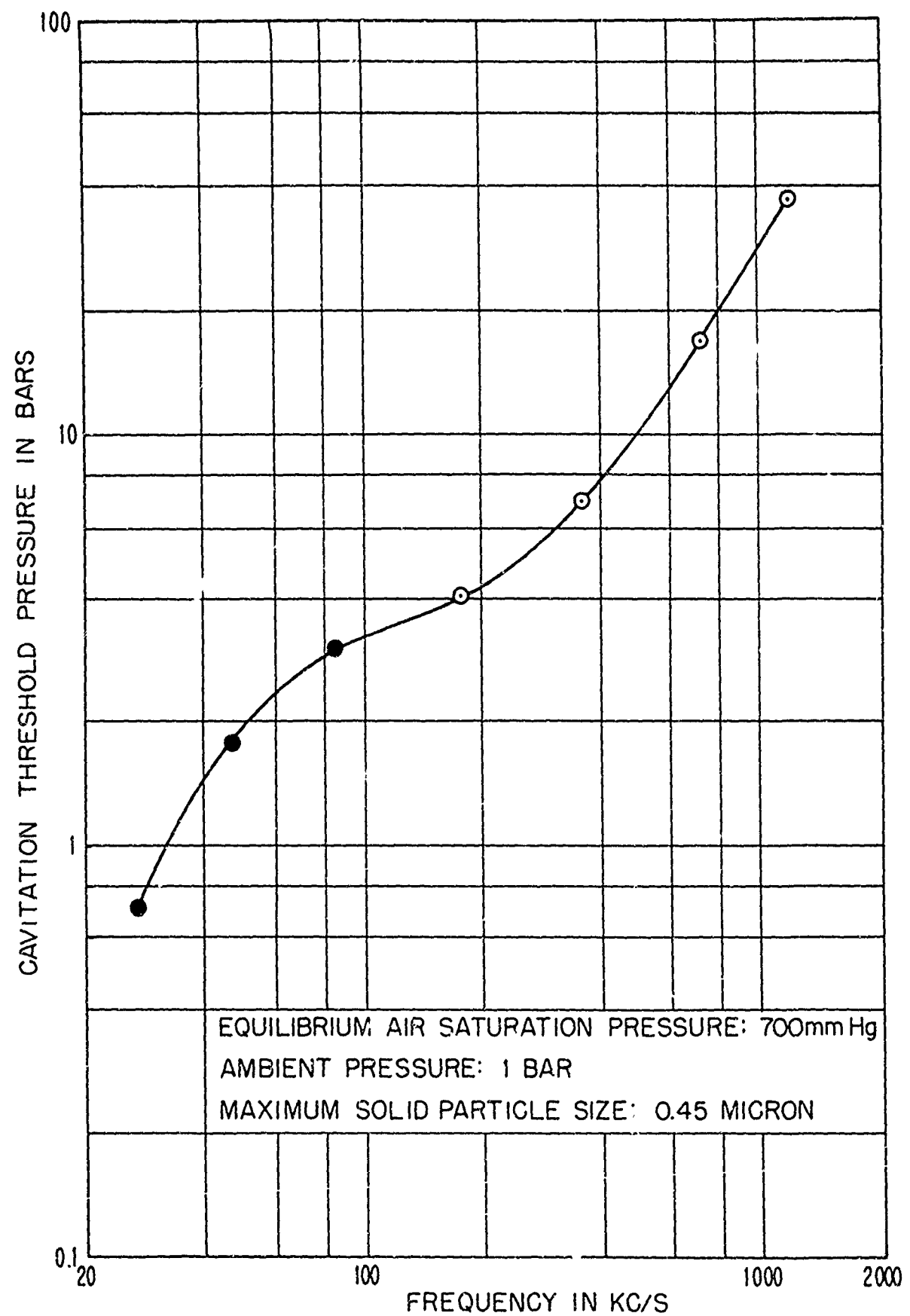


FIG. 16 CAVITATION THRESHOLD FOR WATER

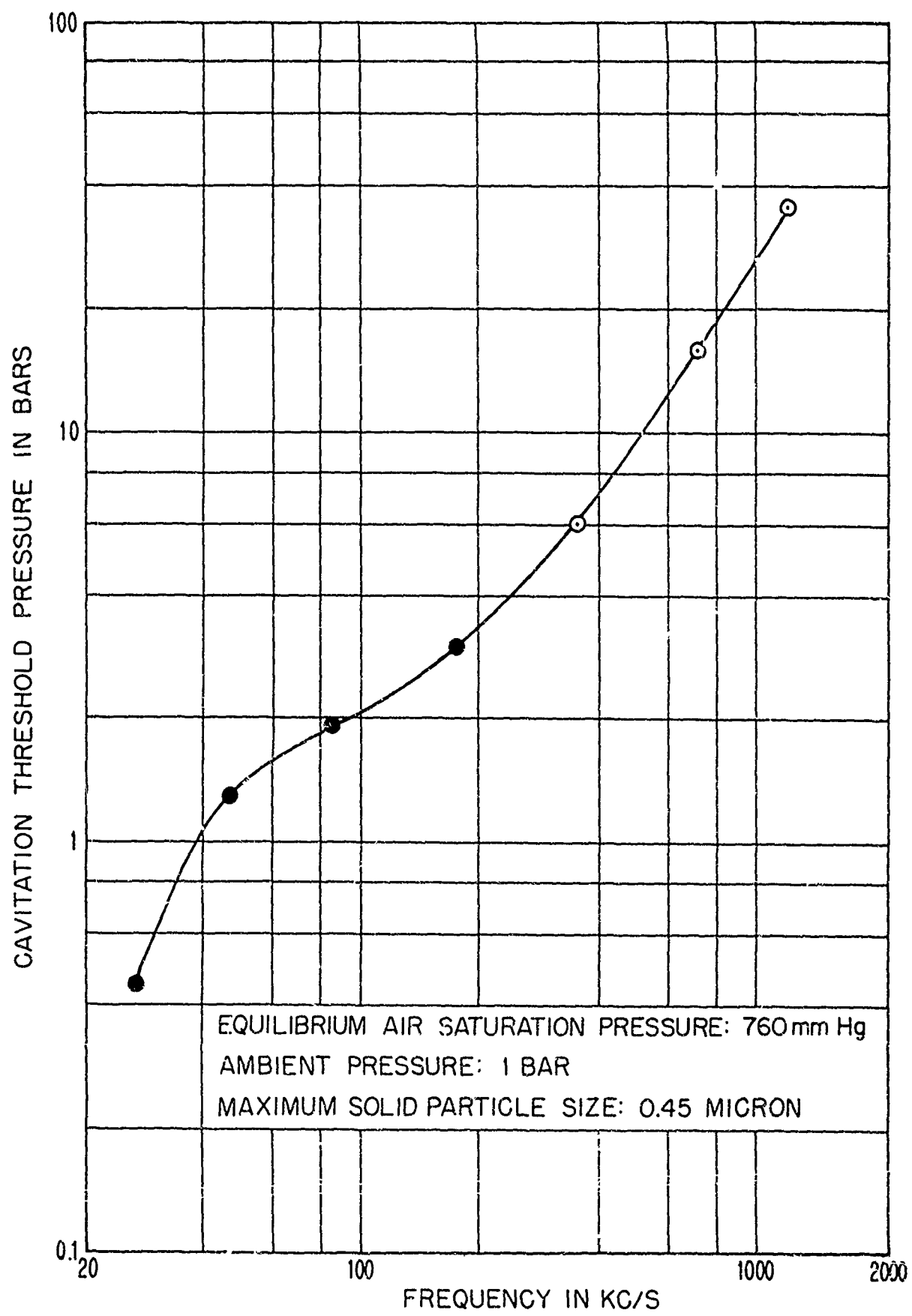


FIG. 17 CAVITATION THRESHOLD FOR WATER

the filled-in circles represent the threshold pressure required to form stable cavities, or air bubbles.

The cavitation thresholds at 27 kc/s that I have measured are tabulated in Table III. These thresholds are within 1.5 dB of Galloway's data\* at 26.3 kc/s. It was not possible to produce acoustic pressures larger than 10 bars at 27 kc/s with my apparatus. For an equilibrium air saturation pressure less than about 100 mm Hg, the threshold is greater than 10 bars at 27 kc/s. The point on Fig. 13 at 27 kc/s corresponds to Galloway's data at an equilibrium air saturation pressure of 10 mm Hg. The minima in the data which result from the large cavitation threshold pressures at low frequencies in degassed water were not anticipated by Esche's data.<sup>†</sup>

The cavitation threshold at 1.16 Mc/s was found to be  $35 \pm 1.9$  bars and to be independent of the amount of dissolved air, provided the water was not supersaturated with dissolved air. At 690 kc/s the threshold pressures were found to be  $16 \pm 0.9$  bars, also independent of the amount of dissolved air. At 353 kc/s, however, the threshold of degassed water was about 20% higher than the threshold of water saturated with air at the ambient pressure. At 183 kc/s and lower the cavitation thresholds were a function of the dissolved air content of the water. At these frequencies the thresholds of degassed water were higher than the thresholds of gassy water.

A minimum in the threshold pressure as a function of frequency occurred for the two most completely degassed samples. For water with

---

\* W. I. Galloway, Reference 28, cited on p. 23.

† R. Esche, Reference 44, cited on p. 29.

an equilibrium air saturation pressure of 10 mm Hg the minimum occurred at about 200 kc/s. When the equilibrium air saturation pressure was increased to 100 mm Hg the minimum shifted to about 80 kc/s. The threshold data for further increases of the equilibrium air saturation pressure did not show a minimum, but continued to decrease with decreasing frequency.

It has been mentioned that the data at 27 kc/s agree with the data reported by Galloway within the limited pressure range of my equipment at that frequency. The data above about 300 kc/s show good qualitative agreement with the data reported by Esche (see Fig. 1), the numerical values of Esche's thresholds being slightly higher than the thresholds that I have measured. For example, at 1 Mc/s Esche reports the median value of his measurements to be about 40 bars, while the threshold pressure I measured at 1.16 Mc/s is about 35 bars. It is also to be noted that both Esche's and my data approach a slope of 12 dB per octave at 1 Mc/s.

Some further comparisons of the thresholds on Figs. 13 through 17 with the thresholds plotted on Fig. 1 are interesting. Blake\* measured the cavitation threshold in water at about 60 kc/s. He measured a threshold of 2.5 bars for water that was saturated with air at atmospheric pressure. The corresponding point of Fig. 17 is 1.8 bars. At an equilibrium air saturation pressure of just over 250 mm Hg he measured a threshold of 3.6 bars, which corresponds exactly to the threshold at 60 kc/s on Fig. 15. The maximum threshold he obtained by degassing was

---

\* F. G. Blake, Jr., Reference 13, cited on p. 7.

10 bars. This compares with the point at 60 kc/s on Fig. 13, which is about 9 bars.

#### Cavitation Threshold as a Function of Ambient Pressure

The cavitation threshold was also measured as a function of ambient pressure at two different frequencies and two different equilibrium air saturation pressures. The results are plotted on Fig. 18. It can be seen that the cavitation threshold remains constant for ambient pressures between 1 bar and a pressure that is about twice the air saturation pressure. At lower air saturation pressures the threshold decreases to 1 bar or less.

The threshold pressures at 164 kc/s (this frequency corresponds to the second lower mode than the one used in the threshold measurements at 183 kc/s) are very nearly the same at 1 bar ambient pressure because the equilibrium air saturation pressure has little effect on the threshold at this frequency. The measurements were terminated at the ambient pressures shown because lower ambient pressures caused air bubbles to form in the water instead of transient cavities. These air bubbles were formed at acoustic pressures of about 1 bar.

The threshold pressures at 46 kc/s are quite different at 1 bar ambient pressure because the equilibrium air saturation pressure has a strong effect on the cavitation threshold at this frequency. The sample for which the air saturation pressure was 0.014 bar (approximately 10 mm Hg) formed bubbles below an ambient pressure of about 7.0 mm Hg. The cavitation threshold at an ambient pressure of 7.6 mm Hg was 1 bar. The

sample for which the air saturation pressure was 0.13 bar (approximately 100 mm Hg) formed bubbles below an ambient pressure of about 76 mm Hg. It was possible to measure a cavitation threshold of about 0.6 bar before the bubble formation began.

In all cases the cavity motions at an ambient pressure represented by the horizontal portions of the curves in Fig. 18 were typical of transient cavities. The cavity motions at ambient pressures represented by the descending portions of the curves were intermediate between transient and stable cavity motion. The cavity would form and collapse relatively slowly, and a small bubble would remain at the point of collapse for a short time. At ambient pressures at the terminal points on the curve, stable cavities would form slowly, with no collapse.

#### Number of Cavitation Events Produced as a Function of Acoustic Pressure

It was mentioned in Chapter III that the cavitation process did not always proceed indefinitely in a sample of water at a given acoustic pressure. This effect was examined in detail for several samples of water which were all degassed at an equilibrium air saturation pressure of 100 mm Hg. The acoustic frequency was 82 kc/s. The results of this experiment are exhibited in Fig. 19.

To measure these curves the acoustic pressure was first set at about 4 bars, which is just below the threshold value (see Table III). The water in the system was circulated by a flow of  $10 \text{ cm}^3/\text{sec}$  through the peristaltic pump. Initially, the acoustic pressure was increased to 6 bars. Each cavitation event that occurred was totalized on the

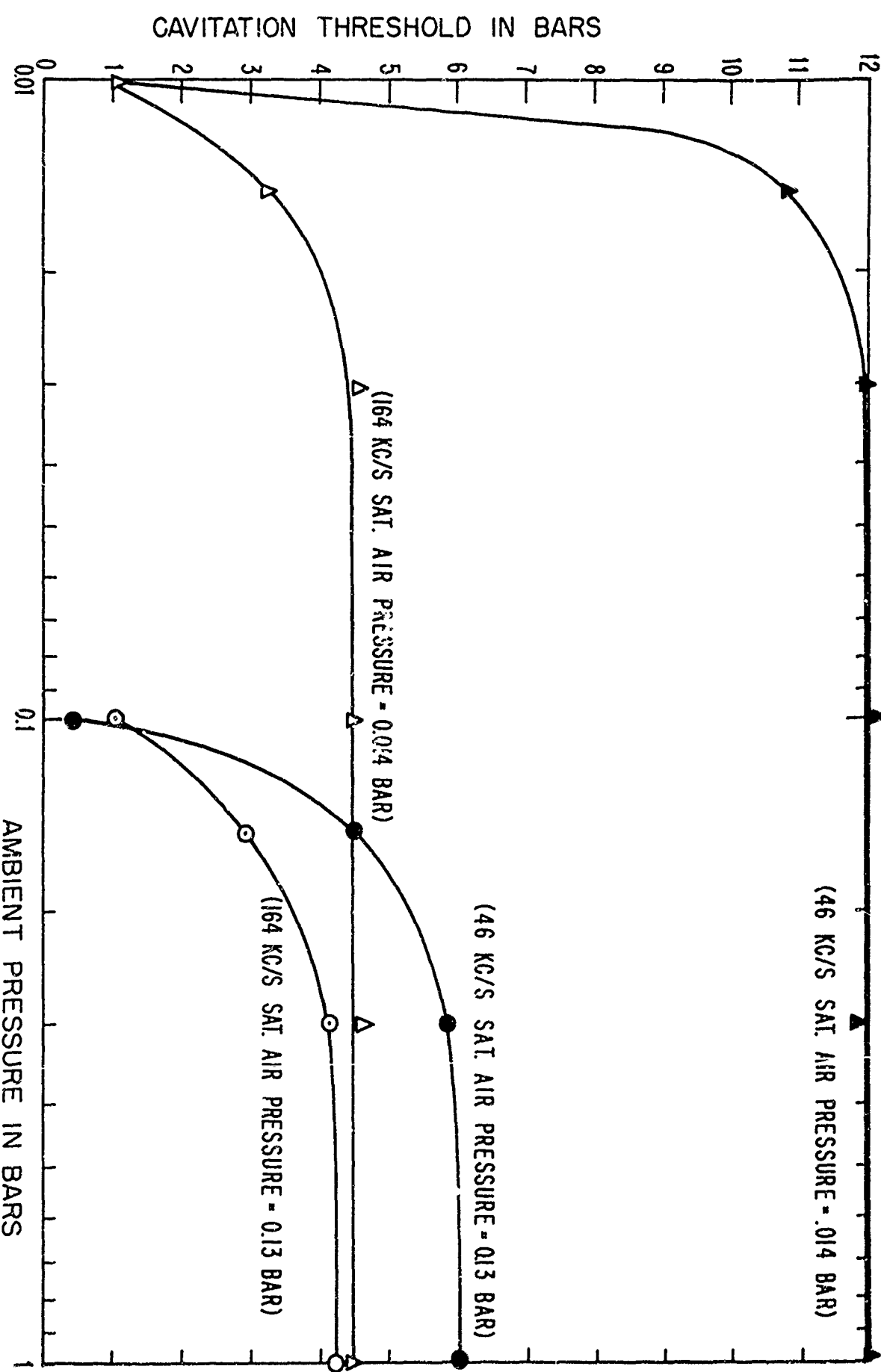


FIG. 18 CAVITATION THRESHOLD AS A FUNCTION OF AMBIENT PRESSURE.

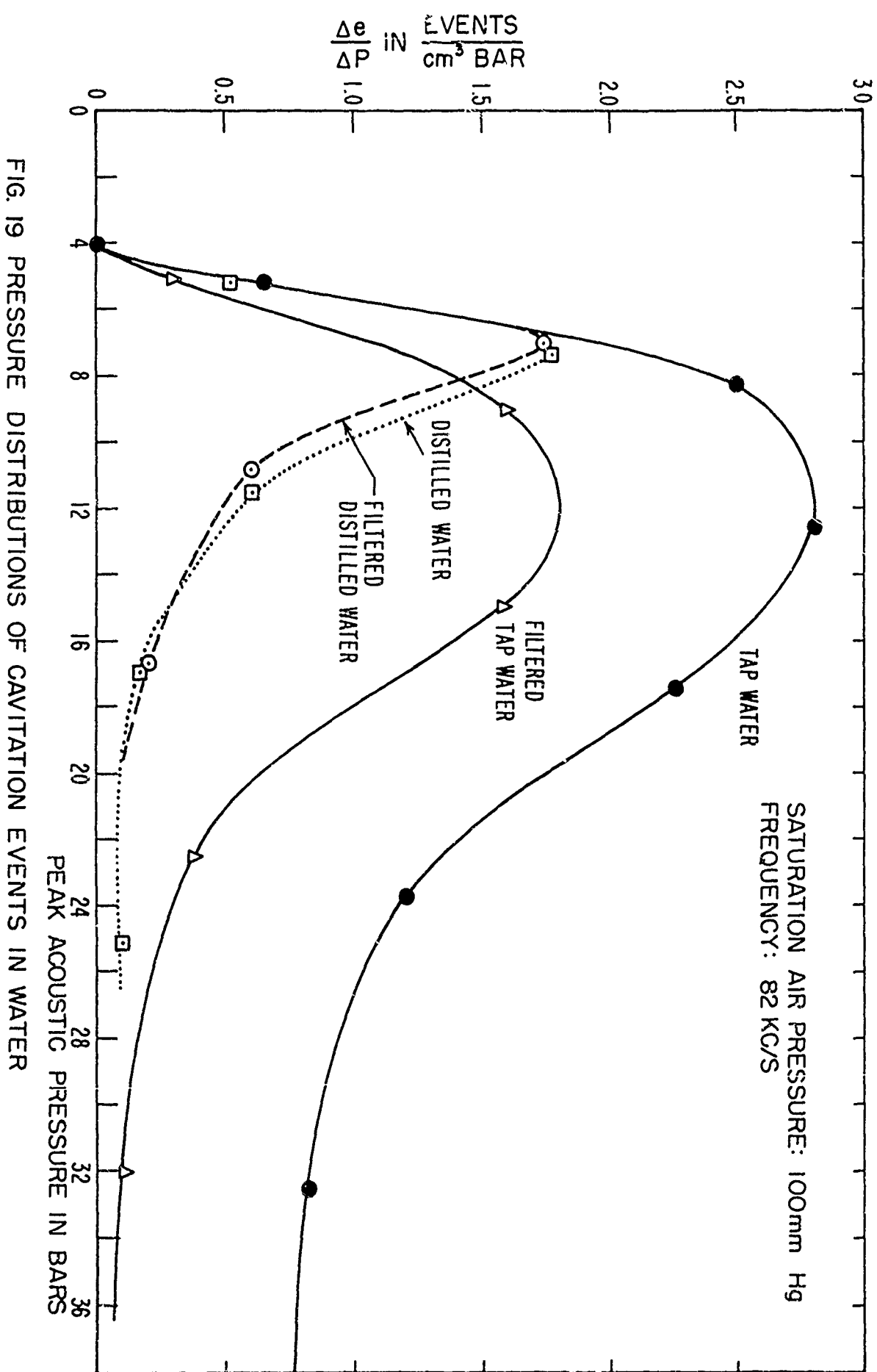


FIG. 19 PRESSURE DISTRIBUTIONS OF CAVITATION EVENTS IN WATER

12

electronic counter. The acoustic pressure was held constant until no further cavitation events occurred.

It took as long as five hours in some cases for the cavitation events to cease, but at least two hours were required in every case. The volume of water that was circulated during the experiment was at least 72 liters, and never more than 180 liters. A very turbulent flow pattern in the spherical resonator was produced by the water flow through the inlet and outlet connections on the top. Since the volume of water circulated was at least 36 times the volume of the water in the resonator, it was assumed that all of the water passed through the focal region at least once during the time of the experiment.

When the cavitation events had ceased, it was assumed that all of the nuclei in the 2-liter sample capable of producing a cavitation event in the pressure range  $\Delta P$  between 4 and 6 bars had been exhausted. The number of events  $\Delta E$  that had been counted was divided by the volume of the sample to obtain  $\Delta e$ , the number of events per  $\text{cm}^3$  of water. The ratio of  $\Delta e$  to  $\Delta P$  is plotted in Fig. 19. The abscissa is the average value of the two limiting pressures of  $\Delta P$ . Thus, the first data points are plotted at  $P = 5$  bars.

After all cavitation events had ceased, the acoustic pressure was increased further by another increment  $\Delta P$ . This increment was chosen to provide an initial cavitation rate that could be accurately counted by the counting apparatus, and was approximately equal to the initial rate of cavitation that occurred when the pressure was raised from 4 to 6 bars. As before, the acoustic pressure was held constant until the cavitation ceased.

123

The continuation of this process determined the curves plotted in Fig. 19. When the acoustic pressure was about 15 bars or more, it was found that the cavitation rate did not become zero, no matter how long the water was cavitated. As before, the pressure increment  $\Delta P$  was selected to produce a particular initial cavitation rate of about 10 events/sec. At 15 bars peak acoustic pressure the cavitation rate decreased from 10 events/sec to 0.089 events/sec in a period of about 2 hours, and it was found that this terminal cavitation rate remained constant in time. In order to proceed with the curves in Fig. 19, at acoustic pressures larger than 15 bars, only those cavitation events were counted that occurred in the period when the cavitation rate was larger than 10% of the initial rate.

The observation that the cavitation rate cannot be reduced to zero by cavitating at acoustic pressures larger than 15 bars indicates that there are at least two kinds of cavitation nuclei. One type of nucleus can apparently be destroyed by cavitation; the other cannot. The scheme used for counting the events occurring at acoustic pressures greater than 15 bars was an attempt to separate cavitation events caused by the two kinds of nuclei. The curves in Fig. 19, therefore, represent the number of nuclei of the kind that can be destroyed as a function of the acoustic pressure required to rupture them.

The total area under the curves of  $\Delta e/\Delta P$  for  $P < P_m$  represents the total number of events that can be produced in one  $\text{cm}^3$  of water by an acoustic pressure  $P_m$ . For  $P_m = 38$  bars, the total number of cavitation events produced in the two-liter samples of water are listed in Table IV.

TABLE IV

Total number of cavitation events produced in two liters of water  
by an acoustic pressure of 38 bars

Tap water	342 000
Tap water ( $1 \mu$ filter)	189 000
Tap water ( $0.45 \mu$ filter)	90 500
Distilled water	30 000
Distilled water ( $0.45 \mu$ filter)	29 800

The total number of events produced per  $\text{cm}^3$  in the various samples are plotted as a function of the reciprocal of the maximum particle size in Fig. 20. The first point on this curve represents the unfiltered tap water. The maximum particle size was estimated to be  $10 \mu$ , although the position of the point will not be affected much by larger particle sizes because of the reciprocal scale of the abscissa. The next two points represent the tap water samples filtered by the  $1 \mu$  and  $0.45 \mu$  filters, respectively. The point on the right-hand end of the curve represents the distilled water. Since filtering the distilled water with a  $0.45 \mu$  filter had a negligible effect on the number of events produced, the maximum particle size that can affect cavitation must have been less than or equal to  $0.45 \mu$ . The range of the abscissa which is indicated for this point represents the assumed range over which the maximum particle size might be expected to vary. The range is centered on one-third micron.

Statistical Distribution of the Time Between Cavitation Events

It was noted in the previous section that a definite terminal rate of cavitation occurred at acoustic pressures above about 15 bars. An experiment was conducted to investigate the effect of a paraffin screen on the terminal cavitation rate. Since this type of experiment is evidently a statistical one, it was necessary to determine the statistics of the time history of the cavitation process in the resonator.

A sample of distilled water whose equilibrium air saturation pressure was 350 mm Hg was cavitated for 40 minutes at an acoustic pressure of 16 bars and a frequency of 82 kc/s. The events were recorded as a function of time by the Brüel and Kjaer level recorder. A total of 264 events was recorded. The time intervals  $\tau$  between successive events were measured. The number of successive events that occurred within a time interval  $\tau$  and  $\tau + \Delta\tau$  was plotted as a function of  $\tau$ . The results of this experiment are plotted in Fig. 21. The time increment  $\Delta\tau$  was chosen to be one second.

It is known that for a process for which the events are statistically independent random variables, the probability of obtaining  $K$  events in a time  $\tau$  is given by the Poisson probability distribution.<sup>57</sup>

$$P(K, \tau) = \frac{(\bar{n}\tau)^K \exp(-\bar{n}\tau)}{K!}, \quad (4-1)$$

where  $\bar{n}$  is the average number of events per second. If  $K$  is considered to be a parameter and  $\tau$  the variable, one can ask the question: What is the probability that the  $K$ th event occurs between  $\tau$  and  $\tau + \Delta\tau$ ? Since

---

57. W. B. Davenport and W. L. Root, Random Signals and Noise, p. 117 (McGraw-Hill, New York, 1958).

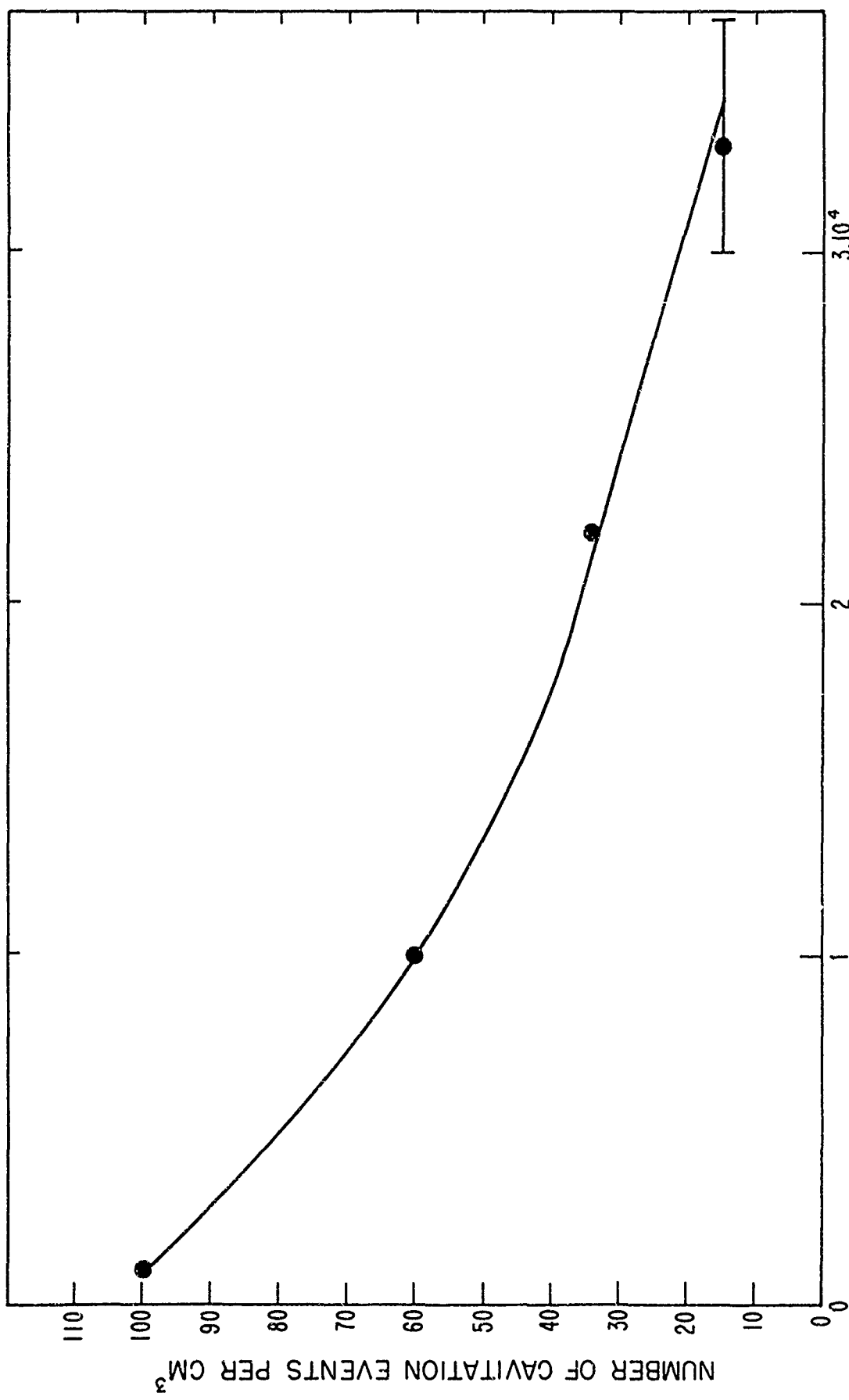


FIG. 20 NUMBER OF CAVITATION EVENTS/CM<sup>3</sup> AS A FUNCTION OF THE MAXIMUM FOREIGN PARTICLE SIZE.

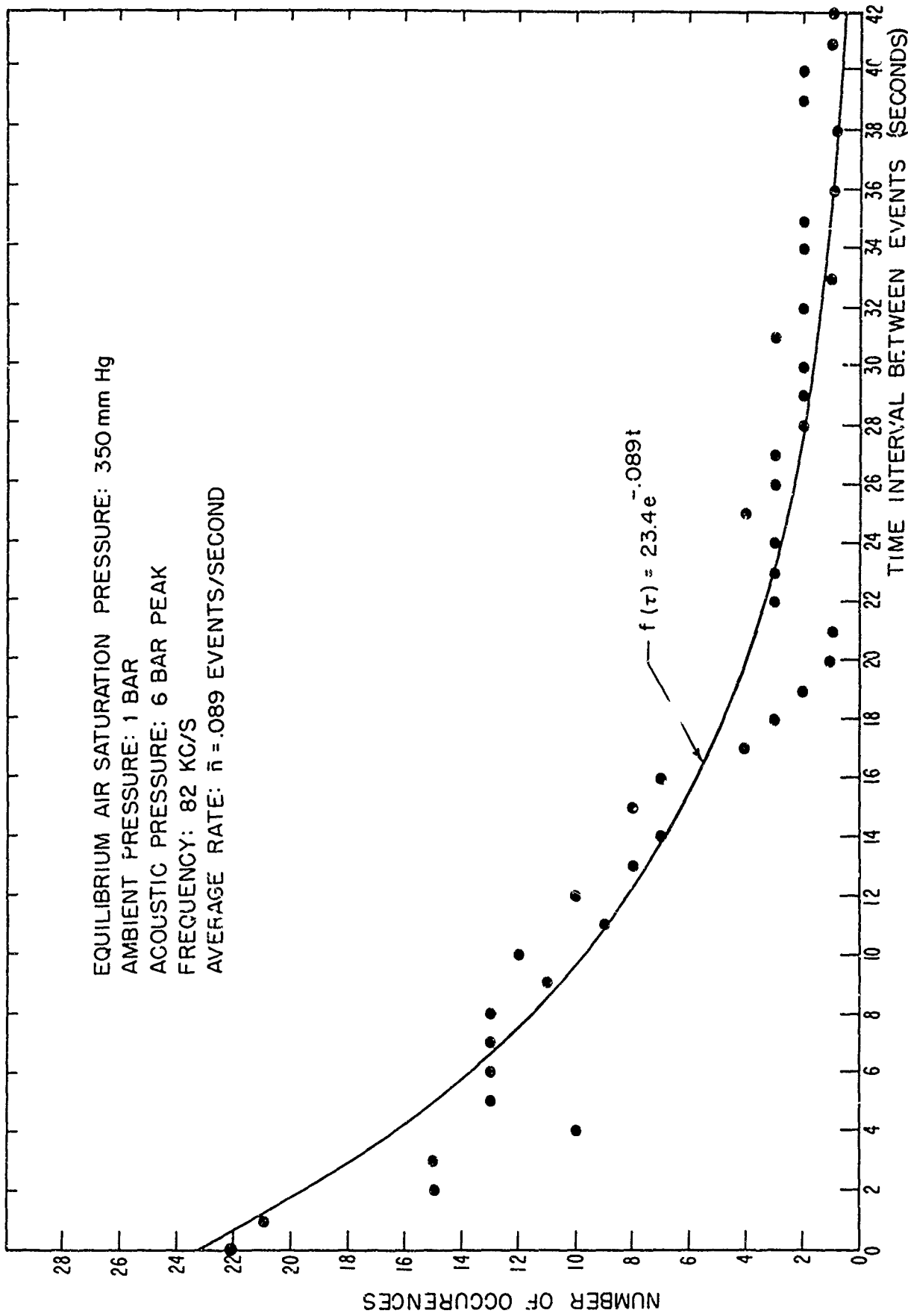


FIG. 2I DISTRIBUTION OF INTERVAL BETWEEN EVENTS

28

the events are statistically independent, this probability is given by the product of the probability to have  $K-1$  events in time  $\tau$  and the probability to have 1 event in the time interval  $\Delta\tau$ . This result can be calculated from Eq.(4-1). Under the assumption that  $\bar{n}\Delta\tau \ll 1$ , we have

$$f_K(\tau)\Delta\tau = \frac{(\bar{n}\tau)^{K-1}}{(K-1)!} \exp(-\bar{n}\tau) \bar{n} \Delta\tau , \quad (4-2)$$

where  $f_K(\tau)$  represents the probability density function of the waiting time  $\tau$  for the  $K$ th event. The probability distribution of the waiting times for the first event can be obtained from Eq.(4-2) by taking  $K=1$ . The result is

$$f_1(\tau)\Delta\tau = \bar{n} \exp(-\bar{n}\tau)\Delta\tau , \quad (4-3)$$

where  $f_1(\tau)\Delta\tau$  is the probability that the first event occurs between  $\tau$  and  $\tau + \Delta\tau$ . Since  $f_1(\tau)$  is a probability density,  $\int_0^\infty f_1(\tau)d\tau = 1$ . The data shown in Fig. 21 are not normalized, so it is necessary to multiply the probability density function by the total number of events, 264. The average cavitation rate over the duration of this experiment was 0.089 events/sec. The probability density function for waiting  $\tau$  seconds to observe the first event is then given by

$$f_1(\tau) = (264)(0.089) \exp(-0.089\tau) . \quad (4-4)$$

Equation (4-4) is plotted in Fig. 21. The good agreement between the data and Eq.(4-4) supports the conclusion that the occurrence of the cavitation events is governed by a Poisson probability distribution. The waiting times between events are, therefore, statistically independent random variables.

### The Effect of a Paraffin Screen on the Cavitation Rate

In a preceding section it was found that the cavitation rate at acoustic pressures greater than about 15 bars did not approach zero, no matter how long the water was cavitated. The terminal rate of cavitation was found to persist as long as the experiment was continued. The cavitation events that occur after the terminal rate of cavitation has been achieved appear to arise from nuclei that cannot be destroyed by the cavitation process. The experiment outlined in this section was conducted to see if the terminal rate of cavitation could be altered by shielding the water with a paraffin screen 3 cm thick.

Figure 22 shows the time history of the experiment conducted with the paraffin screen. The ordinate is the total number of events as a function of time. The time at which the paraffin screen was placed around the resonator, and the time it was removed, are indicated on the abscissa.

The cavitation process has been shown to be a random process with a Poisson probability distribution. For this type of process the standard deviation from the mean is the square root of the average number of events. The data in Fig. 22 have been fitted with three different straight lines, each representing a constant cavitation rate. The standard deviations from the mean,  $\sigma$ , represented by these lines are also plotted. and it can be seen that the data lie inside the standard deviations for the particular choice of lines fitted to the data. There is some latitude in the choice of these rate lines, but it can be clearly seen that there is no single straight line that can be made to pass

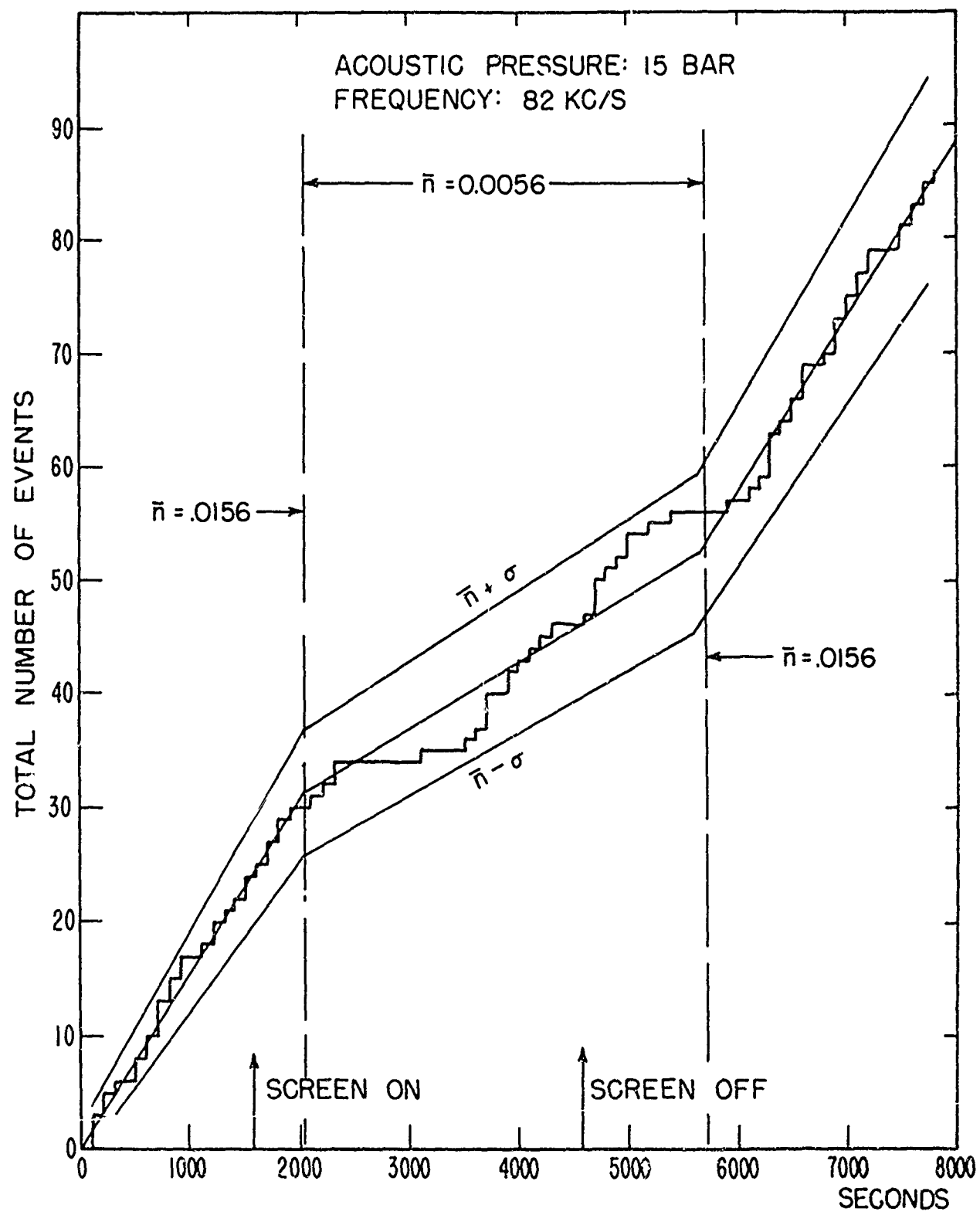


FIG.22 TIME HISTORY OF CAVITATION EVENTS SHOWING EFFECT OF PARAFFIN SCREEN.

through all the data and for which the data will lie between the standard deviations.

The presence of the paraffin screen can be seen to decrease the rate of cavitation by a factor of about three. The cavitation rate that was obtained after the screen was removed was the same as the cavitation rate before the screen had been put in place. There was a time lag before the effect of the screen was reflected in the cavitation rate.

The water sample which was used in this experiment had been previously cavitated for a sufficient length of time at an acoustic pressure of 15 bars so that the cavitation events which occurred were not nucleated by the type of nucleus which can be destroyed by cavitation. The terminal rate of cavitation was constant in time, except when the paraffin shield was placed around the water sample. The reduction of this terminal cavitation rate by the presence of the paraffin shield seems to support the conclusion that the cavitation nuclei that cannot be destroyed by cavitation are continuously created by high-energy particles entering the water. The time lag between the application or removal of the shield and the change of the cavitation rate suggests that these nuclei have a finite lifetime. No further experiments concerning the effects of shielding were conducted, as this was not the primary objective of this investigation. These results are presented, however, in order to show the relative importance of this effect on the behavior of acoustic cavitation in water.

## Chapter V

## DISCUSSION OF THE RESULTS

The nature of the cavities that are formed in water by an acoustic pressure field depends mostly on the frequency and the dissolved gas content of the water. The minimum acoustic pressures required to form these cavities are plotted in Figs. 13 through 17. An examination of these threshold data suggests a natural separation of the parameter variation into three regions. These regions are defined as follows:

Region A ( $P_a < 3$  bars;  $f < 200$  kc/s)

The measured thresholds in this region correspond to the acoustic pressures required to form air bubbles in water. Air bubbles are formed only in relatively gassy water.

Region B ( $P_a > 3$  bars;  $f < 200$  kc/s)

The measured thresholds in this region correspond to the acoustic pressures required to form visible transient cavities. The threshold is a function of the dissolved gas in the water in this region.

Region C ( $P_a > 3$  bars;  $f > 200$  kc/s)

The measured thresholds in this region correspond to the acoustic pressures required to form transient cavities that are detected acoustically, but cannot be seen. The threshold is not a function of the dissolved gas in the water in this region.

Since the nature of the cavities and the dependence of the threshold on gas content and frequency are different in each region, the measured cavitation thresholds will be discussed separately for each region. In addition, the characteristic motions of the cavities will be discussed.

The Threshold for the Formation of Gas Bubbles (Region A)

We will discuss first the thresholds that lie in region (A). It is appropriate to recall the description of the events that occur when air bubbles are formed. A typical datum point in region (A) defines a threshold pressure of 0.45 bar and a frequency of 27 kc/s in water saturated with air at atmospheric pressure. Under these conditions a small bubble whose radius was estimated to be about  $40 \mu$  formed in the region of the focus. This bubble was observed to drift slowly toward the focus, where its radius increased for a period of about one minute. After the short period of bubble growth the bubble surface became frosted, and the bubble began to fluctuate rapidly about the focus. The oscillating bubble was then ejected from the focus, and came to rest at the nearest pressure node. The bubble remained at the node until the pressure was reduced by a factor of about three, after which the bubble rose to the surface.

The first question that we can ask is: How did the bubble grow from sub-visible size to a diameter of  $80 \mu$ ? As a first step in answering this question we must consider the nucleus from which the bubble was formed. In Chapter III it was concluded that cavitation nuclei are small air- or vapor-filled cavities stabilized in cracks on the surface of small particles suspended in the water. Since the water was filtered through a  $0.45 \mu$  filter, it can be assumed that the diameter of these particles must have been less than about  $0.5 \mu$ . It is probable, therefore, that the radius of the small bubbles that were drawn from these cracks was less than about  $0.2 \mu$ .

. 34

Since the bubble that was observed had a mean radius of about  $40\mu$ , it is clear that some mechanism must exist by which the air content of the bubble can increase when the bubble is situated in an acoustic pressure field. This mechanism is undoubtedly rectified diffusion of air into the bubble as it oscillates in the acoustic pressure field. The phenomenon is explained as follows: When the bubble is expanded beyond its equilibrium radius the pressure of the air in the cavity is less than the equilibrium air saturation pressure in the surrounding liquid, and air diffuses into the cavity. When the bubble is contracted below its equilibrium radius the air pressure in the bubble is greater than the equilibrium air saturation pressure in the surrounding liquid, and air diffuses out of the bubble. But the bubble surface area is larger when air diffuses in than it is when air diffuses out. Thus, the bubble experiences a net gain of air during each cycle of motion.

Several calculations have been made to determine the mass transfer of gas by rectified diffusion. The most complete calculations have been presented by Hsieh and Plesset.\* These authors derive the following expression for the rate of influx of mass into the bubble by rectified diffusion:

$$\frac{dm}{dt} = \frac{8\pi}{3} D C_o R_o t^2 , \quad (5-1)$$

where  $D$  is the diffusivity of the gas through the liquid (for air in water,  $D = 2 \times 10^{-5} \text{ cm}^2/\text{sec}$ );  $C_o$  is the concentration of dissolved gas in the liquid when it is saturated at the static pressure  $P_o$ ;  $R_o$  is the

---

\* D.-Y. Hsieh and M. Plesset, Reference 22, cited on p. 17.

average radius of the bubble; and  $\epsilon$  is the ratio of the acoustic pressure amplitude to the ambient pressure. Equation (5-1) was derived under the assumption that  $\epsilon \ll 1$ , which implies small amplitude linear oscillations. It is also assumed that the bubble is in stable equilibrium at the radius  $R_o$ ; i.e.,  $P_{gi} + P_v = P_o + 2\sigma/R_o$ , where  $P_{gi}$  and  $P_v$  are the gas pressure and the vapor pressure. In the absence of sound, therefore, gas would diffuse out of the bubble because the pressure of the gas in the bubble is larger, by the surface tension pressure, than the ambient pressure in the liquid.

If the bubble is to be prevented from dissolving, the gain of air by rectified diffusion must be greater than or equal to the loss of air by the steady outward diffusion. Strasberg<sup>58</sup> found a critical pressure  $P_t$  for which the two rates of mass flow are equal. His result can be expressed

$$\epsilon_t^2 = \left[ \frac{P_t}{P_o} \right]^2 = \frac{3}{2} \left[ 1 + \frac{2\sigma}{R_o P_o} - \frac{C_\infty}{C_o} \right] , \quad \epsilon \leq 0.25 \quad (5-2)$$

where  $C_\infty$  is the actual concentration of dissolved gas in the liquid far from the bubble and  $\sigma$  is the surface tension. The magnitude of  $\epsilon_t$  is limited by the assumption  $\epsilon \ll 1$  that was made in the derivation of Eq.(5-1), on which Eq.(5-2) was based. For water that is saturated with air at the ambient pressure  $P_o = 1$  bar,  $C_\infty = C_o$ , and we find that the inequality  $R_o \geq 39 \mu$  must hold for  $\epsilon \leq 0.25$ . For partially degassed water  $C_\infty < C_o$ , and we find that Eq.(5-2) is limited to even larger values of  $R_o$ .

---

58. M. Strasberg, "Rectified Diffusion: Comments on a Paper of Hsieh and Plesset," *J. Acoust. Soc. Am.* 33, 359 (1961).

The bubbles were observed to grow from sub-visible size, however, so it is evident that Eq.(5-2) cannot be called upon to furnish us with quantitative data.

The actual motion of the sub-visible bubbles will be nonlinear at the acoustic pressure amplitudes we found to be required to form bubbles in region (A). The nonlinearity is caused by the stiffness of the air, which is inversely proportional to the third power of the radius of the bubble. The positive displacements of the bubble surface, therefore, will be larger than the negative displacements. A typical example of such bubble oscillations is provided by a calculation performed by Flynn.\* This calculation shows the oscillations of an air-filled bubble with a radius  $R_0 = 26 \mu$  at an acoustic pressure  $P_a = 1 \text{ bar}$  and a frequency of 83.4 kc/s. The oscillations look very much like a full-wave rectified signal of the same frequency as the acoustic signal. For such nonlinear oscillations, the radius of the bubble is larger than the equilibrium radius for more than half of the period, while the radius of a linearly oscillating bubble is larger than the equilibrium radius for only half of the period. Thus, the inward diffusion will occur over a larger fraction of the period when the motion is nonlinear than when the motion is linear. Rectified diffusion is enhanced, therefore, by the nonlinearity of the motion. A theory of rectified diffusion for bubble oscillations of large amplitude is needed to explain the measured thresholds quantitatively, although the growth of air bubbles from sub-visible size is qualitatively explained by the simple linear theory of rectified diffusion.

---

\* H. G. Flynn, Fig. 16 of Reference 14, cited on p. 8.

### Motion of Small Gas Bubbles in a Radial Sound Field

We will see that the behavior of a gas bubble in a radial sound field depends mostly on the relationship between the frequency of the sound and the resonance frequency of the bubble. The linear resonance frequency of an air bubble in a liquid is given by the following equation,\* which was derived under the assumption that the air in the bubble is compressed isothermally:

$$f_o = \frac{1}{2\pi R_o} \left[ \frac{3P_o + 4\sigma/R_o}{\rho} \right]^{1/2} . \quad (5-3)$$

In this equation,  $R_o$  is the equilibrium radius of the bubble,  $P_o$  is the ambient pressure,  $\sigma$  is the surface tension, and  $\rho$  is the density of the liquid surrounding the bubble. For a bubble radius of  $40 \mu$  in water, at  $P_o = 1$  bar, the resonance frequency is 69 kc/s.

Since the bubble is driven at a frequency well below its resonance frequency, its motion will be primarily controlled by the stiffness of the air. The compression of the air inside a bubble with a  $40 \mu$  radius pulsating at a frequency of 27 kc/s will be approximately isothermal, and the volume of the bubble at any instant can be written

$$V = \frac{P_o V_o}{P_o + P} = \frac{V_o}{1 + (P/P_o)} , \quad (5-4)$$

where the instantaneous pressure in the neighborhood of the bubble has

---

\* B. E. Noltingk, Reference 6, cited on p. 3.

been written as the sum of the ambient ( $P_0$ ) and acoustic ( $P$ ) pressures. The value of the quantity  $P/P_0$  was about one-half for the bubbles observed at 27 kc/s. Under the assumption that  $P/P_0 \leq 1/2$ , Eq.(5-4) can be approximated by

$$R(\tau) = R_0(1 - \frac{1}{3} \frac{P}{P_0}) , \quad (5-5)$$

where  $R(\tau)$  is the instantaneous value of the cavity radius and  $R_0$  is the equilibrium radius of the bubble.

The bubble exists in an acoustic pressure field for which the local acoustic pressure is:<sup>\*</sup>

$$P = P_a \frac{\sin kr}{kr} \sin \tau , \quad (5-6)$$

where  $P_a$  is the peak acoustic pressure at the focus,  $r$  is the radial distance from the focus,  $\tau = wt$ , and  $k$  is the phase constant.

The dimensions of the cavity are small with respect to a wavelength. The acoustic pressure gradient will, therefore, be practically constant over the diameter of the cavity, a situation which exists for a body in a hydrostatic pressure field. The force on the cavity caused by the pressure gradient is, therefore, given by the buoyancy equation:

$$F = -V \nabla P , \quad (5-7)$$

where  $V$  is the volume of the cavity. Since the spatial pressure distribution in the radially symmetric standing wave is a function only of the radius, this force is directed radially.

---

<sup>\*</sup> See Appendix A.

The motion of the bubble will be resisted by a drag force. The nature of the drag force depends on the Reynolds' number of the motion, which for a sphere is defined:

$$R_e = \frac{qd}{v} ,$$

where  $v$  is the kinematic viscosity of the liquid,  $d$  is the diameter of the sphere, and  $q$  is the velocity of the sphere. For water,  $v = 0.012 \text{ cm}^2/\text{sec}$ . The bubbles that were observed had diameters of about  $80 \mu$  and drift velocities less than  $10 \text{ cm/sec}$ . The Reynolds' number, therefore, will be less than 7. In the range of Reynolds' numbers  $0 < R_e < 10$ , the drag force acting on a rigid sphere is given by Stokes' law:

$$D = 6\pi\rho v R q . \quad (5-8)$$

The Stokes' law drag force is computed from the viscous stresses at the boundary of the sphere, assuming that there is no slip between the fluid and the surface of the sphere. For a bubble some slip at the surface can occur, and the drag force can be expected to be smaller. The rigid sphere drag force will be used to approximate the drag of the bubble.

The equation of motion of the bubble is obtained by equating the two forces  $D$  and  $F$  given by Eqs.(5-8) and (5-7). Thus, with the use of Eq.(5-5) for the radius of the bubble, the translational velocity of the bubble is given by

$$q = - \frac{2}{9} \frac{R_o^2}{\rho v} \left(1 - \frac{P}{3P_o}\right)^2 \nabla P . \quad (5-9)$$

Under the assumption that the bubble is situated close enough to the focus so that  $kr \ll 1$ , the acoustic pressure  $P$  and its gradient  $\nabla P$  are, by Eq.(5-6):

$$P = P_a \sin \tau ; \quad P = -\frac{1}{3} P_a k^2 r \sin \tau . \quad (5-10)$$

Substitution of these values into Eq.(5-9) gives:

$$q = \frac{2}{9} \frac{P_a R_o^2}{\rho v} \frac{k^2 r}{3} \left(1 - \frac{P_a}{3P_o} \sin \tau\right)^2 \sin \tau . \quad (5-11)$$

The average velocity of the bubble then becomes:

$$\bar{q} = -\frac{2}{81} \frac{P_o^2 R_o^2 \omega^2}{\rho v P_o c^2} \bar{r} , \quad (5-12)$$

where  $c$  is the speed of sound in water and  $\bar{r}$  is the average position of the center of the cavity.

The average velocity is negative, indicating that the bubble is driven toward the center of the sphere. Equation (5-12) predicts an average velocity of 7 cm/sec for an air bubble of radius  $40 \mu$  located 0.5 cm from the focus with a peak acoustic pressure at the focus of 0.5 bar. This is consistent with my experimental observation that the drift velocity was slightly less than 10 cm/sec.

Equation (5-12) shows that the average bubble velocity will decrease to zero at the focus, where  $\bar{r}=0$ . Thus, the focus (an antinode) is a point of stable equilibrium for a small air-filled cavity located in an acoustic standing wave of frequency less than the resonance frequency of the cavity.

While the bubble is located at the focus it will continue to grow in size by rectified diffusion. The time required for a linearly oscillating bubble to double its size is given by the following result due to

547

Hsieh and Plesset:<sup>\*</sup>

$$t = \frac{9R_o^2 \rho_g}{4C_\infty D\epsilon^2} , \quad (5-13)$$

where  $\rho_g$  is the density of the gas inside the cavity,  $C_\infty$  is the concentration of gas dissolved in the liquid at equilibrium,  $D$  is the coefficient of diffusion of the gas through the liquid, and  $\epsilon$  is the ratio of the maximum pressure variation in the liquid to the ambient pressure.

For the gas bubble considered in the preceding analysis, Eq.(5-13) predicts  $t \approx 120$  seconds. Thus, after two minutes the bubble radius will double. This will cause the bubble resonance frequency to drop to 34 kc/s, which is close to the driving frequency of 27 kc/s. As the bubble approaches resonance size the amplitude of oscillation will increase. This corresponds to the observation that after a period of one or two minutes the bubble surface developed a frosted appearance.

After the cavity has grown to be larger than its resonance size, the cavity will oscillate in phase with the pressure in the neighborhood of the cavity. The amplitude of the oscillations will then be primarily controlled by the mass reactance of the cavity. The calculation of the motion of a mass-controlled cavity is performed in a later section. The final result is shown to be

$$R(\tau) = R_o \left( 1 + \frac{P}{\rho \omega^2 R_o^2} \right) , \quad (5-14)$$

where  $P$  is the acoustic pressure,  $\rho$  is the density of the liquid

\* D.-Y. Hsieh and M. S. Plesset, Reference 22, cited on p. 17.

surrounding the cavity, and  $R_o$  is the average cavity radius about which small oscillations take place. The air bubble at the focus of the resonator was observed to grow to a radius of about 0.5 mm. The peak acoustic pressure was 0.45 bar, and the frequency was 27 kc/s. The ratio of the amplitude of oscillation to the average radius for this bubble is, from Eq.(5-14), equal to  $7.2 \times 10^{-3}$ . It is clear that the linearization process which led to the derivation of Eq.(5-14) is valid for these conditions of bubble oscillation.

The equation for the translational velocity of this enlarged bubble is obtained by equating the forces given by Eqs.(5-7) and (5-8), and by using Eq.(5-14) for the radius of the bubble. The velocity  $q$  is then given by

$$q = -\frac{2}{9} \frac{R_o^2}{\rho} \left(1 + \frac{P}{\rho \omega^2 R_o^2}\right)^2 \nabla P , \quad (5-15)$$

where  $P$  is given by Eq.(5-6). For  $kr \ll 1$  the acoustic pressure  $P$  and its gradient  $\nabla P$  are given by Eq.(5-10). Equation (5-15) becomes

$$q = \frac{2}{27} \frac{P^2 R_o^2 k^2 r}{\rho v} \left(1 + \frac{P}{\rho \omega^2 R_o^2} \sin \tau\right)^2 \sin \tau , \quad (5-16)$$

and the time average of the translational velocity of the bubble becomes

$$\bar{q} \approx \frac{2}{27} \frac{P_a^2}{\rho^2 v c^2} \bar{r} , \quad (5-17)$$

where  $\bar{r}$  is the average position of the bubble.

The average velocity of a bubble whose motion is mass controlled is positive, and thus is directed away from the focus. For the bubble being discussed, Eq.(5-17) predicts that the average velocity of a cavity larger than resonance size will be about 40 cm/sec at a distance of 0.5 cm from the focus. It was observed that the bubble left the center of the resonator at a much larger velocity than the velocity of approach, which is consistent with this calculation.

Since the average velocity of a bubble larger than resonance size is directed away from the focus and is proportional to the distance from the focus, the focus will be a position of unstable equilibrium for the bubble. This fact undoubtedly accounts for the erratic behavior of the bubble about the focal point just prior to the time it was ejected.

The approximation to the pressure and the gradient of the pressure in the acoustic standing wave that was given in Eq.(5-10) is valid only near the focus. Since the cavity will soon approach the region of the nearest pressure node as it moves away from the focus, it is necessary to represent the pressure and the pressure gradient in the region of the nearest pressure node. Since the radial distance to this point from the focus is  $\lambda/2$ , the acoustic quantities can be calculated for  $r = \frac{\lambda}{2} - \xi$ , where  $\xi$  is the distance measured toward the focus from the first pressure node.

From Eq.(5-6) the pressure at  $r = \frac{\lambda}{2} - \xi$ , for  $\xi \ll \frac{\lambda}{2}$ , becomes  $P = P_a \frac{\omega \xi}{\pi c} \sin \tau$ . The pressure gradient near  $r = \frac{\lambda}{2}$  becomes  $\nabla P = -P_a \frac{\omega}{\pi c} \sin \tau$ . To obtain the equation for the translational velocity  $q$  near the first pressure node,  $P$  in Eq.(5-15) is replaced by  $P_a \frac{\omega \xi}{\pi c} \sin \tau$  and  $\nabla P$  is

replaced by  $-P_a \frac{\omega}{\pi c} \sin \tau$ . Equation (5-15) for the translational velocity of the bubble then becomes

$$q = \frac{2}{9} \frac{P_a R_o^2}{\rho v} \frac{\omega}{\pi c} \left(1 + \frac{P_a \xi}{\rho \omega \pi c R_o^2} \sin \tau\right)^2 \sin \tau , \quad (5-18)$$

and the average velocity is

$$\bar{q} = \frac{2}{9} \frac{P_a^2}{\rho^2 v \pi^2 c^2} \xi . \quad (5-19)$$

As the cavity approaches the pressure node,  $\xi$  is positive and the velocity is positive. At the node the velocity is zero. If the cavity is perturbed toward the focus the velocity will be positive, and the cavity will return to the node. If the cavity is perturbed along a radius away from the focus, the velocity will be negative and the cavity will return to the node. Thus, the node is a position of stable equilibrium for a cavity that is larger than resonance size. Since there is no acoustic pressure at the node, however, the cavity oscillations will cease and no additional change in the cavity size can then arise from rectified diffusion. This predicted stability of large bubbles at pressure nodes was observed.

We have seen how the motions of air bubbles that are formed at low acoustic pressures and low frequencies (region A) can be explained by the dynamic forces that act on them. The bubbles grow from sub-visible size by rectified diffusion to resonance size. During the growth phase the bubbles are stabilized at the pressure antinode of the stationary wave system. When the bubble grows to resonance size the pressure

antinode becomes a position of unstable equilibrium, and the bubble dances around the antinode; then it is ejected to the nearest pressure node, which is a position of stable equilibrium. It is necessary to disrupt the standing wave before the buoyancy of the stabilized bubbles can carry them to the surface.

#### The Formation of Transient Cavities at Low Frequencies (Region B)

The cavities formed in region (B) are transient cavities; i.e., the lifetime of the cavity is relatively short (about 10 msec or less). Transient cavities are described in detail in Chapter III. Unlike the air bubbles discussed in the previous section, which produced very little noise, each transient cavity produces a burst of noise in the water when it collapses. In region (B) it was possible to hear the collapse of each transient cavity that was detected visually, both by the unaided ear and by the listening apparatus. We recall that the cavities formed at 82 kc/s appeared to be elongated cracks about 10 mm in length and 1 mm in diameter. When these cavities were photographed with a flash of 1 $\mu$ sec duration the pictures show them to be small spherical cavities, indicating that the elongated appearance was caused by a high translational speed.

The growth of transient cavities in region (B) cannot be explained by rectified diffusion. At least half of the dissolved air had been removed from the water samples in which transient cavities were formed in this region. In addition, the complete collapse of cavities in this region indicates that the air content of the cavities must be negligible with respect to the amount of air that would be necessary to stabilize

the final pre-collapse cavity radius. For these reasons, the growth of the cavities in region (B) cannot be explained by rectified diffusion and must be explained on the basis of the motions of a cavity that contains a relatively small, constant amount of air.

In Chapter I it was shown that the peak negative pressure in the vicinity of a small spherical cavity must be larger than the static strength of the cavity if the radius of the cavity is subsequently to reach a value much larger than the initial radius. The acoustic pressure required to exceed the strength of a small air- or vapor-filled cavity was found to be

$$P_a = P_c + 0.77 \frac{\sigma}{R_0} - P_v , \quad (5-20)$$

where  $P_v$  is the vapor pressure. For a cavity with a radius of  $R_0 = 0.2 \mu$  in water at 1 bar ambient pressure the value given by Eq.(5-20) is  $P_a = 4$  bars. This pressure is close to the minimum pressure of 3.2 bars that was found to be required to form a transient cavity in region (B).

Although most of the measured thresholds were larger than the minimum pressure predicted by the static strength theory, this theory is not consistent with two of the conclusions drawn in Chapter III. It was pointed out that the invariance of the measured threshold with filtration pore size implies that the threshold pressure is independent of the initial radius of cavitation nuclei. But the static strength theory implies that the threshold pressure is inversely proportional to the initial radius. Figures 13 through 17 also show clearly that the cavitation threshold does vary with frequency, whereas frequency does not appear in Eq.(5-20) and the term "static" strength obviously refers to

43

an asymptotic low-frequency measure of strength. It follows that neither the size nor the frequency dependence of the threshold data are explained by the static strength of the cavitation nucleus.

The experimental threshold pressure data increase with decreasing frequency in region (B). It is interesting to extrapolate these threshold pressures to zero frequency. The maximum acoustic cavitation pressure measured by Galloway<sup>58</sup> at 26.3 kc/s was 190 bars. This value was obtained by degassing the water at a pressure of 1 mm Hg. The lowest frequency at which my apparatus was capable of cavitating such completely degassed water was 82 kc/s. At this frequency the maximum cavitation threshold that could be obtained by degassing the water (with an equilibrium air saturation pressure slightly less than 1 mm Hg) was 6.5 bars. If these two points are extrapolated to zero frequency, we obtain a cavitation threshold pressure of 270 bars. This value compares well with the highest reported value of the static strength of water, which is 277 bars.<sup>59</sup> Perhaps the close correspondence between the static measurement and the extrapolated acoustic measurements is an indication of the fact that the state of purity of the water sample used by Briggs was about the same as the purity of the water samples used by Galloway and me.

Since the static strength of a nucleus does not seem to explain the measured thresholds, it is apparently necessary to consider the dynamic behavior of a sub-visible nucleus in an acoustic field. The motion of a spherical cavity interface in an acoustic pressure field has been

---

<sup>58</sup> W. I. Galloway, Reference 28, cited on p. 23.

59. Lyman Briggs, "Limiting Negative Pressure of Water," J. Appl. Phys., 21, 721 (1950).

considered by three authors.<sup>50,\*</sup> This work was reviewed in Chapter I, but we will consider the solutions in more detail here. Each author worked from essentially the same equation of motion for a cavity in water. The derivation of this equation is given by Noltingk. The equation can be written:

$$\rho(\ddot{R}R + \frac{3}{2}\dot{R}^2) + \frac{2\sigma}{R} + P_o - P_a \sin \omega t - P_{gi} \left[ \frac{R_o}{R} \right]^3 = 0 , \quad (5-21)$$

where  $P_{gi}$  is the initial gas pressure in the cavity and all other symbols have their usual meaning. The first term in the equation represents the mass reactance, per unit area of cavity surface, of the water that moves with the cavity. This term was calculated with the aid of the assumption that the water is incompressible. The second term is the pressure caused by the surface tension. The magnitude of the surface tension  $\sigma$  is assumed to be a constant. The third and fourth terms represent the ambient and acoustic pressures in the vicinity of the cavity. Both Noltingk and Flynn took the phase of the acoustic pressure to be  $-\sin \omega t$ . The last term represents the pressure of the gas in the cavity. This term was obtained under the assumption that the compression of the gas is isothermal.

Noltingk and Neppiras present a series of solutions of Eq.(5-21) indicating that the cavity opens up over the first acoustic period to a radius  $R_m$  and then collapses. Their solutions are presented graphically,

---

50. B. E. Noltingk, and E. A. Neppiras, "Cavitation Produced by Ultrasonics," Proc. Phys. Soc. (London) F3B, 674 (1950).

\* H. G. Flynn, Reference 1, cited on p. 8.

but it is possible to represent their curves for  $R_m$  by the following empirical equation:

$$R_m = 0.15 P_a^{2/3} \omega^{-1}, \quad (5-22)$$

where cgs units are employed.

After the maximum radius  $R_m$  was achieved, Noltingk and Neppiras found that the cavity began to collapse. At the end of the first acoustic period, they found that the radius was equal to or less than the initial radius. They did not continue their calculations beyond this point because the calculated cavity interface velocity became larger than the speed of sound in water, a condition that invalidates the incompressible assumption. Noltingk and Neppiras assumed that this cavity motion, characterized by expansion and collapse of the cavity within one acoustic period, was characteristic of all acoustic cavitation. Since our observations of cavitation in region (B) indicate that the lifetime of a transient cavity is measured in hundreds of acoustic periods, we can assume that Noltingk's calculations are not germane to the phenomenon we have observed.

It is interesting, however, to compare the values of  $R_m$  predicted by Noltingk and Neppiras with the maximum cavity radii we have observed. At 27 kc/s the cavity that formed in the water with an acoustic pressure of 10 bars had a maximum radius of about 5000  $\mu$ . According to Eq.(5-22), the maximum radius under these conditions is  $R_m = 410 \mu$ . At 82 kc/s the cavity that formed in the water with an acoustic pressure of 6 bars had a maximum radius of about 500  $\mu$ . Under these conditions the maximum radius, according to Eq.(5-22), is about  $R_m = 86 \mu$ . We can see that the

maximum cavity radii predicted by Noltingk for one-cycle expansions are about an order of magnitude less than the maximum many-cycle expansions observed.

We now turn to the solutions of Eq.(5-21) that have been obtained by Flynn (Flynn refers to Eq.(5-21) as D.E. I). These solutions show, indeed, that the cavity oscillates over many acoustic periods before collapsing. It is not possible, however, to compare Flynn's solutions with our experimental observations because the magnitudes of several parameters he used are not germane to the parameters we have found to cause cavitation. For example, Flynn calculates the oscillations of cavities with initial radii of either 26  $\mu$  or 260  $\mu$  at acoustic pressures of 1 bar or less.

Since it has not been possible to find any solutions of Eq.(5-21) that pertain to our experimental results, we shall examine the equation more closely. It is useful to non-dimensionalize Eq.(5-21) by introducing the variables  $\tau = wt$  and  $\xi = R/R_o$ , where  $R_o$  is the initial cavity radius. Equation (5-21) becomes

$$\xi \xi'' + \frac{3}{2} \xi'^2 + \delta \left[ \frac{2\sigma}{R_o P_a} \xi^{-1} + \frac{P_o}{P_a} - \sin \tau - \frac{P_{gi}}{P_a} \xi^{-3} \right] = 0 , \quad (5-23)$$

where the primes denote differentiation with respect to  $\tau$ , and where  $\delta = P_a / \rho \omega^2 R_o^2$ . The parameter  $\delta$  can be seen to play a dominant role in the nature of the solutions. If  $\delta \gg 1$ , the magnitudes of the acceleration and the velocity will be large, and the solution will be highly nonlinear. If  $\delta \ll 1$ , however, the solution will represent small amplitude quasi-linear

51

oscillations. The majority of solutions presented by Flynn represent the case for which  $\delta < 1$ .

The values of the parameter  $\delta$  are very large for the cavitation experiments we have performed. For example, cavitation in water filtered through a  $0.45 \mu$  filter was observed at 8 bars acoustic pressure at 82 kc/s. The value of  $\delta$  at this datum point in region (B) (assuming  $R_o = 0.225 \mu$ ) is  $\delta = 5.9 \times 10^4$ . For such large values of  $\delta$  the nonlinear terms in (5-23) are dominant, and the solutions are very difficult to obtain by any analytic means. The question about the details of the mechanism of cavity growth from sub-visible size to sizes characteristic of cavities formed in region (B) remains unanswered.

Upon examination of Eq.(5-23), we can deduce several requirements for cavitation. For example, if the cavity is to grow explosively, the acceleration will be large and positive. During this period of growth both left-hand terms will be large and positive, requiring the remaining terms to be large and negative. Thus, at least initially, we require that  $\delta \gg 1$  and that the term in brackets be negative. The latter requirement is related to the static strength of the nucleus (initial cavity of radius  $R_o$ ). For example, at  $r=0$  we have  $\xi \rightarrow 1$  and the term in brackets must satisfy

$$\left[ \frac{2\sigma}{R_o} + P_o - P_{gi} - P_a \tau \right] < 0 . \quad (5-24)$$

But Eq.(5-24) is related to the static strength of a small gas-filled bubble, which can be expressed as

$$\left[ 0.77 \frac{\sigma}{R_o} + P_o - P_a^* \right] < 0 , \quad (5-25)$$

where we recall that the explicit dependence on  $P_{gi}$  vanishes because it depends on  $P_0$  and  $R_0$  for initial equilibrium.

The other requirement, for  $\delta \gg 1$ , is automatically satisfied at low frequencies because  $\delta \sim \omega^{-2}$ . Thus the static strength, as expressed by Eq.(5-25), should provide an adequate representation of the cavitation threshold as long as  $\delta \gg 1$ . This is in order, because  $\delta \gg 1$  implies low frequency. At high frequencies, Eq.(5-25) will no longer be sufficient as  $\delta \rightarrow 1$ . Specifically, we might expect that a detailed analysis of Eq.(5-23) would predict some number  $a \leq \delta$  for which cavitation is assured. An attempt will be made to determine  $a$  from the solutions of Eq.(5-23) presented by Flynn. This will be done in the section devoted to consideration of cavitation in region (C), the high-frequency region of the data.

An examination of the threshold data reveals that acoustic pressures of at least 3 bars peak were required to form transient cavities. If we assume that the largest initial radius of cavitation nuclei is equal to one half the filter pore size, Eq.(5-25) predicts a threshold pressure of 3.5 bars for cavitation in region (B). The dependence of the threshold on the dissolved air content, which was observed, is not explained by Eq.(5-25).

#### Translational Motions of Transient Cavities

The transient cavities were observed to undergo a translational velocity in a direction away from the focus before they collapsed.

Figure 12 shows a photograph of transient cavities occurring at 82 kc/s

at an acoustic pressure of about 10 bars. In one photograph, the illumination was supplied by a stroboscope flashing at a rate of 417 flashes per second. As many as four cavities can be seen in one row, indicating that this particular cavity was photographed in five different positions. The distance between two of the cavities is 3 mm. The average velocity of this cavity must have been  $(0.3)(417) = 125 \text{ cm/sec}$ . This cavity is located about 5 mm from the focus and has a radius of about  $500 \mu$ . We can calculate the translational velocity of this cavity as we did for a mass-controlled air bubble. The Reynolds' number is very different in this case, however.

The Reynolds' number for the translational motion of this cavity is about

$$R_e = \frac{qd}{v} = \frac{(125)(0.1)}{0.012} \approx 1000$$

For translational motion of a sphere at this Reynolds' number the drag force is given by

$$D = C_d A \frac{\rho q^2}{2} , \quad (5-26)$$

where  $C_d$  is the drag coefficient,  $A$  is the projected area of the spherical cavity,  $\rho$  is the density of the liquid, and  $q$  is the translational velocity of the sphere. The drag coefficient can be found by reference to Prandtl and Tietjens.<sup>60</sup> These authors report that  $C_d \approx 0.4$  over a range of Reynolds' numbers extending from  $6 \times 10^2$  to about  $2 \times 10^5$ . Because

---

60. L. Prandtl and O. Tietjens, Applied Hydro- and Aerodynamics, p. 100 (Dover, New York, 1957).

$C_d$  is nearly constant over this range, the drag coefficient will not be considered to be a function of Reynolds' number.

The amplitude of the mass-controlled oscillations of the cavity is easy to calculate, if we regard the oscillations to have commenced at a time when the radius corresponded to the observed size,  $\delta \ll 1$ . Specifically, in this case  $\delta = 0.015$ . Equation (5-23) can now be linearized, and with the use of  $P_o \ll P_a$ , the linear solution is

$$R = R_o(1 + \delta \sin \omega t) . \quad (5-27)$$

The equation for the translational velocity of the spherical cavity is obtained by equating the drag force given by Eq.(5-26) to the pressure gradient force given by Eq.(5-7). Thus, with the use of Eq.(5-27) for the radius of the cavity:

$$q^2 = - \frac{8R_o}{3\rho C_d} \left(1 + \frac{P_a \sin \tau}{\rho \omega^2 R_o^2}\right) \nabla P , \quad (5-28)$$

where  $P_a \sin \tau$  is the acoustic pressure in the neighborhood of the cavity. The acoustic pressure and its derivative with respect to  $r$ , the position of the cavity, are given for  $kr \ll 1$  by Eq.(5-10). Equation (5-28) becomes, with the substitution  $\nabla P = - \frac{1}{3} P_a k^2 r \sin \tau$ :

$$q^2 = \frac{8R_o \omega^2 P_a r}{9\rho C_d c^2} \left(1 + \frac{P_a}{\rho \omega^2 R_o^2} \sin \tau\right) \sin \tau . \quad (5-29)$$

The time average of Eq.(5-29) is:

$$\frac{\bar{r}^2}{q^2} = \frac{4 p_a^2 \bar{r}}{9^2 R_o C_d c^2} , \quad (5-30)$$

where  $\bar{r}$  is the average position of the cavity. If the cavity forms at the focus  $\bar{r} = 0$  the translational velocity of the cavity will be zero. This is a point of unstable equilibrium, however, because the velocity is positive and increases as the distance from the focus increases. Equation (5-30) predicts a translational velocity of 210 cm/sec for the cavity that was observed at 8½ kc/s. This is within a factor of two of the observed velocity, which was 125 cm/sec.

Before we conclude the discussion of the cavity motions that are characteristic of the cavities formed in region (B), it is necessary to consider one additional problem. The surfaces of the cavities shown in the photographs (Fig. 12) are very rough. This suggests that the oscillating surfaces are unstable. Hsieh and Plesset\* have attempted to apply the theory of "Taylor instability" to the case of an accelerated spherical interface between water and a medium of negligible density. They conclude that for a spherical cavity with a radius given by

$$\bar{R}(t) = R_o(1 + \gamma \sin \omega t) , \quad (5-31)$$

the interface will be stable if

$$R_o \leq \left[ \frac{24\sigma}{5\rho\gamma\omega^2} \right]^{1/3} . \quad (5-32)$$

---

\* D.-Y. Hsieh and M. S. Plesset, Reference 22, cited on p. 17.

If  $\gamma$  is eliminated by using Eqs.(5-27) and (5-31), the largest stable radius can be written as

$$R_o \leq \left[ \frac{24\sigma R_o^2}{5P_a} \right]^{1/3}. \quad (5-33)$$

If the equality is assumed to hold, the largest stable radius is found to be  $4\mu$  with one bar peak acoustic pressure in water. Thus, all cavity interfaces that have been observed should be unstable. The photographs showed no smooth-surfaced spherical cavities, a result that is explained by this calculation.

In our discussion of the thresholds in region (B), we have noted that the threshold pressures are larger than the minimum threshold pressures predicted by the static strength theory, but the details of the threshold data are not explained by this simple concept. We have seen that the maximum cavity radius that is predicted to be achieved in one acoustic period is at least an order of magnitude less than the maximum cavity radii that we observe experimentally. In addition, the lifetime of the observed cavities was much larger than one acoustic period. Thus, we were led to consider the motions of cavities over many acoustic periods as described by the equation of motion. It was not possible to find any solutions of the equation of motion that pertained to the experimental conditions of region (B), and so we were led to consider the non-dimensionalized equation of motion. In region (B) this procedure reduced to the static strength theory. Finally, we were able to show that the observed high-speed radial translation and the rough surfaces of cavities

with mass-controlled small-amplitude oscillations are in good agreement with theoretical predictions.

#### Cavitation Thresholds at High Frequencies (Region C)

The cavitation produced at frequencies higher than 200 kc/s was detected acoustically; it was not possible to see the individual cavities. At a frequency as high as 353 kc/s, however, it was possible to see a twinkling in the focal region when the acoustic pressure was large enough to produce a cavitation rate of about 10 events per second.

Flynn includes three solutions of Eq.(5-21) that are appropriate to the conditions characteristic of region (C).<sup>\*</sup> The initial cavity radius is  $R_0 = 5 \mu$ , and the frequency is 500 kc/s. Three different acoustic pressures are considered: 100, 20, and 5 bars. Thus, the values of  $\delta$  considered are: 40, 8, and 2. The cavity radius is predicted to reach a maximum of about  $18 \mu$  and then collapse, when the acoustic pressure is 5 bars. The solutions obtained for acoustic pressures of 20 bars and 100 bars show that the cavity oscillates about an expanded radius for two periods and three periods, respectively. These short periods of oscillation are followed by collapse.

It is not possible to discuss the motion of the transient cavities formed in region (C) because they could not be individually resolved. The sizes of the cavities observed in region (B) decreased with increasing frequency, although their lifetimes were measured in hundreds of

---

\* H. G. Flynn, Reference 14 (Fig. 34), cited on p. 8.

periods, regardless of frequency. If it can be inferred that the lifetimes of the cavities formed in region (C) are also measured in hundreds of periods, it would appear that the three-cycle oscillations predicted for  $\delta = 40$  fall short of what we measure as cavitation. If  $\delta$  is a good measure of the threshold, we can write

$$P^* > a \omega^2 R_0^2 , \quad (5-34)$$

where  $a > 40$  is a constant to be determined. It is understood that Eq.(5-25) must also hold, the threshold being given by the larger of the two predictions. If the value of  $R_0$  is determined as before, the value of  $a$  can be found from the datum point at 1.16 Mc/s. The result is  $a \approx 10^3$ .

Equation (5-34) further implies that the threshold pressure should increase by 12 dB/octave. The slope of the threshold data at 1.16 Mc/s is about 11 dB/octave, but the data appear to be approaching an asymptote whose slope is 12 dB/octave. It is interesting to recall at this point that Esche's threshold data\* were also seen to approach a slope of 12 dB/octave at about 1 Mc/s.

A final observation about the threshold data in region (C) can be made with regard to the effect of gas content in the water. We have assumed that the cavity motion in this region is controlled by  $\delta^2 a$ , resulting in increasingly large acoustic pressures with increased frequency. The effect of the gas-pressure term when this type of motion occurs is shown by Eq.(5-23). We observe that the gas-pressure term is

---

\* R. Esche, Reference 44, cited on p. 23.

of order  $P_{gi}/P_a$ , whereas the inertial term and the acoustic-pressure term are both of order 1. Since  $P_{gi}/P_a$  is of order 0.1 or less in region (C), we can expect that the gas content of the cavity will have a negligible effect. This fact was observed to be one of the defining characteristics of the data in region (C).

#### The Cavitation Nucleus

Certain assumptions have been made about the probable nature of the cavitation nucleus. It is appropriate to discuss these assumptions in the light of those experimental results which have bearing on the nucleus.

It was observed that the cavitation threshold in distilled water filtered through a  $0.45 \mu$  filter was the same as the cavitation threshold for tap water, although many more cavitation events were produced in the tap-water sample than in the filtered distilled water. Thus, cavitation nuclei can apparently be as small as  $0.45 \mu$ , although such nuclei are not as plentiful as larger ones.

In Chapter III it was concluded that the solid particles are actually dust particles, or "motes," that are supplied by the atmosphere. There are some experiments that indicate that this conclusion is reasonable. It has been shown by Dalla Valla<sup>61</sup> that the mean size of atmospheric dust is roughly  $0.5 \mu$ . Bickerman<sup>62</sup> shows that interferometer and

61. J. M. Dalla Valla, Micrometrics (Pitman Co., New York, 1948).

62. J. J. Bickerman, Surface Chemistry for Industrial Research (Academic Press, New York, 1948).

electron microscope measurements indicate that the surfaces of these particles are very irregular. Rosenberg<sup>63</sup> concludes, on the basis of microscopic examination of water, that the cavitation nuclei consist chiefly of dust particles ranging from 0.5  $\mu$  to 10  $\mu$  in diameter.

The cavitation nucleus must be capable of producing, or of being, a small cavity in the water when the pressure in the vicinity of the cavity becomes negative. It is reasonable to assume that this cavity is formed when a negative acoustic pressure draws out a small gas- and vapor-filled bubble from a crack in the surface of the nucleus.

A simple calculation can demonstrate the plausibility of this. Consider the geometry of the sketch shown in Fig. 23. In this figure, the following quantities are identified:

$\alpha$  = contact angle between the interface and the solid;

$\alpha_a$  = advancing contact angle;

$\alpha_r$  = receding contact angle;

$\beta$  = slope of the solid boundary of the crack at the point where the interface meets the solid;

$\gamma = \alpha - \beta - \frac{\pi}{2}$ ;

$R$  = radius of curvature of the interface =  $\frac{2\sigma}{P_e - P_g}$ ;

$\sigma$  = surface tension in dynes per cm of interface;

$a$  = effective radius of interface =  $R \sin \gamma = R \cos(\alpha - \beta)$ ;

$P_g$  = gas pressure inside the cavity;

$P_e$  = pressure in water external to the cavity.

---

63. M. D. Rosenberg, "Gaseous-Type Cavitation in Liquids," Tech. Memo. No. 26, Acoustics Research Lab., Harvard Univ. (1953).

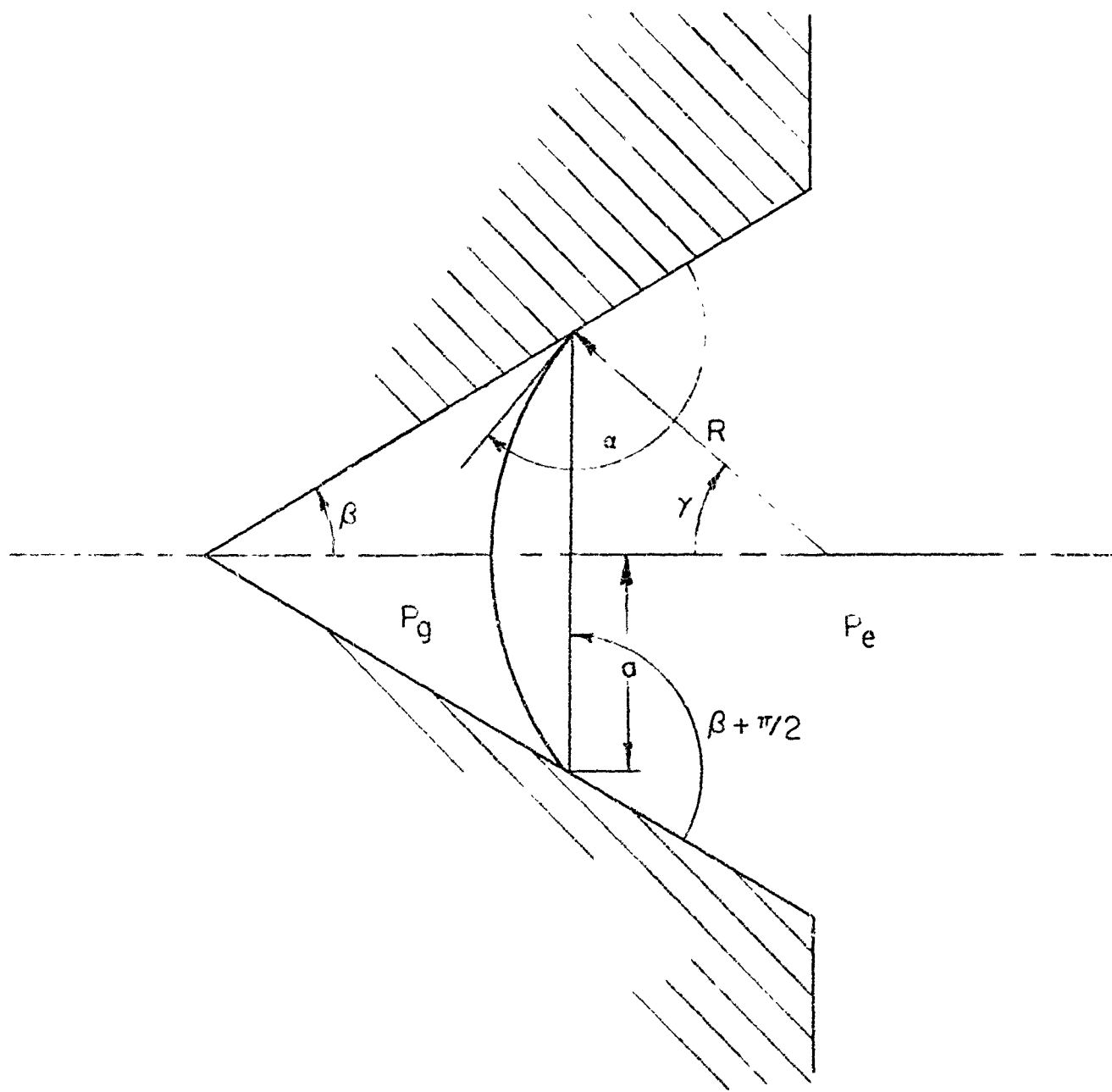


Fig. 23. Geometry of an interface in a crack

The static strength of the interface in the crack can be estimated by considering the details of the history of the water sample. We will parallel an argument presented by Strasberg.<sup>64</sup> To begin with, we will

---

64. M. Strasberg, "Onset of Ultrasonic Cavitation in Tap Water," J. Acoust. Soc. Am., 31, 163 (1959).

assume that the water is initially saturated with gas at the ambient pressure  $P_o$ . The various parameters for the original water sample are:

$$P_e = P_g = P_o, \quad R_o = \infty, \quad a = a_o, \quad \text{and} \quad \alpha = \beta + \pi/2. \quad (5-35)$$

These initial conditions imply that the air-water interface is plane.

The contact angle  $\gamma$  must always lie in the range  $\alpha_r < \gamma < \alpha_a$ , where  $\alpha_r$  and  $\alpha_a$  are the receding and advancing contact angles, respectively. Thus, from (5-35) we have the following requirement for the half-apex angle :

$$0 < \alpha_r < \beta + \pi/2 < \alpha_a < \pi. \quad (5-36)$$

The first step of the degassing operation was effected by lowering the ambient pressure to the desired equilibrium air saturation pressure  $P_s$ . When this is done, the interface will become concave to the gas. The point of contact of the interface will not move ( $a_o$  will not change) if  $\alpha_r \leq \alpha$ . All interfaces for which  $a_o \leq a_{\max}$  will remain fixed to the wall of the crevice under the effect of the ambient pressure drop. All interfaces for which  $a_o > a_{\max}$  will become unstable and form an air bubble in the liquid. The conditions describing the largest (and weakest) interfaces after the ambient pressure is lowered are:

$$P_e = P_s = P_g + \frac{2\sigma}{R_I}, \quad a = a_{\max} = R_I \cos(\alpha_r - \beta), \quad \text{and} \quad \alpha = \alpha_r. \quad (5-37)$$

The reason for the instability of interfaces for which  $a_o > a_{\max}$  is demonstrated by (5-37). Suppose that  $a_o > a_{\max}$ . This would require a larger interfacial radius  $R_I$ . But the applied pressure differential could not be supported by the interface of larger radius of curvature and the interface will recede explosively.

63

The second step is achieved by allowing the gas in the crack to diffuse into the liquid until equilibrium is reached. These conditions are expressed by.

$$P_g = P_e = P_s, \quad R_{II} = \infty, \quad \text{and} \quad a = a_{\max}. \quad (5-38)$$

After diffusion equilibrium has been established, the ambient pressure is restored. During this process, the curvature of the interface becomes convex to the gas. In fact, when the interface becomes so convex as to cause  $a = a_a$ , the interface will advance toward the apex of the crevice until the contact angle is  $\alpha_a$ . The conditions of the interface are now:

$$P_s + \frac{2\sigma}{R_{III}} = P_o, \quad a = R_{III} \cos(\alpha_a - \beta), \quad \text{and} \quad \alpha = \alpha_a. \quad (5-39)$$

The final step involves applying a large enough pressure to rupture the interface (to make  $\alpha < \alpha_r$ ). In our experiments this is done, in the low-frequency range, by applying an acoustic pressure to the water. The external pressure to rupture the interface is  $P_e^*$ , where

$$P_e^* = P_g' + \frac{2\sigma}{R_{IV}} = P_o - P_a^*, \quad a = R_{IV} \cos(\alpha_r - \beta), \quad \text{and} \quad \alpha = \alpha_r. \quad (5-40)$$

In Eq.(5-40),  $P_g'$  represents the gas pressure in the crevice when the interface is concave to the gas and just ready to rupture. The value of  $P_g'$  is given by the product of  $P_s$  and the ratio of the volume of the crevice in step III to the volume of the crevice in step IV. Thus,  $P_g' < P_s$ . Since  $P_e^*$  is much larger (experimentally) than  $P_s$ , we can neglect  $P_g'$  in Eq.(5-40). Thus, the peak acoustic pressure to rupture the interface is given by Eqs.(5-40) and (5-39);

$$P_a^* = P_o + (P_o - P_s) \left| \frac{\cos(\alpha_r - \beta)}{\cos(\alpha_a - \beta)} \right| . \quad (5-41)$$

In principle it is possible to calculate  $\alpha_r$  from the relations given by (5-37). The form of (5-41) is sufficient, however. We see that  $P_a^*$  is linearly dependent on  $P_s$ , being larger for small  $P_s$ . This relationship was observed by Galloway.

When the acoustic pressure exceeds the value given by Eq.(5-41), the interface will become unstable and recede from the apex of the crevice. This motion is limited only by the inertia of the fluid moving with the interface. It is of interest to see if the frequency range covered by our experiments includes frequencies for which the inertia loading on the moving interface will alter Eq.(5-41). This question can be answered by considering the resonance frequency of the interface. It is apparent that negative pressures of about 5 bars must be supplied to deflect the interface sufficiently to cause instability. The displacement suffered by the interface could not be more than  $0.5 \mu$  because of the dimensions of the nucleus particle. Thus, the interface stiffness must be at least  $A \times 10^4$  dyne/cm where A is the area of the interface. The effective mass load of the water on the interface can be estimated by considering the interface to be a small radiator of area A set in a spherical enclosure.<sup>65</sup> At the frequencies in question, this mass is given by  $M = \rho A a$ , where a is the radiator radius. On this basis, the resonance frequency of the interface will be

---

65. P. M. Morse, Vibration and Sound, p. 324 (McGraw-Hill, New York, 1948).

$$f_o = \frac{1}{2\pi} \sqrt{k/M} = 7 \text{ Mc/s} , \quad (5-42)$$

where  $a$  was taken to be  $0.5 \mu$ . This frequency is 7 times larger than the highest frequency for which the cavitation threshold was measured. It is not likely that interface resonances were encountered.

Equation (5-42) indicates that all interfaces in suspended particles are below resonance in this experiment, and thus Eq.(5-41) should be valid at all frequencies. But there is a marked frequency dependence for the cavitation threshold. It is clear that Eq.(5-41) is a necessary condition, for the gas bubble at the bottom of the crevice must issue from the crevice. But, once the gas bubble is transported to the liquid it exists, temporarily at least, as an approximately spherical bubble of radius  $R_o$ . Cavitation will result only if this nucleus bubble is unstable in the sound field.

This discussion has been presented to demonstrate the plausibility of the crevice gas bubble theory. It is not possible to be quantitative in these conjectures, because the geometry of the crevices and the dynamic behavior of the contact angles are not known quantitatively.

#### Recommendations for Future Study

We have seen that the cavitation thresholds observed in these experiments were all substantially below the theoretical strength of water. Almost all previous experimenters have reached the conclusion that these below-theoretical cavitation thresholds can be explained by the presence of cavitation nuclei. That is, the cavitation threshold is

CC

not determined by the tensile stress required to form an interior interface in the liquid, but rather by the stress required to produce a gross enlargement of an internal cavity already existing. If an experimental measurement of the theoretical strength of water is attempted, we have shown that the presence of atmospheric dust particles, or motes, in the water sample must be eliminated.

One of the results of our experiments suggests a new way to remove the cavitation nuclei from water, i.e., by repeated cavitation of the sample at acoustic pressures well above the threshold for ordinary distilled, filtered water. It was not possible to produce acoustic pressures as large as the theoretical strength of water (about 1300 bars) in my apparatus. It might be possible, however, to design a resonator for efficient operation at one frequency, thereby providing larger acoustic pressures than I was able to produce. With such a device in hand, it would be a very interesting experiment to show how far the cavitation threshold can be raised by repeated cavitation, or by any other purification means.

We have seen that there are no solutions of the equation of motion of a spherical cavity that have been obtained with parameter values corresponding to the parameter values we have observed to cause cavitation. It would be interesting, therefore, to compare the experimental observations we have made with solutions obtained from the equation of motion with parameter values suggested by the experiments. Specifically, the following set of parameters would be especially appropriate:

C&gt;

$$R_o = 0.2 \mu$$

$f = 82 \text{ kc/s}$		$f = 11 \text{ kc/s}$		$f = 27 \text{ kc/s}$	
$P_a$ (bars)	$P_{gi}$ (mm Hg)	$P_a$ (bars)	$P_{gi}$ (mm Hg)	$P_a$ (bars)	$P_{gi}$ (mm Hg)
..	10	12	10	40	10
4.2	100	4.9	100	8.1	100
4.1	250	3.5	..	3.1	250

It is quite possible that the simplifications that have been made in deriving the existing equations of motion of a spherical cavity will be found to preclude the observed kinds of behavior. This question can be answered only by extending the range of parameters for which the equation of motion has been solved to include the relevant parameters.

The details of the motions of cavities could be supplied by high-speed photographic techniques. Such techniques have been developed to a high degree by Ellis,<sup>\*</sup> for recording the collapse of relatively large cavities formed by an electric spark in water. It would be of particular interest to photograph the growth of cavities in a low-frequency sound field (below about 50 kc/s). In this frequency range the maximum diameter of the cavity can be as large as 1 cm, thus facilitating observation.

One subject on which almost no quantitative information exists is the mechanism by which a foreign body in water can become a cavitational nucleus. It might be possible to make a model study of this mechanism. By using large scale models, the behavior of a liquid-gas interface in a crack on the surface of a body could be studied. In particular, the

---

\* A. T. Ellis, Reference 17, cited on p. 9.

dependence of wetting angle and boundary geometry on the interface motion could be studied. There is a large number of parameters to consider, and the scaling laws will not be simple. Nevertheless, a study guided by the rules of dimensional analysis should be feasible, and could certainly be of interest to the subject of cavitation nucleation.

In an earlier section we noted that the linearized theory of rectified diffusion cannot be applied to small bubbles with an initial radius less than about  $40 \mu$ . It is certain that a reasonably pure sample of water will not contain any bubbles of this size. We concluded that nonlinear bubble oscillations, resulting from the large acoustic pressures required to form visible bubbles, will be able to cause bubble growth by rectified diffusion. There is a clear requirement for an analysis of rectified diffusion based on the nonlinear motions of small air bubbles. Such a calculation should be able to show what critical bubble sizes are required to explain the experimental cavitation threshold data. The clear delineation of these critical bubble sizes will provide useful knowledge about the cavitation nucleus.

A series of experiments is suggested by our conclusions about the cavitation nucleus. One kind of nucleus was found to be destroyed by cavitation; another kind was not. The first kind are apparently pre-existing air- or vapor-filled bubbles stabilized in water. It has been suggested that this kind of nucleus might be investigated by model studies. Some evidence has been presented in this paper that suggests that the mechanism responsible for a low rate of continuous cavitation nucleation in water is the "thermal spike" phenomenon suggested by

Messino, Sette, and Wanderlingh.\* It is possible that a detailed study of this kind of nucleation could lead to the design of a very sensitive bubble chamber, in which the liquid is stressed to a point just below its threshold by acoustic means rather than by large superheat

Finally, it is appropriate to discuss the usefulness of my equipment as a general tool for cavitation research. Many of the faults of this apparatus are a result of its primary virtue: the wide operational frequency range. The most important fault is the low acoustic pressure capability at low frequencies. There are several ways this deficiency can be corrected. The simplest way is to lower the fundamental resonance frequency of the driver transducers. This can be done by lengthening the backing cylinder; a three-inch-long brass cylinder would provide a fundamental resonance frequency of 20 kc/s. The focal pressures can also be increased by using a larger sphere, the variational pressure at the focus being proportional to the radius of the sphere for a constant driving velocity. Each of these two methods of increasing the variational pressure at the focus will limit the pressures at high frequencies because of increased losses in the transducers and in the water.

A different approach would be to raise the Q of the resonator modes. This can be accomplished by decreasing the coupling between the resonator and its drivers (for example, by decreasing the contact area between the two systems). The reduced coupling will require larger driver velocities to produce a given pressure at the focus, however. Thus, the transducers would need to be made resonant at all frequencies

---

\* Messino, Sette, and Wanderlingh, Reference 37, cited on p. 26

for which cavitation is to be produced in order to obtain sufficient driving velocities.

The apparatus in its present form requires about two liters of water. If ultra-pure water samples are to be employed, a separate thin-walled container for the sample could be placed at the center of the resonator. The ultra-pure water sample will probably require a much larger acoustic pressure to cause it to cavitate than will be required by the large volume of water in the remainder of the sphere. Thus, the sample container should be several wavelengths in diameter to insure that the maximum acoustic pressure in the coupling water is not too large. Considering that the diameter of a sample contained can be no larger than the opening in the top of the resonator (4.4 cm), the acoustic frequency will probably need to be at least 200 kc/s (allowing the radius of the container to be two wavelengths). Since much of the interest is for low frequency thresholds, this requirement would suggest the use of a larger sphere, or at least a larger opening in the top.

With the exception of modifications in size to accommodate different frequency ranges, it appears that this apparatus provides a compact and versatile device for the study of many aspects of acoustic cavitation. The use of a high-Q spherical resonator is an economical and convenient way to produce large acoustic pressures, when used in conjunction with an automatic frequency control system. The visibility of the cavitation region afforded by the all-glass construction renders qualitative assessments easy to make. The possibility of apocryphal judgments about the phenomenon is thereby eliminated.

## ACKNOWLEDGMENTS

I am happy to take this opportunity to acknowledge my indebtedness and to return my thanks to Professor F. V. Hunt and the staff of the Acoustics Research Laboratory for their help and encouragement. In addition, the support offered by the Office of Naval Research and administered by Mr. Aubrey Price is gratefully acknowledged.

12

## Appendix A

### RESONATOR MODAL FREQUENCIES AND DRIVING SENSITIVITIES

If a means could be found to support a spherical volume of water in a massless and infinitely compliant vessel, the radially symmetric resonance frequency of the nth mode would be  $f_n = nc/2R$ , where n is the mode number, c is the velocity of sound in water, and R is the radius of the sphere. We consider here a thin glass spherical shell to contain the water, and this shell must become part of the resonant system. The resonance frequencies of the composite glass-water system will be calculated. Perhaps of more importance, the effect of the shell on the focal pressure must be determined. In the absence of the shell, the external surface of the water is a pressure release surface at the modal resonance frequencies. An expression for the focal pressure as a function of the radial driving velocity at the external surface can easily be derived. The presence of the shell alters the situation somewhat. At any of the radially symmetric resonances of the combined glass-water system, the pressure release surface is transferred to the external surface of the glass shell. The impedance at the external surface of the water will not be zero in this case. The effect that this has on the focal pressure must be determined.

Only radially symmetric motion will be considered in this analysis. This reduces the problem to one dimension, which will be taken as the radius r, measured from the origin of coordinates taken to be coincident with the center of the sphere. Since the velocity at the glass-water

interface must be continuous, the impedance of the two individual systems are to be connected in series.

The acoustic pressure and particle velocity in a spherical standing wave can be expressed:<sup>\*</sup>

$$p(r) = P_0 \frac{\sin kr}{kr} e^{j\omega t} \quad (A-1)$$

$$q(r) = j \frac{p(r)}{\rho_w c_w} (\cot kr - \frac{1}{kr}) ,$$

where  $k = \frac{\omega}{c}$  is the phase constant,  $\rho_w$  and  $c_w$  are the density and sound velocity in water respectively, and  $P_0$  is the peak acoustic pressure at the focus.

The specific acoustic impedance of a spherical surface at a distance  $r$  from the focus becomes

$$Z_s = j\rho_w c_w \left( \frac{1}{kr} - \cot kr \right)^{-1} . \quad (A-2)$$

The specific acoustic impedance of the mass of the glass envelope is the ratio of the inertial force acting on a unit area of the shell divided by the radial velocity of the shell:

$$Z_s = \frac{[\text{mass of unit area of shell}][\text{radial acceleration}]}{[\text{radial velocity}]} = \rho_g h(j\omega) , \quad (A-3)$$

where  $\rho_g$  is the density of the glass,  $h$  is the thickness of the shell, and  $\omega$  is the angular frequency. The specific acoustic impedance of the shell due to its mass is an inductive reactance, with an inductance

$$L = \rho_g h .$$

---

\* P. M. Morse and H. Feshbach, Reference 55, cited on p. 66.

7/1

A uniform radial displacement of the spherical shell also encounters a stiffness reactance. The tangential stress  $\sigma_\theta$  in the shell of radius  $R$  and thickness  $h$  due to an external pressure  $P_e$  is equal to the total force acting across any plane which passes through the center of the sphere divided by the cross-sectional area of the shell cut by that plane.

$$\sigma_\theta = \frac{P_e \pi R^2}{2\pi Rh} = \frac{P_e R}{2h} .$$

The tangential stress at any point on the shell is uniform in all directions in a plane tangent to the spherical surface at that point. Selecting two mutually perpendicular directions in that plane centered at the point of tangency and labeling them the  $x$  and  $y$  directions, we have from Hooke's law:

$$\epsilon_x = \frac{1}{Y} [\sigma_x - v\sigma_y]$$

$$\epsilon_y = \frac{1}{Y} [\sigma_y - v\sigma_x] ,$$

where  $\epsilon_x$  and  $\epsilon_y$  are the strains in the  $x$  and  $y$  directions and  $v$  is Poisson's ratio. Since  $\epsilon_x = \epsilon_y = \epsilon_\theta$  and  $\sigma_x = \sigma_y = \sigma_\theta$  because the stresses and strains are uniform in all directions, we have:

$$\epsilon_\theta = \frac{1}{Y} (1-v)\sigma_\theta ,$$

By definition,  $\epsilon_\theta$  is the change in the circumference of the sphere divided by the unstrained circumference, e.g.,  $\epsilon_\theta = \frac{\Delta R}{R}$ . For harmonic motion the radial velocity of the shell is  $q(r) = j\omega\Delta R$ ,

The specific acoustic impedance of the stiffness of the shell thus becomes

$$Z_s = \frac{P_e}{q} = \frac{2hY}{j\omega R^2(1-v)} . \quad (A-4)$$

This impedance is a capacitive reactance, with a capacitance  $C = \frac{R^2(1-v)}{2Yh}$ .

The radial specific acoustic driving-point impedance at the surface of the spherical glass shell is the sum of the impedance expressed in Eqs.(A-2), (A-3), and (A-4).

$$Z_{s(\text{driving})} = j\omega \rho_g h \left[ 1 - \frac{\omega_0^2}{\omega^2} + \frac{\rho_w r}{\rho_g h} (1 - kr \cot kr)^{-1} \right] . \quad (A-5)$$

The definition of the resonance frequency of the glass sphere itself has been made as follows:

$$\omega_0^2 = \frac{1}{LC} = \frac{2Y}{R^2(1-v)\rho_g} .$$

The frequency equation is obtained by equating the driving impedance to zero at  $r=R$ , the external surface of the glass shell. After some algebra, this equation becomes

$$\frac{\tan k_n R}{k_n R} = \frac{(\omega_0/\omega_n)^2 - 1}{(\omega_0/\omega_n)^2 - 1 + [\rho_w R/(\rho_g h)]} , \quad (A-6)$$

where  $k_n = \frac{\omega_n}{c}$ .

This equation was solved numerically by successive interpolation for the resonant modal frequencies. An experimentally determined value of  $\omega_0$  was used in the frequency equation. To measure this frequency a

Western Electric 640-AA condenser microphone was placed inside the sphere at the center. The sphere was placed in the sound field of a loudspeaker. The pressure response of the microphone was recorded as a function of the frequency of the sound field. A peak response of the microphone was recorded at 18.45 kc/s. The frequencies of the two adjacent resonance peaks were 16.64 kc/s and 19.32 kc/s.

The physical constants of the glass shell are:

$$Y = 8.7 \times 10^{11} \text{ dyne cm}^{-2}$$

$$\rho = 2.4 \text{ gm cm}^{-3}$$

$$v = 1/4 \text{ (approximately)}$$

$$R = \text{inside radius plus half the thickness} = 7.93 \text{ cm}$$

$$h = 2 \text{ mm} .$$

These constants when substituted into the equation for the resonance frequency of the shell predict a resonance frequency,  $f_o = 18.34 \text{ kc/s.}$

The experimentally measured resonance frequency at 18.45 kc/s must have been the frequency of the radially symmetric mode of vibration of the shell.

The solutions of Eq.(A-6) for the resonator modes which were used in the experiment are presented in Table II.

The equation for the radial velocity in (A-1) can be used in connection with the frequency equation to determine the peak acoustic pressure  $P_o$  at the focus as a function of the driving velocity at the external surface  $r = R$  at the resonance frequencies  $\omega_n$ . The peak pressure is found to be:

$$P_o = -jq(R) \frac{\omega_n^2 R \rho h}{c} \left[ \frac{\omega_0^2}{\omega_n^2} - 1 \right] \text{ cosec}(\omega_n \frac{R}{c}) . \quad (\text{A-7})$$

Both of the last two terms are found to be nearly unity for the sixth and higher modes. The magnitude of the peak acoustic pressure at the focus can be approximated by

$$|P_o| = q(R) \frac{\omega^2 R \rho h}{\frac{n^2 g}{c}} = q(R) f^2 \times 10^{-3} \text{ dyne/cm}^2 , \quad (\text{A-8})$$

where the values of the parameters used correspond to the glass envelope.

If the resonator is to be able to provide peak acoustic pressures of 200 bars, the velocity required from the transducers is

$$q(R) = 2 \times 10^{11} \text{ f}^{-2} \text{ cm/sec} . \quad (\text{A-9})$$

Equation (A-9) demonstrates why a nonresonant piezoelectric ceramic material cannot be used as a transducer. The best ceramics have a displacement sensitivity of only  $2.5 \text{ \AA/volt}$ . The voltage required to achieve 200 bars would be

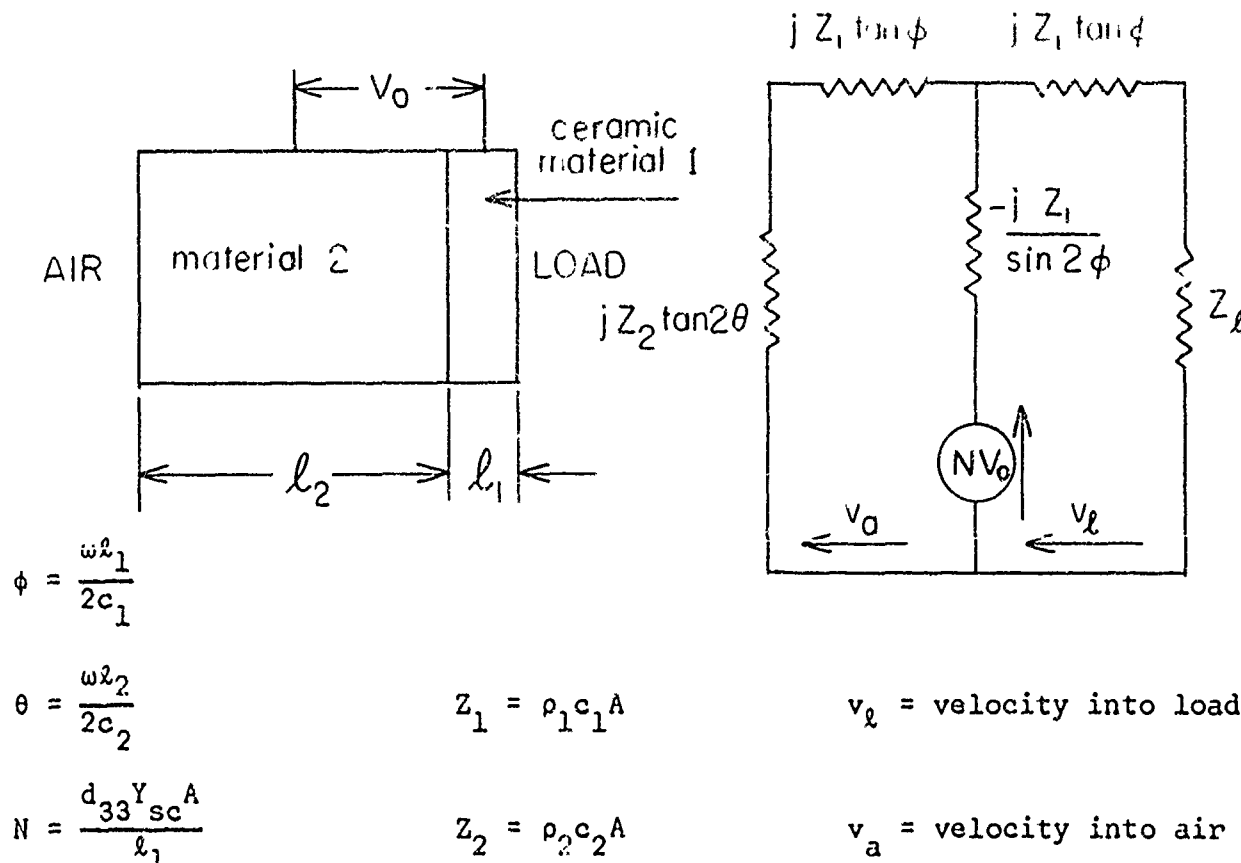
$$V = 1.33 \times 10^{18} f^{-3} \text{ volt} .$$

At 100 kc/s,  $V = 1330$  volts. A ceramic bar would need to be at least 1 cm thick to keep the strain below the breaking strain at this voltage. A ceramic bar of this thickness would have a fundamental resonance of 500 kc/s, which would make it unusable over part of the frequency range of interest. In addition, the large voltages would be a problem in a practical sense.

## Appendix B

## MULTIRESONANT TRANSDUCER CALCULATIONS

It has been pointed out in Chapter II and Appendix A that a multi-resonant piezoelectric transducer is needed to drive the resonator to the desired pressure amplitudes. The transducer is to operate efficiently at all of the harmonic frequencies of its fundamental frequency. It is anticipated that a composite bar transducer made of a thin piezoelectric ceramic disk attached to the end of a metal cylindrical bar will have these resonances as well as sufficient velocity amplitudes at resonance. The geometry of the system and its equivalent mechanical impedance analog is given in the figure below.



The impedance of the backing material #2 is represented by its transmission line equivalent, assuming it to be terminated by a zero impedance. The impedance of the ceramic element is represented by its transmission line equivalent. In this representation the force generated across the blocked ceramic element is represented as a force generator as shown. The magnitude of the force is numerically equal to the product of the driving voltage  $V_o$  and the electromechanical transduction ratio  $N$ , the force in newtons developed when one volt is applied across the blocked electrodes.

The equations which describe the circuit were solved, with the following result for the velocity into the load:

$$v_l = -jV_o N \frac{\left[ \frac{Z_2}{Z_1} \tan 2\theta + \tan \phi \right]}{Z_1 \left[ \frac{Z_2}{Z_1} \tan 2\theta \cot 2\phi + 1 \right] + jZ_l \left[ \frac{Z_2}{Z_1} \tan 2\theta - \cot 2\phi \right]} . \quad (B-1)$$

The load impedance has zero reactance because the resonator is operated at a radially symmetric resonance frequency. The load impedance  $Z_l$  will be real but very small because of the low losses in the resonator as indicated by the very high Q's of the resonator modes. The second term in the denominator is expected, therefore, to be very small with respect to the first term except at resonance. The frequency equation for the transducer can be closely approximated by the condition for the first term in the denominator to be zero. The resonance frequencies of the transducer are the solutions of:

780

$$\frac{\omega^2}{Z_1} \tan 2\theta_n \cot 2\phi_n + 1 = 0 , \quad (B-2)$$

At the resonance frequencies the magnitude of the velocity into the load as a function of the magnitude of the applied voltage is, from (B-1) and (B-2),

$$|v_L| = \frac{2NV}{Z_L} \sin^2 \phi_n . \quad (B-3)$$

For the materials employed in the construction of the transducers, brass and PZT-4 ceramic, the characteristic impedances  $Z_1$  and  $Z_2$  are practically identical. This fact simplifies the frequency equation (B-2), whose solutions when  $Z_1 = Z_2$  are:

$$f_n = \frac{n}{2} \left[ \frac{\ell_1}{c_1} + \frac{\ell_2}{c_2} \right]^{-1} .$$

It was decided to match the fundamental transducer resonance frequency to the 82 kc/s resonance frequency of the resonator. The ceramic element has the values  $\ell_1 = 0.1$  in. and  $c_1 = 2.79 \times 10^5$  cm/sec. For brass,  $c_2 = 3.4 \times 10^5$ . To match the fundamental ( $n = 1$ ) mode to 82 kc/s the length of the brass  $\ell_2 = 0.70$  inch.

The equation for the velocity delivered to the load, (B-3), can only be used in an approximate way because  $Z_L$  is not accurately known.  $Z_L$  can be estimated, however.

The instantaneous power delivered to the resonator at a resonance frequency  $\omega_n$  is the product of the pressure, velocity, and area at the external surface. The average input power is  $p(R)q(R)A_s/2$ , where  $p(R)$  and  $q(R)$  are peak values of the acoustic pressure and velocity at the

external surface, and  $A_s$  is the area of the spherical surface. The average power delivered to the resonator is equal to the average power dissipated in the resonator. The latter quantity is given by Eq.(2-5). By equating the average power dissipated to the average power input, the peak acoustic pressure at the surface becomes:

$$p(R) = \frac{2P_o^2 R^2}{\rho cnQ_n q(R) A_s} . \quad (B-4)$$

It will be assumed that the external surface at  $r = R$  is a pressure release surface. From this assumption,  $k_n = \frac{n\pi}{R} = \frac{\omega_n}{c}$ . The value of the velocity at  $r = R$  is given by Eq.(A-1). The result, for the peak velocity is  $q(R) = jP_o/\rho\omega_n R$ . Equation (B-4) becomes:

$$p(R) = -j \frac{P_o}{2Q_n} . \quad (B-5)$$

Equation (B-5) shows that the peak acoustic pressure at the focus leads by  $90^\circ$  the pressure which provides the power dissipated in the system. The pressure  $p(R)$  will be in phase with  $q(R)$ . Since the surface pressure is applied over an area  $A_t$  covered by the transducers, the magnitude of the driving pressure at the surface of the sphere will be

$$p(R) = \frac{P_o}{2Q_n} \frac{A_s}{A_t} .$$

The mechanical load impedance presented to the transducers becomes:

$$Z_L = \frac{p(R)A_t}{q(R)} = \frac{P_o A_s}{2q(R)Q_n} \text{ dyne sec cm}^{-1} . \quad (B-6)$$

62

When this expression is substituted into Eq.(B-3), with the assumption that the transducer load velocity  $v_l$  equals the velocity at the surface of the sphere  $q(R)$ , we obtain:

$$\frac{P_o}{V_o} = \frac{A_t}{A_s} Q_n \frac{4d_{33}Y_{sc}}{\lambda_1} \sin^2 \frac{\omega_n \lambda_1}{2c_1} , \quad (B-7)$$

where  $N$  and  $\phi_n$  have been replaced by their definitions in terms of the material constants.

Equation (B-7) is an approximate expression for the driving sensitivity of the resonator in terms of the peak acoustic pressure at the focus for 1 volt peak input to the transducer. It is understood that the expression only holds at the resonance frequencies of the transducers. The only assumption that was made to obtain Eq.(B-7) from (B-3) and (B-6) was that the velocity of the surface of the resonator was uniform. In practice the velocity of the surface of the glass shell can be different at the transducers and the space between them.

The material constants that appear in Eq.(B-7) are as follows:

$$d_{33} = 2.55 \times 10^{-10} \text{ m/V} ;$$

$$Y_{sc} = 6.7 \times 10^{10} \text{ N/m}^2 ;$$

$$\lambda_1 = 2.54 \times 10^{-3} \text{ m} ;$$

$$c_1 = 2.79 \times 10^3 \text{ m/sec} ;$$

$$\frac{A_t}{A_s} = \frac{1}{12} .$$

For the resonance frequency at 82 kc/s, the measured Q was 2990.

Equation (B-7), with these values of the parameters, gives:

$P_o/V_o = 3.6$  bars/volt. The measured sensitivity for the completed resonator was:  $P_o/V_o = 0.5$  bar/volt (see Table II). The calculations provide an order of magnitude agreement with the measured sensitivities. The calculations correctly indicate that the proposed transducer design will be adequate to drive the proposed resonator to sufficient acoustic pressures.

## Appendix C

## PROBE-HYDROPHONE RECEIVING-SENSITIVITY CALCULATIONS

Thin-wall piezoelectric ceramic cylinders have been used as pressure hydrophones by many experimenters. It has been common practice to mount the cylindrical shell on a pressure release core. The sensitivity of this type of hydrophone has been calculated by Langevin.<sup>66</sup> The calculation can be extended to include a central core of general elastic properties. It will be shown that a ceramic cylinder mounted on a relatively stiff core can have a larger sensitivity and a higher fundamental resonance frequency than the same cylinder mounted on a pressure release core. For these reasons, the hydrophone constructed with a stiff core can be superior to the hydrophone constructed with a pressure release core.

The objective of this calculation is the determination of the receiving sensitivity of a pressure hydrophone constructed from a thin-wall piezoelectric ceramic cylinder mounted on an elastic core. The construction of this device is shown in Fig. 8. The outer and inner radii of a hollow piezoelectric ceramic cylinder are taken to be  $b$  and  $a$ , respectively. The length of the cylinder is of no consequence in this calculation. The inner surface of the piezoelectric cylinder is bonded to a solid core of the same radius.

---

66. R. A. Langevin, "The Electro-Acoustic Sensitivity of Cylindrical Ceramic Tubes," J. Acoust. Soc. Am. 26, 421 (May 1954).

15

The boundary conditions are as follows: The stress on the outside surface of the ceramic cylinder is equal to the instantaneous acoustic pressure  $P$ . The radial displacement of the inner surface of the ceramic cylinder is equal to the radial displacement of the outer surface of the solid core. The radial stress on the inner surface of the ceramic cylinder is equal to the radial stress on the outer surface of the solid core. These boundary conditions are expressed

$$\sigma_{rs}(r=b) = -P ,$$

$$\sigma_{rs}(r=a) = \sigma_{rc}(r=a) , \quad (C-1)$$

$$\xi_s(r=a) = \xi_c(r=a) ,$$

where  $\sigma_{rs}$  and  $\sigma_{rc}$  are the radial stresses in the cylindrical ceramic shell and the solid core, respectively.  $\xi_s$  and  $\xi_c$  are the radial displacements of the shell and the core, respectively. The stresses and displacements for the shell and core are:<sup>67</sup>

$$\sigma_{rs} = Ar^{-2} + C ; \quad \sigma_{\theta s} = -Ar^{-2} + C ; \quad \xi_s = \frac{1}{Y_s} [-A(1-v_s)r^{-1} + C(1-v_s)r] ; \quad (C-2)$$

$$\sigma_{rc} = \sigma_{\theta c} = E \text{ (constant)} ; \quad \xi_c = \frac{1}{Y_c} E(1-v_c)r ;$$

where  $v_s$  and  $v_c$  are the Poisson's ratios of the shell and core, and  $Y_s$  and  $Y_c$  are the Young's moduli of the shell and core. The constants  $A$ ,  $C$ , and  $E$  are to be determined by the boundary conditions.

67. S. Timoshenko and J. Goodier, Theory of Elasticity (McGraw-Hill, New York, 1951), p. 66.

When Eqs.(C-2) are substituted into the boundary conditions (C-1), the resulting set of three simultaneous equations can be solved for the constants A, C, and E. When the values of these constants are substituted into Eqs.(C-2), there results for the stresses in the ceramic shell:

$$\sigma_{rs} = -P \left[ \frac{\frac{b^2}{1+\rho^{-2}G-1} r^{-2} + \frac{1}{1+\rho^2G}}{r} \right] , \quad (C-3)$$

$$\sigma_{\theta s} = -P \left[ -\frac{\frac{b^2}{1+\rho^{-2}G-1} r^{-2} + \frac{1}{1+\rho^2G}}{r} \right] ,$$

where  $\rho = \frac{a}{b}$ , and  $G = \left[ \frac{\frac{Y_c}{Y_s} \frac{1-v_s}{1-v_c} - 1}{\frac{Y_s}{Y_c} \frac{1-v_c}{1-v_s} - 1} \right] \left[ \frac{\frac{Y_c}{Y_s} \frac{1+v_s}{1-v_c} + 1}{\frac{Y_s}{Y_c} \frac{1+v_c}{1-v_s} + 1} \right]^{-1}$ .

The cylindrical ceramic shell is assumed to be polarized radially. The electric field in the radial direction resulting from the radial and tangential stress components are:

$$E_{rr} = g_{33}\sigma_{rs} , \quad E_r = g_{31}\sigma_{\theta s} , \quad (C-4)$$

where  $g_{33}$  is the electric field produced in the radial direction due to the application of unit radial stress, and  $g_{31}$  is the electric field produced in the radial direction by the application of a unit stress in the tangential direction.

The voltage developed across the two surfaces of the ceramic shell is:

$$V = \int_a^b (E_{rr} + E_{r\theta}) dr . \quad (C-5)$$

When Eqs.(C-3) and (C-4) are substituted into Eq.(C-5) and the integration is performed, there results for the absolute pressure sensitivity of the hydrophone:

$$\left| \frac{v}{p} \right| = \frac{b(1-\rho)(1-\rho G)}{1 + \rho^2 G} \left[ g_{33} \frac{1+\rho G}{1-\rho G} + g_{31} \right] . \quad (C-5)$$

If the central core is infinitely compliant (pressure release), the value of  $Y_c \rightarrow 0$ , and  $G \rightarrow -1$ . The sensitivity of the hydrophone with a pressure release core can be obtained from Eq.(C-6) with the substitution  $G = -1$ .

$$\left| \frac{v}{p} \right|_{G=-1} = b \left[ g_{33} \frac{1-\rho}{1+\rho} + g_{31} \right] . \quad (C-7)$$

This result agrees with the sensitivity of a hollow ceramic cylinder as calculated by Langevin.\*

The behavior of the receiving sensitivity is best explained by a graph. In Fig. 24, the sensitivity of a solid core ceramic cylinder made of PZT-5 is plotted as a function of the ratio of the inner and the outer radii of the ceramic shell. The parameter is  $G$ .

The curve for which  $G = -1$  represents the sensitivity of a PZT-5 ceramic cylindrical shell with a pressure release inner surface. Considering that the Poisson's ratio for any material must lie between 0 and  $1/2$ , it can be seen that  $-1 \leq G < 1$ . Since the sensitivity curve for  $G = 1$  is the highest curve for shells with a solid core, it is evidently desirable to make  $G$  as large as possible. All of the sensitivities for

---

\* R. A. Langevin, Reference 66, cited on p. 163.

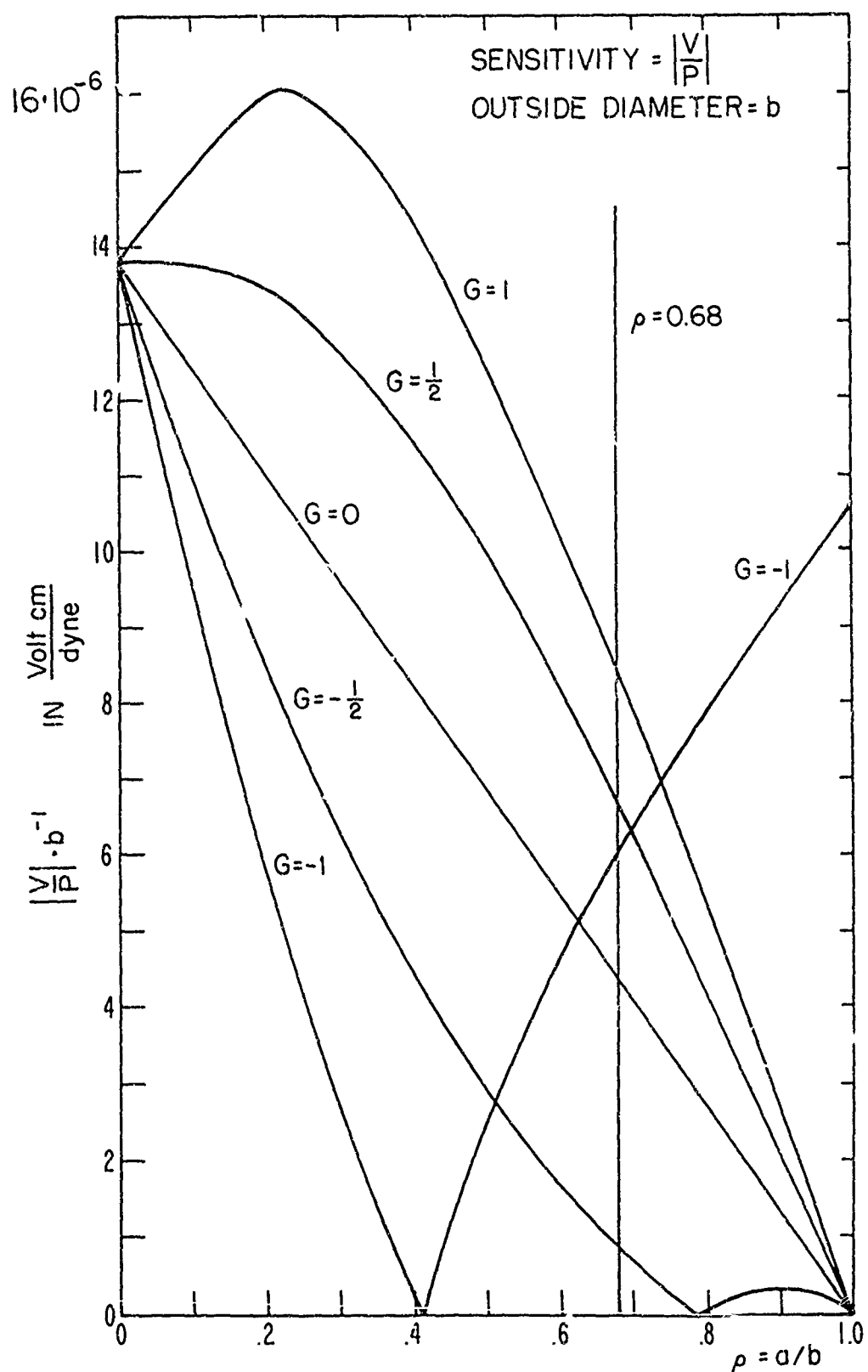


FIG. 24 RECEIVING SENSITIVITY OF SOLID CORE HYDROPHONES OF PZT-5.

$G \neq -1$  are higher than the pressure release sensitivity, except for very thin shells, e.g.,  $\rho \rightarrow 1$ . All of the curves converge at  $\rho = 0$  because the transducer becomes a solid cylinder of ceramic.

The expression for  $G$  becomes.

$$G = \left[ \frac{\frac{Y_c}{5.8 \times 10^{10}} \frac{2}{3(1-v_c)}}{3(1-v_c)} - 1 \right] \left[ \frac{\frac{Y_c}{5.8 \times 10^{10}} \frac{4}{3(1-v_c)}}{3(1-v_c)} + 1 \right]^{-1}, \quad (C-8)$$

where the Poisson's ratio for the ceramic has been taken as  $1/3$  and the Young's modulus for PZT-5 in cgs units has been substituted for  $Y_s$ . It can be seen from Eq.(C-8) that for PZT-5 the maximum value of  $G$  is  $1/2$  when  $Y_c \rightarrow \infty$ . The values of  $G$  for various core materials used with PZT-5 are given in the table below:

hard rubber	$G = -0.86$
PZT-5	$G = 0$
lead	$G = -0.09$
brass	$G = 0.148$
steel C 38	$G = 0.30$
beryllium	$G = 0.35$
tungsten	$G = 0.45$

The core material chosen for the probe hydrophone was brass. The ratio of the inside to the outside radius for the ceramic shell was 0.68. Reference to Fig. 24 shows that the sensitivity for this probe will be about 16% less than the sensitivity of a hydrophone with a pressure release inner surface. If the core material had been tungsten, the

sensitivity of the probe would have been about 12% greater than the sensitivity of a probe with a pressure release inner surface.

The sensitivity of the probe can be calculated from the information given in Fig. 24. The outside radius of the probe,  $b = 1/32$  inch.

$$S = 4.9 \times 10^{-6} \left( \frac{2.54}{32} \right) = 3.9 \times 10^{-7} \text{ volt}/\mu\text{bar}$$

$$= -128.2 \text{ dB//1V}/\mu\text{bar} .$$

The sensitivity calculations are valid at frequencies lying well below the lowest resonance frequency of the hydrophone. In this range of frequencies the pressure sensitivity of the hydrophones will not be a function of frequency. As the acoustic frequency approaches the fundamental resonance frequency of the hydrophone the strain amplitudes in the transducer will increase as will pressure sensitivity.

The fundamental resonance frequency of the cylindrical shell of radius  $b$  with a pressure release core occurs when the circumference of the shell is one wavelength long. This condition may be expressed:  $kb = 1$ , where  $k = \omega/c$ . The fundamental resonance frequency of a solid cylinder of radius  $b$  is the smallest solution of  $J_0(kb) = 0$ . This solution is  $kb = 2.405$ .<sup>68</sup> Thus, the fundamental resonance frequency of a solid cylinder of PZT-5 would be 2.405 times the fundamental resonance frequency of a thin cylindrical shell of the same outside radius. The specific acoustic impedances of brass and PZT-5 are almost identical, being  $290 \times 10^4$  and  $285 \times 10^4 \text{ gm cm}^{-3} \text{ sec}^{-1}$ , respectively. The fundamental

---

68. Eugene Jahnke and Fritz Emde, Tables of Functions (Dover, New York, 1945).

resonance frequency of the solid ceramic cylinder and the composite ceramic and brass cylinder will be practically identical. The fundamental resonance frequency of the ceramic shell was 600 kc/s. The fundamental resonance frequency of the composite structure will be about 1.44 Mc/s. This places the fundamental resonance frequency of the probe hydrophone above the frequency range over which the probe is to have a flat frequency response.

## LIST OF REFERENCES

1. Sir John Thornycroft and Sidney W. Barnaby, "Torpedo Boat Destroyers," Proc. Inst. Civil Engrs. 122, 51 (1895).
2. Lord Rayleigh, "On Pressure Developed in a Liquid During the Collapse of a Spherical Cavity," Phil. Mag. 34, 94 (1917).
3. J. Olaf, "Oberflachenreinigung mit Ultraschall," Acustica 7, 253 (1957).
4. K. Bisa, K. Dirnagl, and R. Esche, Siemens-Zeitschrift 28, 341 (1954).
5. W. L. Nyborg, R. K. Gould, F. J. Jackson, and C. E. Adams, "Sonically Induced Microstreaming Applied to a Surface Reaction," J. Acoust. Soc. Am. 31, 706 (1959).
6. B. E. Noltingk, "The Effects of Intense Ultrasonics in Liquids," Handbuch der Physik, Vol. XI/2, S. Flugge, ed. (Springer-Verlag, Berlin, 1962).
7. M. del Duca, E. Yeager, M. Davies, and F. Hovorka, "Isotopic Techniques in the Study or the  $\alpha\gamma$ -chemical Formation of Hydrogen Peroxide," J. Acoust. Soc. Am. 31, 301 (1958).
8. C. Campbell, "Ultrasonic Soldering of Aluminum," Electronic Progress 2, 4 (Raytheon Manufacturing Co., Waltham, Mass., 1958).
9. E. Heidmann, "Metallurgical Effects of Ultrasonic Waves," J. Acoust. Soc. Am. 26, 831 (1954).
10. W. Roberts, E. Yeager, and F. Hovorka, Ultrasonic Research Lab., Western Reserve Univ., Cleveland, Ohio; Tech. Rept. No. 18 (1957).
11. E. Meyer and H. Kuttruff, "Zur Phasenbeziehung zwischen Sonolumineszenz und Kavitationsvorgang bei periodischer Anregung," Z. Physik 11, 325 (1959).
12. N. A. Roi, "The Initiation and Development of Ultrasonic Cavitation," Soviet Phys.-Acoustics 3, 3 (1957).
13. F. G. Blake, Jr., "The Onset of Cavitation in Liquids," Tech. Memo. No 12, Acoustics Research Lab., Harvard Univ. (1949).
14. H. G. Flynn, "Physics of Acoustic Cavitation in Liquids," Physical Acoustics, Vol. 1B (Academic Press, W. P. Mason, ed.), in press.

15. G. Willard, Ultrasonically Induced Cavitation in Water: A Step-by-Step Process," J. Acoust. Soc. Am. 25, 667 (1953).
16. W. Mohr, "Über Schwingungskavitation bei kurzen Schallimpulsen," Acustica 7, 267 (1957).
17. A. T. Ellis, "Techniques for Pressure Pulse Measurements and High-Speed Photography in Ultrasonic Cavitation," Cavitation in Hydrodynamics, London, H. M. S. O., 8-1-8-32 (1956).
18. R. T. Knapp and A. Hollander, "Laboratory Investigations of the Mechanism of Cavitation," Trans. A. S. C. Mech. Engrs. 70, 419 (1948).
19. G. I. Taylor, "The Instability of Liquid Surfaces When Accelerated in a Direction Perpendicular to Their Planes," Proc. Roy. Soc (London), Ser. A, 201, 192 (1950).
20. A. M. Binnie, "The Stability of the Surface of a Cavitation Bubble," Proc. Cambridge Phil. Soc. 49, 151 (1953).
21. M. D. Rosenberg, "Pulsations and Growth of Gas-Filled Bubbles in Sound Fields," Tech. Memo. No. 25, Acoustics Research Lab., Harvard Univ. (1952).
22. D.-Y. Hsieh and M. S. Plesset, "Theory of Rectified Diffusion of Mass into Gas Bubbles," J. Acoust. Soc. Am. 33, 206 (1961).
23. F. G. Blake, Jr., "The Tensile Strength of Liquids: A Review of the Literature," Tech. Memo. No. 9, Acoustics Research Lab., Harvard Univ. (1949).
24. J. C. Fisher, "The Fracture of Liquids," J. Appl. Phys. 19, 1062 (1948).
25. D. Turnbull and J. C. Fisher, "Rate of Nucleation in Condensed Systems," J. Chem. Phys. 17, 71 (1949).
26. F. E. Fox and U. F. Herzfeld, "Gas Bubbles with Organic Skin as Cavitation Nuclei," J. Acoust. Soc. Am. 26, 984 (1954).
27. G. Kurtze, Nachr. Akad. Wiss. Göttingen, Math.-Phys. Kl. 1 (1958).
28. W. I. Galloway, "An Experimental Study of Acoustically Induced Cavitation in Liquids," J. Acoust. Soc. Am. 26, 849 (1954).
29. D. C. Pease and R. L. Blink, "Cavitation from Solid Surfaces in the Absence of Gas Nuclei," J. Phys. Colloid. Chem. 51, 556 (1947).
30. E. N. Harvey, Barnes, McElroy, and Whitely, "Removal of Gas Nuclei from Liquids and Surfaces," J. Am. Chem. Soc. 67, 156 (1945).

31. E. N. Harvey, W. C. McElroy, and A. H. Whitely, "On Cavity Formation in Water," *J. Appl. Phys.* 18, 162 (1947).
32. M. Strasberg, "Undissolved Air Cavities as Cavitation Nuclei," Cavitation in Hydrodynamics, London, H. M. S. O. 6-1-6-13 (1956).
33. R. B. Lindsay, "Acoustics and the Structure of Liquids," *Sci.* 120, 409 (1945).
34. D. Sette, "Sonic Cavitation and Ionizing Radiation," Proc. III Intern. Cong. Acoust., Stuttgart, 1959, V. I. Elsevier Publ., Amsterdam, 330 (1961).
35. D. Sette and F. Wanderlingh, "Nucleation by Cosmic Rays in Ultrasonic Cavitation," *Phys. Rev.* 125, 409 (1962).
36. F. Seitz, "On the Theory of the Bubble Chamber," *Phys. Fluids* 1, 2 (1958).
37. D. Messino, D. Sette, and F. Wanderlingh, "Effects of Uranium Salts on Sound Cavitation in Water," *J. Acoust. Soc. Am.* 35, 926 (1963).
38. D. Lieberman, "Radiation-Induced Cavitation," *Phys. Fluids* 2, 456 (1959).
39. H. N. V. Temperley and L. G. Chambers, "The Behavior of Water Under Hydrostatic Tension," *Proc. Phys. Soc. (London)* 58, Part 1, 420 (1946).
40. L. B. Briggs, J. B. Johnson, and W. P. Mason, "Properties of Liquids at High Sound Pressures," *J. Acoust. Soc. Am.* 19, 664, (1947).
41. H. Eyring, "Viscosity, Plasticity, and Diffusion as Examples of Absolute Reaction Rates," *J. Chem. Phys.* 4, 283 (1936).
42. A. M. Thorndike, "Experiments of Cavitation in the Range 10 kc to 50 kc," O. S. R. D. Section C-4, N. D. R. C., Univ. of Cal., San Diego, Pub. Bd. Rept. No. 81496.
43. R. B. Dean, "The Formation of Bubbles," *J. Appl. Phys.* 15, 446 (1944).
44. R. Esche, "Untersuchung der Schwingungskavitation in Flüssigkeiten," *Akust. Beihefte* 4, 208 (1952).
45. M. G. Sirotyuk, "Ultrasonic Cavitation," *Soviet Phys.-Acoustics* 8, 201 (1963).
46. M. G. Sirotyuk, "Behavior of Cavitation Bubbles at Large Ultrasonic Intensities," *Akust. Zh.* 7, 499 (1961); *Soviet Phys.-Acoustics* 7, 405.

47. B. E. Noltingk, "Comments on Ultrasonically Induced Cavitation in Hydrodynamics," Cavitation in Hydrodynamics, London, H. M. S. O., X-XII (1956).
48. H. Fuchtbauer and M. Thelsman, "Wirkung des Ultraschalls und Badterien," Naturwissenschaften 36, 246 (1949).
49. D. Doynon and Y. Simont, "Cavitation et Hemolyse par Ultrasons de Fréquences Différentes," C. R. Acad. Sci. Paris 232, 2011 & 2411 (1951).
50. B. E. Noltingk and A. E. Neppiras, "Cavitation Produced by Ultrasonics," Proc. Phys. Soc. (London) 63B, 674 (1950); 64B, 1032 (1951).
51. C. W. Willard, "Focusing Ultrasonic Radiators," J. Acoust. Soc. Am. 21, 360 (1949).
52. Th. Lange, "Methoden zur Untersuchung der Schwingungskavitation in Flüssigkeiten mit Ultraschall," Akust. Beih. 2, 75 (1952).
53. W. Connolly and F. E. Fox, "Ultrasonic Cavitation Thresholds in Water," J. Acoust. Soc. Am. 26, 843 (1954).
54. W. I. Galloway, "A Simple Calibration Technique for Low-Sensitivity Transducers," J. Acoust. Soc. Am. 25, 1127 (1953).
55. P. M. Morse and H. Feshbach, Methods of Theoretical Physics, (McGraw-Hill Book Co., New York, 1953).
56. F. G. Blake, Jr., "Apparatus and Techniques for a Study of Cavitation," Tech. Memo. No. 11, Acoustics Research Lab., Harvard Univ. (1949).
57. W. B. Davenport and W. L. Root, Random Signals and Noise (McGraw-Hill, New York, 1958).
58. M. Strasberg, "Rectified Diffusion: Comments on a Paper of Hsieh and Plesset," J. Acoust. Soc. Am. 33, 359 (1961).
59. Lyman Briggs, "Limiting Negative Pressure of Water," J. Appl. Phys. 21, 721 (1950).
60. L. Prandtl and O. Tietjens, Applied Hydro- and Aeromechanics (Dover, New York, 1957).
61. J. M. Dalla Valla, Micrometrics (Pitman Co., New York, 1948).
62. J. J. Bickerman, Surface Chemistry for Industrial Research (Academic Press, New York, 1948).

63. M. D. Rosenberg, "Gaseous-Type Cavitation in Liquids," Tech. Memo. No. 26, Acoustics Research Lab., Harvard Univ. (1953).
64. M. Strasberg, "Onset of Ultrasonic Cavitation in Tap Water," J. Acoust. Soc. Am. 31, 163 (1959).
65. P. M. Morse, Vibration and Sound (McGraw-Hill, New York, 1948).
66. R. A. Langevin, "The Electro-Acoustic Sensitivity of Cylindrical Ceramic Tubes," J. Acoust. Soc. Am. 26, 421 (1954).
67. S. Timoshenko and J. Goodier, Theory of Elasticity (McGraw-Hill, New York, 1951).
68. E. Jahnke and F. Emde, Tables of Functions (Dover, New York, 1945).